THE VOLTAGE-CURRENT CHARACTERISTIC OF THE HUMAN SKIN

by

Georg Philip Lochner

Submitted in partial fulfillment of the requirements for the degree

Master of Engineering (Bio-Engineering)

in the

Faculty of Engineering, Built Environment and Information Technology

UNIVERSITY OF PRETORIA

April 2003

ABSTRACT

The objective of this dissertation is to provide insight into the mechanisms that are responsible for the nonlinearities and asymmetries of the voltage current characteristic of the human skin. Furthermore to provide an explanation for the partially reversible breakdown of the electrical resistance of the skin that results in a rapid decrease of the skin resistance and occurs when the skin is stimulated with a dry electrode.

The skin resistance and impedance was investigated with low frequency constant voltage pulses and with sinusoidal stimulation over a range of amplitudes (10 - 20 V) and frequencies (3 - 30 Hz), using a dry 79 mm^2 Ag/AgCl electrode.

Evidence is presented that electroporation of the lipid bilayer membranes occurs in the dry skin over in the voltage range 10-20 V, a wider range than previously thought; it is further shown that experimental results are predicted by electroporation theory, if it is assumed that a small percentage of the total surface area of the dry skin consists of 15 lipid bilayers in series, rather than the generally accepted estimate of 70-100 layers. By modeling the dry skin as 15 lipid bilayers in series undergoing electroporation, the non-linearity of voltage-current characteristic of the skin is accurately predicted.

Evidence is presented in support of a new hypothesis that the asymmetry of the skin's voltage-current characteristic can be attributed to electro-osmosis occurring within the lipid bilayers of the stratum corneum. It is further suggested that the existing mathematical description of electro-osmosis would not accurately describe this situation and equations were introduced to model the effect of electro-osmosis on the voltage-current characteristic of the skin.

An electrical model of the skin is presented based on the hypothesis that the voltage-current characteristic of the skin is due to the combined effect of electroporation and electro-osmosis on the lipid bilayers in the stratum corneum. In addition the model accounts for the effect of trans epidermal water loss.

Experimental evidence is presented contradicting existing hypotheses in the literature regarding the origin of the resistance breakdown of the dry skin. A new hypothesis is proposed that is consistent with measured data namely that the resistance breakdown of the dry skin is due to rupture of the lipid bilayer membranes in the stratum corneum.

OPSOMMING

Die mikpunt van die proefskrif is om insig te verskaf oor die meganismes wat verantwoordelik is vir die nie-linieere en asimmetriese spanning-stroom karakteristiek van die menslike vel. Verder, om 'n verduideliking te verskaf vir die gedeeltelik omkeerbare deurbraak van die elektriese weerstand van die vel, wat lei tot 'n skielike verlaging van die vel weerstand en wat plaas vind tydens elektriese stimulering van die vel met 'n droë elektrode.

Die velweerstand en impedansie word bestudeer met lae frekwensie konstante spanning pulse en met wisselspanning oor 'n bereik van spannings (10 - 20 V) en frekwensies (3 - 30Hz) met 'n droë 79mm^2 Ag/AgCl elektrode.

Bewys word gelewer dat die lipiede membrane van die vel elektroporasie ondergaan oor die spanningsbereik 10-20V, 'n wyer bereik as wat huidiglik aanvaar word; dit word verder gewys dat eksperimentele resultate voorspel word deur elektroporasie teorie, indien dit aanvaar word dat 'n klein persentasie van die oppervlak van die droë vel uit 15, eerder as die algemeen aanvaarde 70-100, lipiede lae bestaan. Deur die droë vel te modeleer as 15 lipiede lae wat elektroporasie ondergaan, kan die nie-lineariteit van die stroom-spanning karakteristiek van die vel akuraat voorspel word.

Eksperimentele resultate word voorgelê ter ondersteuning van 'n nuwe hipotese naamlik dat die assimetrie van the stroom-spannings karakteristiek van die vel veroorsaak word deur elektro-osmose wat binne the lipiede lae van die vel plaas vind. Dit word verder uitgewys dat die huidige beskrywing van elektro-osmosie nie toepaslik is op die situasie nie en vergelykings word voorgestel om die effek van elektro-osmose op die strook-spanning karakteristiek van die vel te modeleer.

'n Elektriese model van die vel word voorgelê wat gebaseer is op die hipotese dat die stroom-spannings karakteristiek van die vel toegeskryf kan word aan die gekombineerde effek van elektroporasie en elektro-osmose op die lipiede lae van die stratum corneum. Verder maak die model voorsiening vir die effek van trans epidermiese water verlies.

Eksperimentele bewyse word voorgelê wat teenstrydig is met huidige hipoteses in die literatuur aangaande die oorsprong van die weerstand deurbraak van die droë vel. 'n Nuwe hipotese word voorgestel wat deur die gemete data ondersteun word, naamlik dat die weerstand deurbraak van die droë vel die gevolg is van skeuring van die lipiede membrane in die stratum korneum.

ACKNOWLEDGEMENTS

I would like to thank Prof. P.J.Cilliers for his assistance and patience.

I am grateful to Dr.J.Z.Szopinski for his inspiration and patience.

I thank the Department of Electrical, Electronic and Computer Engineering for its patience.

I wish to express my sincere thanks to my parents for moral and nutritional support during completion of this dissertation.

Quote:

"The beginning is the most important part of the work" - Plato

"The ending is the most important part of the work" - Georg Lochner

List of abbreviations

CNS	Central Nervous System
TEWL	Transepidermal water loss
VCC	Voltage current characteristic
1D	One dimensional
2D	Two dimensional

TABLE OF CONTENTS

1 INTRODUCTION

1.1 GOAL AND MOTIVATION

The application of electricity to the skin has found widespread diagnostic and therapeutic application in medicine [1]. A common use is the enhancement of the transdermal flux of charged molecules through the skin, primarily for the purposes of transdermal drug delivery (usually in the form of iontophoresis) [1],[2] and non-invasive sampling for diagnostics where analytes are to be extracted for external assay [2]. Electrical enhancement of charged molecule transfer is limited in the size and type of molecule that can be transported [2] and by undesired side-effects of electricity such as tissue damage and pain [1]. For this reason a detailed understanding of the electrical properties of the skin is valuable [1],[3].

Recently skin resistance measurements have found new application in organ diagnostics [4]. The authors statistically demonstrated a link between the degree of electrical rectification measured with a dry electrode at specific skin locations and the health condition of particular internal organs. Since this technique is quick, cheap and non-invasive it could be a potentially useful screening tool for detecting asymptomatic pathologies such as early cancer or ulcers. An understanding of the skin resistance phenomena that are exploited by this technique is therefore of particular importance. The phenomena of interest include the electrical breakdown and asymmetry of the skin resistance.

Although skin impedance has been well characterized using wet electrode stimulation both in vivo and vitro [1], research on dry skin impedance is more limited. Historically dry electrode stimulation has been used for electro-tactile speech processing [1],[5] and for electro-acupuncture [6]. Three primary phenomena are observed in the dry condition. The voltage current characteristic (VCC) of the skin changes from (a) linear to non-linear and from (b) symmetric to asymmetric, dependant on the amplitude and duration of the electrical stimulus, and (c) the skin resistance exhibits a partially reversible electrical breakdown [7],[8],[9].

The peculiarities of the VCC have been attributed to electro-osmosis [9] and more recently to joule heating [7]. The electro-osmosis approach was found to be inadequate since it cannot explain why VCC can be non-linear but still symmetric [7]. The thermal model is based on in vivo impedance measurements and proposes a hypothetical relationship between current and temperature. In vitro measurements have found a different relationship between skin current and temperature [10],[11]. The breakdown effect has been linked to the appendages in the skin and attributed either to thermal activation of sweat glands [7] or electroosmotic filling of sweat ducts with electrolyte [9]. However Yamamoto [8] reported that the breakdown effect also occurs on the skin of nude mice and snakes that do not possess sweat ducts. In addition, during undocumented investigations by the author, the breakdown effect was also found to occur on the human lips, which are devoid of appendages [12]. Furthermore, no data that relates the applied voltage or current to the time to breakdown have been reported. The current models of the dry skin are therefore inadequate.

Subsequent to the development of these models, it was discovered that when an electric field is applied across the skin, microscopic pores are induced in the lipid bilayers of the stratum corneum [3],[13],[14], a process known as electroporation. The stratum corneum is the primary electrical barrier in the skin [15]. These pores are known to have a non-ohmic electrical resistance [16]. Electroporation is also reversible, with the pores disappearing over time when the electric field is removed [3],[13],[14]. The skin impedance phenomena (a) and (c) therefore appeared consist with electroporation. However electroporation has only been shown to occur in vitro in the voltage range 30-50 V [3],[13],[14], whereas the phenomena (a)-(c) are known to occur in the voltage range 10-20 V [7],[9].

The objectives of the research reported here were the following:

- characterize the non-linearity of the skin resistance in vivo using a dry electrode
- statistically characterize the breakdown phenomenon
- create a model that will explain the nonlinearities and asymmetries of the skin VCC
- explain the electrical breakdown of the dry skin
- develop a hypothesis regarding the link between skin electrical parameters and internal organs [4]

1.2 STRUCTURE OF DISSERTATION

The background section is an outline of the literature relevant to this dissertation. An overview of the anatomy of the skin is presented. The literature linking skin electrical phenomena to the anatomical structures in the skin is discussed. This is followed by a discussion of existing electrical models of the skin and their shortcomings.

The design of experimental equipment is described. The experimental section is divided into experiments concerning the nonlinearities and asymmetries of the skin VCC (chapter 4) and experiments investigating the electrical breakdown of the skin (chapter 5). A motivation for the experiment is followed by a description of the experimental setup. The result of the experiment is then presented along with a discussion. The relevant theoretical background, briefly mentioned in the background section, is explained in more detail in the motivation or discussion where necessary.

The conclusion and final model is presented along with a description and results of simulations. This is followed by the concluding discussion.

2 BACKGROUND

2.1 ANATOMICAL STRUCTURE OF THE SKIN

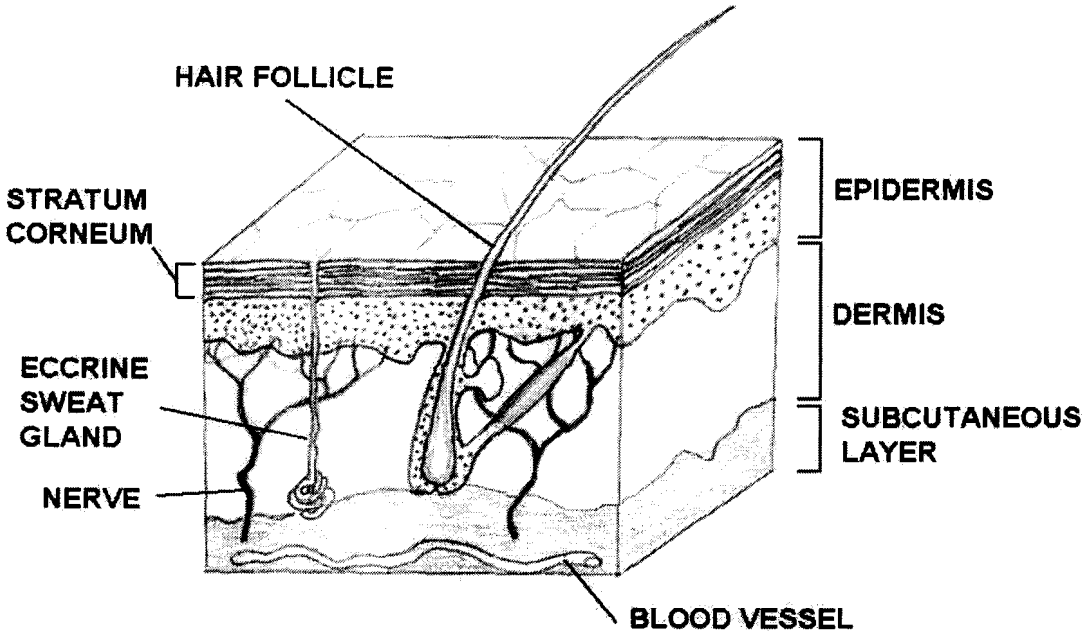

Fig. 2.1 Schematic of the structure of human skin (based on Chizmadzhev [3])

An anatomical description of the skin is presented according to Revis [12].The skin consists of distinct principle layers namely the epidermis, the dermis and the subcutaneous layer (Fig. 2.1). The dermis and subcutaneous layer contains the vascular and nervous components of the skin as well as the sweat glands, sweat ducts and hair follicles. These layers are similar to other tissues in the body and do not contribute significantly to the electrical characteristics of the skin.

The epidermis contains no blood vessels and is entirely dependent on the underlying dermis for nutrient delivery and waste disposal via diffusion through the dermoepidermal junction. The epidermis is a stratified squamous epithelium consisting primarily of keratinocytes in progressive stages of differentiation from deeper to more superficial layers. As keratinocytes divide and differentiate, they move from this deeper layer to the more superficial layers. Once they reach the stratum corneum, they are fully differentiated keratinocytes devoid of nuclei and are subsequently shed in the process of epidermal turnover. Cells of the stratum corneum are the largest and most abundant of the epidermis.

The stratum corneum consists of approximately 15-20 layers of corneocytes (flattened cells filled with keratin, originally keratinocytes) that are surrounded by lipid lamellae [17], consisting typically of 5 stacked lipid bilayers (Fig. 2.2).

The stratum corneum has been shown to be by far the most important current barrier [15]. Tape stripping of the skin has shown that when the stratum corneum is removed the rest of the epidermis and dermis can be modeled as a resistance of about 500 Ω. The stratum corneum and the appendages which traverse it are therefore primarily responsible for the electrical properties of the skin.

Skin appendages such as sweat glands and hair follicles traverse the stratum corneum. Sweat ducts are approximately 10 μm in diameter [17] and account for approximately 0.1% of the skin surface. Sweat ducts act as shunt pathways for electrical current through the skin [18].

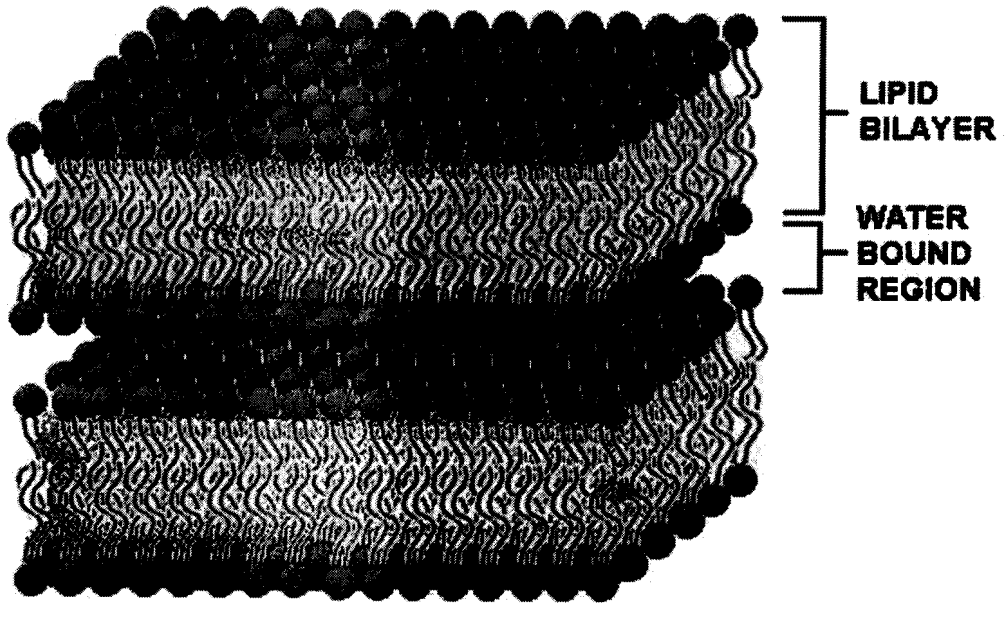

Fig. 2.2 Lipid Bilayer

2.2 FACTORS AFFECTING SKIN IMPEDANCE

Factors affecting skin impedance can be divided into those of anatomical origin, which influence both in vivo and in vitro measurements and those of physiological origin, which only affect in vivo measurements.

2.2.1 Anatomical Factors

As has been indicated, the structures present in the skin are primarily appendages, lipid bilayers and corneocytes. The contribution of each to skin resistance is debated in literature.

2.2.1.1 Appendages

Hair follicles, sweat glands and other appendageal structures may be the primary route of ion transport through the skin in the domain of low transdermal voltages (<20 V). Evidence in support of shunt pathways is derived from microscopic visualization studies [18],[19],[20] and direct electrical measurements [21]. The results of the latter study shows that current density during ion transport is greatest in the vicinity of hair follicles and sweat ducts.

2.2.1.2 Lipid-Corneocyte Matrix

It has been shown that the stratum corneum lipid bilayers are primarily responsible for the electrical properties of the skin [10]. The thermoelectrical properties of these layers have been studied in recent literature [22]-[24]. Between 20 and 120°C four thermal transitions take place in the human stratum corneum namely at 40, 70, 85 and 107°C [22]. These thermal transitions have been studied by X-ray diffraction and Fourier transform infrared spectroscopy and could be attributed to phase transitions of free lipids, protein-bound lipids or proteins [23],[24].

The first transition is not associated with any change in the electrical properties of the skin. X-ray diffraction studies have shown that this transition changes the lateral arrangement of the intercellular lipids from a primarily orthorhombic packing to a hexagonal packing [10]. Measurements of the stratum corneum resistance and capacitance across this temperature range [10],[11],[25] has shown that between 60 and 75°C and abrupt increase in both the stratum corneum conductance and capacitance occurs. This corresponds to the temperature interval of the second thermal transition, namely the phase transition of unbound intercellular lipids. This change in conductance and capacitance is irreversible. X-ray

diffraction studies have shown that the originally predominant lamellar structure with a repeat distance of 6.4 nm did not reappear after recrystallization but lipids preferentially recrystallized in a lamellar structure with a repeat distance of 13.4 nm [23]. The latter structure was only present in small amounts before heating. Below 60°C increased temperature is associated with a much less dramatic but reversible increase is capacitance and conductance [10],[11].

The similarity between the temperature dependence of the stratum corneum conductance and capacitance and the fact that lipid extraction removes the resistive component of the skin impedance indicates that the electrical barrier and charge storage capacity of the stratum corneum resides within the intercellular lipid lamellae [10].

The studies that cite appendages as main current carriers do not rule out charge flow through the surrounding stratum corneum. Moreover, since the appendages only account for about 0.1% of the skin surface, there may be considerable ion flow through the surround lipid matrix. Other studies [11],[17] suggest that current through the lipid matrix may even predominate. Non-appendageal current flow through the lipid matrix probably occurs through defects in the lipid matrix at sites of lipid phase separation, that are present across the temperature range, but more abundant at higher temperatures [11].

2.2.1.3 Electroporation

Under normal conditions the lipids in the stratum corneum exist as stacked bilayers (Fig. 2.2) Due to lateral thermal fluctuations of individual lipid molecules, hydrophobic pores are spontaneously formed in the lipid membrane. These hydrophobic pores are randomly and continuously created and destroyed. At a certain radius, pore energy is reduced by the formation of a hydrophilic pore, which exists in an energy well and is therefore in a metastable condition (Fig. 2.3). The height of the energy barrier to be overcome before a stable pore can be created is reduced by applying a potential difference across the membrane. The hydrophilic pores allow ions to traverse more freely across the membrane and therefore increases membrane conductance [14],[16]. Once a metastable pore is created it's size depends on the voltage across the membrane [26]. An electroporated membrane therefore has a non-linear conductance. Pores induced by the application of voltage continue to exist after stimulation is stopped. The mean lifetime of these pore

depends on the type of membrane and range from seconds for artificially created lipid membranes to hours for cell membranes.

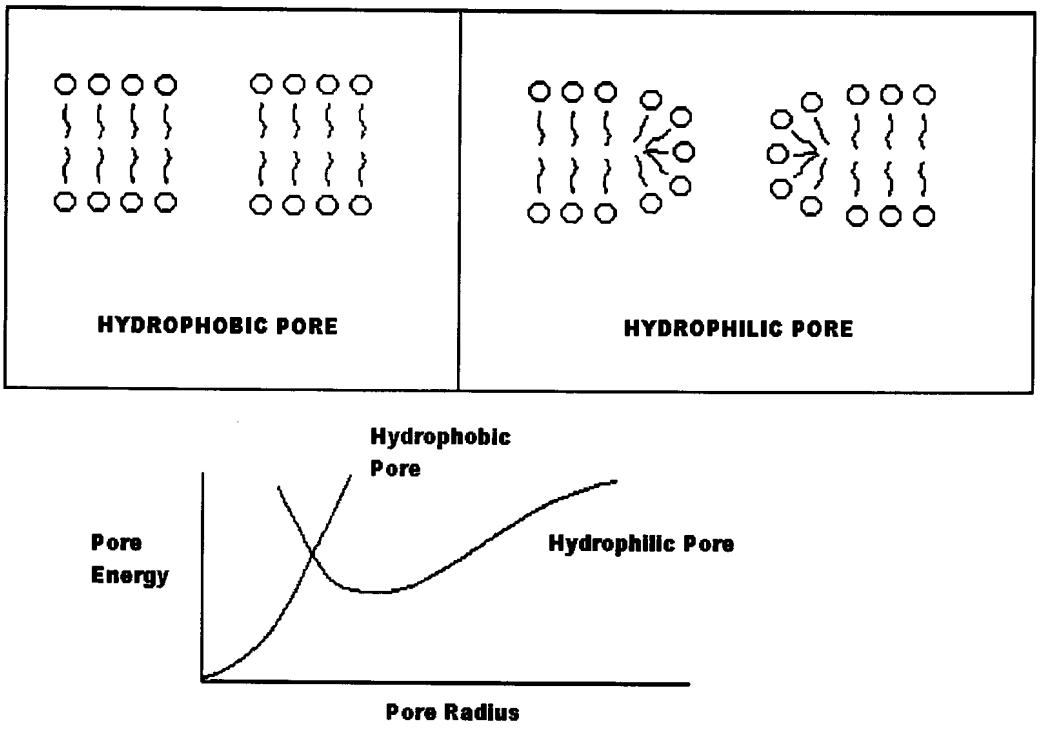

Fig. 2.3 Schematic of different types of pores in a lipid bilayer and pore energy as a function of it's radius, according to Glaser [16].

2.2.2 Physiological Factors

2.2.2.1 Sweat Gland Activity

Sweat gland activity can have a significant impact on skin impedance particularly when the skin is stimulated with a dry electrode. This phenomenon is utilized in devices such a lie detectors. A sweat duct filled with electrolyte forms a low conductivity path through the epidermis. In addition, moisture, which accumulates under the electrode, improves contact with the skin.

Sweat gland activity can be influenced by psychological and environmental factors. The skin plays a key role in thermoregulation. Changes in skin blood flow alone can regulate the body temperature over a range of environmental temperatures (25-30°C) known as the

thermoneutral zone. Above 30°C vasodilation is no longer sufficient and sweating is strongly stimulated [27].

2.3 VOLTAGE CURRENT CHARACTERISTIC OF THE SKIN

The skin impedance is known to be non-linear and is a function of many factors including the intensity, duration, history and frequency of the applied electrical stimulus [7],[8],[9] Different phenomena are seen when the skin is stimulated with a wet electrode than with a dry electrode. The skin VCC is known to take on three forms during sinusoidal stimulation.

2.3.1 Quasilinear Range

For small sinusoidal voltages (less than 10 V) the VCC is quasilinear [7],[13]. The amplitude range for quasilinear behavior is larger at higher frequencies and is practically non-existent at low frequencies (<2 Hz). Moist skin behaves quasilinearly over a wider amplitude range than dry skin. Unless the stimulus voltage is very small, the skin becomes non-linear with continued stimulation. The time required for these changes can vary from seconds to minutes depending on the stimulus, electrode placement and individual skin characteristics.

2.3.2 Non-Linear and Symmetric Range

Under dry electrode stimulation the VCC becomes nonlinear between 10 V and about 30 V but remains symmetric [7],[8],[9]. In vitro tests of hydrated skin indicates that non-linearity starts at around 1 V [13],[3]. The time required for the skin to regain its initial conductance, once the voltage stimulus has been removed, is typically a few seconds.

2.3.3 Non-Linear and Asymmetric Range

When the skin is stimulated with a dry electrode, at voltages in excess of about 20 V, the VCC becomes asymmetric [7],[9],[20],[26] .The skin is said to "break down" i.e. undergo a conductance increase of several orders of magnitude within milliseconds. This will be referred to as electrical breakdown and must not be confused with dielectric breakdown,

which occurs in the skin at hundreds of volts. After breakdown a pricking sensation can be felt. This breakdown is reversible but several minutes are required for skin properties to return to normal. Breakdown occurs as a result of applying a negative voltage stimulus through a dry electrode. Breakdown voltages as low as 12 V have been reported [26]. Breakdown is not observed when skin is stimulated with a wet electrode.

The skin exhibits rectification when stimulated with a dry electrode, i.e. the VCC becomes asymmetric. For positive applied voltages the skin resistance is significantly higher than for negative voltages and the breakdown effect is not observed.

In vitro tests indicate that the hydrated skin undergoes a dramatic increase in conductance above about 30 V, although no mention is made of the polarity of the stimulus [2],[3],[13]. There is no data concerning hydrated in vitro skin that suggests asymmetry. The time required for the skin to regain its original properties is in the order of several minutes.

2.4 EXISTING MODELS OF THE SKIN

Various electrical models have been proposed that attempt to provide a theoretical explanation for the low frequency characteristics of the skin and the electrical breakdown phenomenon.

Grimnes [9] modeled the skin as a membrane with empty pores and an electrolytic reservoir on one side. He concluded that electro-osmosis is responsible for low frequency phase shifts and the breakdown effect. When an electric potential is applied to opposite sides of a capillary, water in the capillary will be transported towards the negative electrode by a mechanism known as electro-osmosis. In dry skin most of the sweat ducts are empty. Sweat ducts underneath a negatively polarized electrode fill with electrolyte due to electro-osmosis. When the ducts are filled and the electrolyte comes into contact with the electrode, a rapid resistance decrease is observed. If the electrode is polarized positively, water molecules are repelled from the electrode and the resistance increases. Although not ruling out the possibility that electro-osmosis is a factor influencing the skin VCC, Panescu [7] points out that the electroosmotic model cannot explain the nonlinear but still symmetric form of the skin VCC.

Panescu and Webster [7],[20] proposed an electrical-thermal model of the skin and linked most of the skin electrical phenomena to thermal effects. The authors showed that high local current densities prevail particularly under dry electrode stimulation conditions. The authors hypothesize that joule heating at sites of high current density causes the local skin temperature to increase. The increased skin temperature increases ion diffusion through the skin, and results in the non-linear VCC of the skin. A power law relationship was postulated between the temperature and the current through the skin and parameters were adjusted to fit the data. Independent in vitro measurements of the current through the skin as a function of temperature at constant applied voltage does not verify a power law relationship. Instead over the relevant temperature range the skin resistance falls linearly with increasing temperature [10],[11]. The thermal model is derived from parameters used to describe the macroscale exchange of heat between the skin as a whole (including epidermis, dermis and subcutaneous layer), the internal body and the ambient medium, where the body is modeled as a cylinder and heat flows only in the radial dimension. However beneath a dry electrode, electrical energy would be dissipated almost exclusively in the stratum corneum [15], that accounts for less than 1% of the skin volume [12], and has significantly different thermal properties from the rest of the skin [28]. In addition since the conductive pathways through the stratum corneum are highly localized [20] the generated heat would flow not only along an axis normal to the electrode, but also radially away from this axis. Therefore this simplification does not appear justified. The authors noted that the energy applied before electrical breakdown occurs, stays relatively constant irrespective of voltage and concluded that sweat gland excitation is responsible for electrical breakdown. However, their assertion that breakdown occurs when the applied energy exceeds a certain threshold is not supported by a rigorous statistical investigation, instead it appears to be a casual observation. The authors themselves note that when a wet electrode is used to stimulate the skin, no breakdown occurs, despite the current being sufficient to cause blisters due to joule heating. Furthermore this theory is also contrary to the observation that breakdown occurs on the skins of animals that do not possess sweat glands [6] and on the skin of the human lips where no sweat glands are found.

Craane-van Hinsburg [10] measured the electrical properties of the skin in vitro as a function of temperature. Stimulus parameters were used which would not influence the skin's electrical properties. The model consists of two parallel resistance-capacitance elements in series (Fig 2.4). Each element has an exclusive and unique dependence on temperature which were linked to different anatomical substructures in the skin. It was

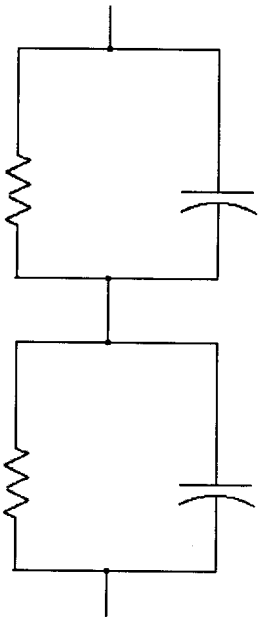

Fig 2.4 Electrical model of skin by Craane-van Hinsburg [10]

shown that the skin resistance decreases dramatically around 65°C while capacitance increases. The author did not attempt to explain the breakdown effect in terms of skin temperature. A separate in vitro study by Pliquett [25] demonstrated that during high voltage pulsing (60-300 V), the skin temperature can exceed 65°C, creating permanent high conductivity defects measuring several hundred micrometers in diameter.

Chizmadzhev [3] measured the electrical resistance of the skin in vitro using constant voltage pulses to investigate the effects of electroporation on the stratum corneum. The skin is modeled as two parallel resistance-capacitance elements connected in parallel. One represents the appendageal route while the other represents contribution of the stratum corneum lipids. The appendageal duct is modeled as a semi-infinite cylindrical tube filled with electrolyte. The tube crosses the stratum corneum, which is considered a high resistivity medium. Inside the body the tube walls are formed by two layers of epithelial cells. Under low voltage stimulation the four cell membranes surrounding the tube undergo electroporation resulting in a non-linear skin resistance. At higher voltages (> 30 V) electroporation of the stratum corneum takes place resulting in a significant drop in skin resistance. The skin completely recovered its electrical properties after dozens of minutes. The authors did not investigate the skin impedance. The voltage range where electroporation of the stratum corneum occurs (30-50 V) does not coincide with the voltage range where the nonlinearities and asymmetries of the dry skin are witnessed (10-20 V). However, the stimulation parameters (e.g. pulse duration) were different from those used for the in vivo studies. In addition the conditions under which in vitro tests are done differ significantly from in vivo conditions. Skin samples are soaked in electrolyte solution and remain immersed in electrolyte during measurements. Therefore the sweat ducts are filled with electrolyte and consequently provide high conductivity pathways through the skin. During in vivo measurements at ambient temperatures that do not induce active sweating, the sweat ducts are empty or semi filled [9], and are therefore not likely to be good conductors.

3 EXPERIMENTAL DESIGN

The non-linearity and asymmetry of the VCC of the skin are best measured using a dry measuring electrode, i.e. no external electrolyte is applied between the measuring electrode and the skin. An indifferent electrode is used that is much larger than the measuring electrode and is typically covered with an electrolyte to ensure good contact. Since the dry stratum corneum has a very high impedance (>100KΩ), the contribution of the indifferent electrode and the tissues below the skin (< 1 KΩ) to the total impedance is insignificant. The electroporation phenomenon is known to be a voltage dependant phenomenon usually studied in the literature using square voltage pulses [2],[3]. Therefore particular attention will be paid in this study to low frequency square voltage wave stimulation of the skin.

The typical arrangement for measuring the skin resistance with a dry electrode is a voltage source in series with a current sensing resistor, connected to the electrodes that are applied to the skin. The skin has been studied using this experimental setup, with electrodes of various sizes, materials and over a range of frequencies. A list of such studies are shown in table 3.1. In each case the authors concluded that the VCC of the skin was similar for different materials and that the polarization resistance of the electrode was sufficiently small, relative to the skin resistance, to be neglected.

Table 3.1 Experimental design of studies of the dry skin VCC in the literature

Reference	Electrode Type	Frequency Hz	Duration s	Stimulus	Electrode Area mm^2
Grimnes [9]	Ag-AgCl, Aluminium, Brass, Copper, Stainless Steel, Platinum	0.2 - 500	20	Square, 24 Vpp Sine, 20-60 Vpp	56
Grimnes [29]	Silver	DC	9	250-600 V	0.018
Yamamoto [8]	Ag-AgCl	0.01-100	500	Sine, 200-300 $\mu A/cm^2$	100
Panescu [20]	Ag-Agcl	0.01-5	40	Sine, up to 110 Vpp	100
Yamamoto [6]	Silver,Copper Gold, Platinum Carbon	DC	40	15 V	0.15

The skin resistance measured with a dry electrode varies by orders of magnitude, from exceeding 100 MΩ to less than 100 kΩ. These changes can take place over time intervals of milliseconds to hours. Due to the significant changes in skin resistance, different stimulus parameters are required to measure skin resistance before, during and after such changes. Due to the rapidity of these changes, the stimulus parameters cannot be controlled in real time by a human operator.

For these reasons it was necessary to design a custom programmable impedance measuring device. The device was designed to the following criteria:

Output voltage range	±40 V
Output current range	±3 mA
Sampling frequency	< 50 μS
Resolution	8 bit resolution

Channels	Two channels were included to allow different measurement ranges to be accommodated during different phases of a single stimulus train.

A block diagram of the circuit is shown in Fig. 3.1.

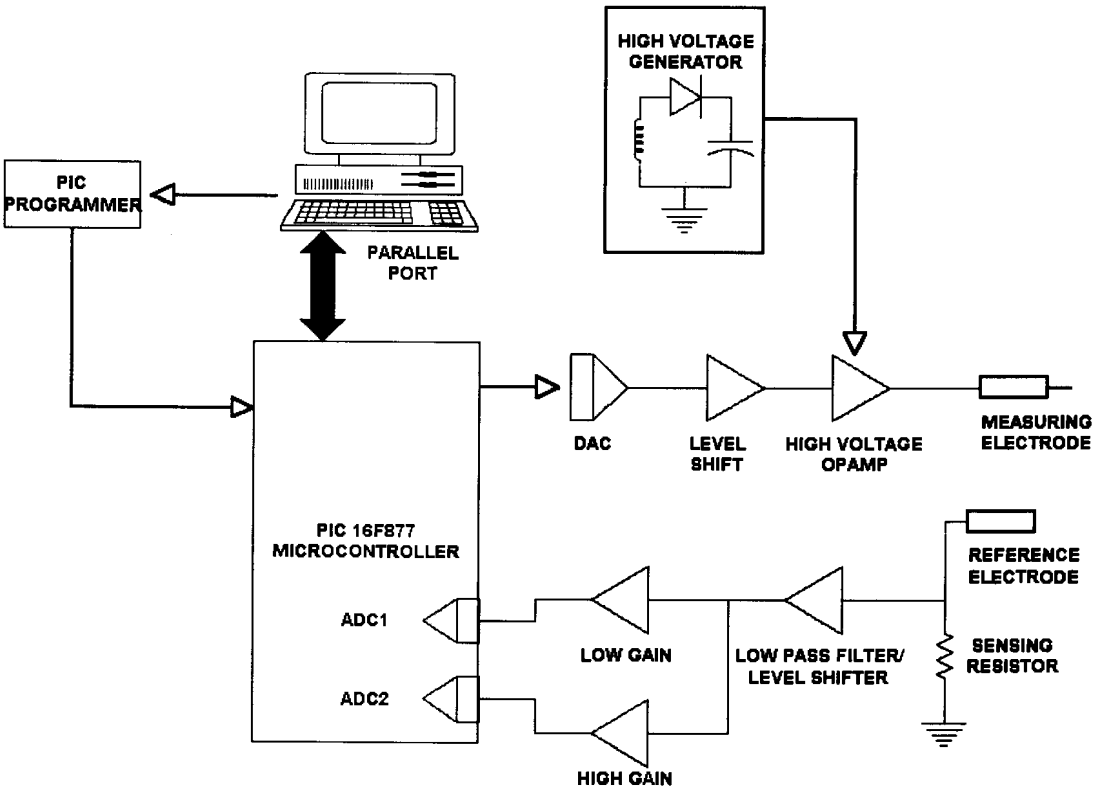

Fig. 3.1 Block diagram of measurement circuit

3.1 Computer software

Software on the computer was developed under Windows 98. The software communicates with the Pic microcontroller via the parallel port. The parallel port was chosen since the serial port is too slow to handle the required data throughput. The computer instructs the microcontroller to initiate a preprogrammed test. The computer then reads data samples from the Pic until the test is complete. A viewing facility was incorporated into software allowing the captured data to be displayed. The data can be viewed on different time scales by zooming in or out. To analyze the data, cursors were included to allow particular parameters (e.g. energy or the current integral) to be measured between arbitrary points in the data series. These parameters once measured could also be saved. Since a particular experiment could consist of many individual measurements, a facility was included to

export measured parameters from groups of data files to a format readable by Microsoft Excel. The Analysis Toolpak in Microsoft Excel was used to do statistical analyses.

3.2 Microcontroller software

A PIC16F877 microcontroller was used to control the measurement process. The microcontroller operates at 20 MHz, which allowed adequate sampling rates to be achieved. The microcontroller has on-board analogue to digital converters, timers, counters and a parallel port. The PIC16F877 is also in-circuit programmable. The microcontroller software could therefore be changed quickly and easily. This made it feasible to create more complex software for the microcontroller, which allowed great flexibility in experimental design.

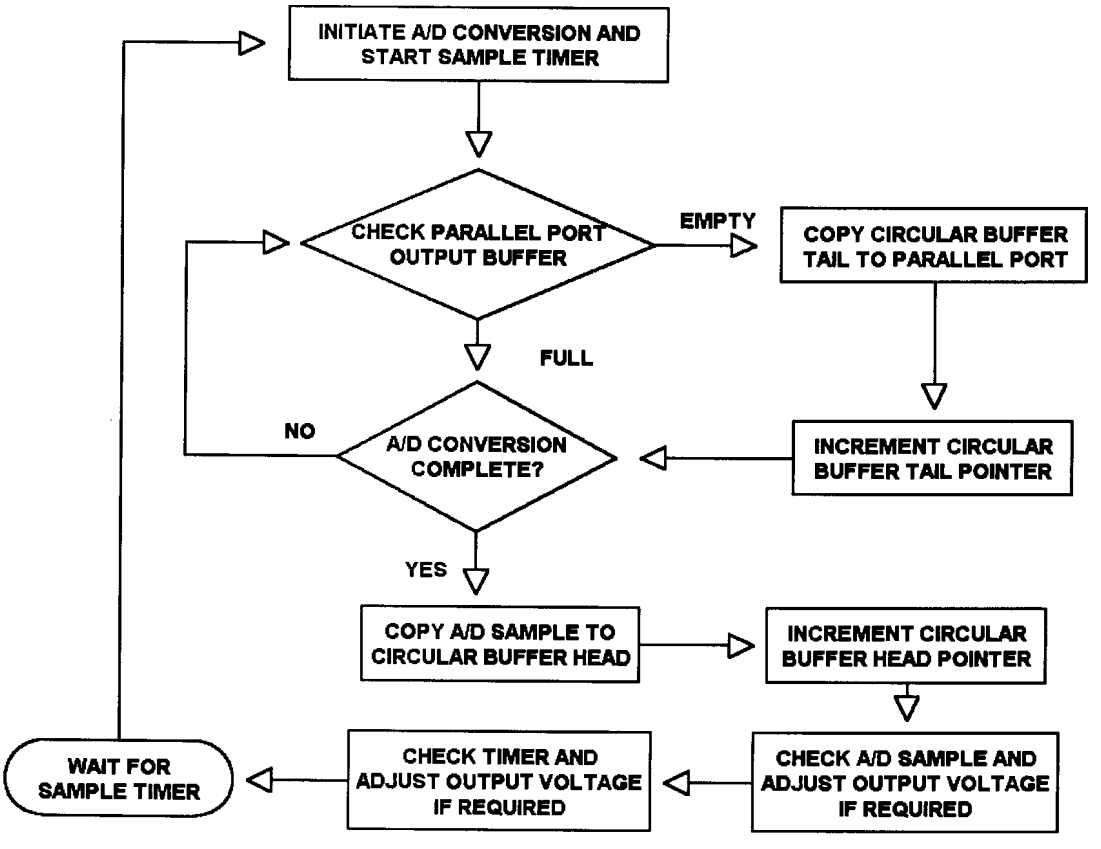

Fig. 3.2 Microcontroller software flow diagram showing sample acquisition cycle.

A typical sample acquisition cycle is shown in Fig. 3.2. Each acquisition cycle is timed with a counter (sample counter), which is linked to the external clock. This ensures that samples are acquired at a constant frequency irrespective of the number of instructions that

are executed by the microcontroller, which may vary from cycle to cycle. After setting up the output voltage or current stimulus, the microcontroller resets the sample counter and starts the data acquisition procedure. The microcontroller initiates a digital to analogue conversion. This process takes place in the background. While this is being completed the microcontroller continuously checks the parallel port output buffer and updates it when the computer has read the value currently in the buffer. A 64 byte circular FIFO buffer is implemented in the microcontroller. Converted samples are inserted at the back of the queue while they are read out from the front by the computer. This was necessary since the computer software is running under Windows 98, which is not a real time operating system, therefore read times cannot be guaranteed. Software checks were implemented to ensure that buffer overruns do not occur.

When data sampling is complete, the microcontroller places the acquired value in the circular buffer. Depending on the requirements of the particular experiment, the microcontroller then has a chance to adjust the output voltage or current as a function of the acquired sample. Alternatively the output stimulus could be adjusted as a function of time using the microcontroller's internal counters. This allowed complex pulse protocols to be generated and allowed decision making to be incorporated into the data acquisition process.

The microcontroller then waits for the sample counter to count up to a specified value before starting the next sample acquisition cycle.

3.3 Analogue Circuit

The microcontroller generates analogue voltages by means of a TLV5619 parallel DAC. The output of the DAC is buffered by a CA3130E opamp connected as a level shifter. The buffer drives a PA81J precision high voltage opamp (HVO). The HVO can be configured in to operate in voltage output or current output mode. High voltage supplies for the HVO are generated by two inductive charge pump circuits generating ±40 V. The PA81J features high power supply noise rejection. In addition a passive low pass filter band limits the high voltage amplifier output to 15 kHz.

The output current is measured through a sensing resistor. A sensing resistor between 1 and 10 kΩ was used depending on the current range to be measured. The voltage over the

sensing resistor is amplified by a LM308 opamp in a first order low-pass filter configuration with 10 kHz bandwidth since the maximum sampling frequency is 20 kHz.. The output of this amplifier drives two level-shift circuits connected in parallel. Each of these connect to an ADC on the microcontroller. The level-shift circuits use LM308 opamps first order narrow banded to 10 kHz. The gain and offset on each are separately adjustable.

The circuit is housed in a grounded metallic case.

The microcontroller was programmed to set the output voltage to zero when the measured current exceeded a particular threshold. This was done to avoid painful sensations due to the rapid increase in current through the skin after breakdown.

3.3.1 Filter Characterisitics

The response of the filter is shown in Fig 3.3.

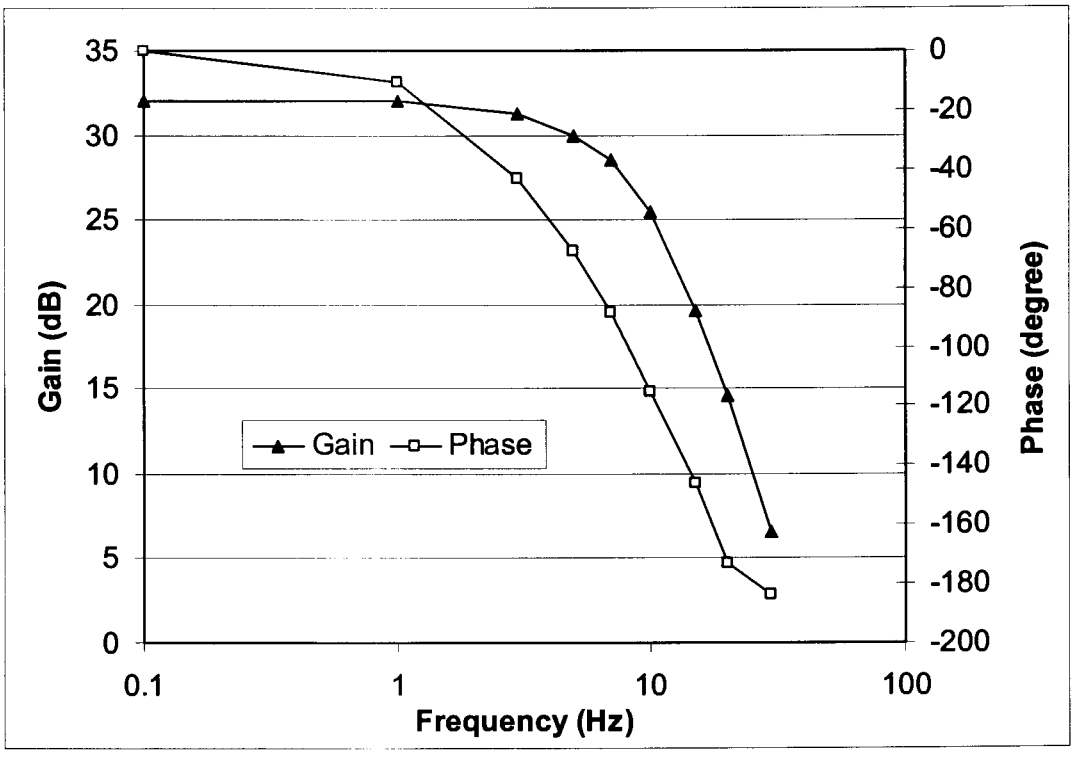

Fig 3.3 Amplitude and phase angle plot of the input filter in Fig 3.1, measured between the reference electrode and ADC1.

3.3.2 Drift

The measurement circuit was calibrated before each series of measurements. To quantify drift during a measurement series the output amplifier was programmed to output a constant 10V signal. The current through a 200 kΩ resistor was measured by taking 1000 12 bit samples at 2.5 KHz. 12 bit samples were acquired using 8 times oversampling. This process was repeated every 15 minutes for 1 hour. Fig 3.4 shows the mean and standard deviation of the binary value of each group of 1000 samples. Drift is not a concern since the mean does not trend up or down.

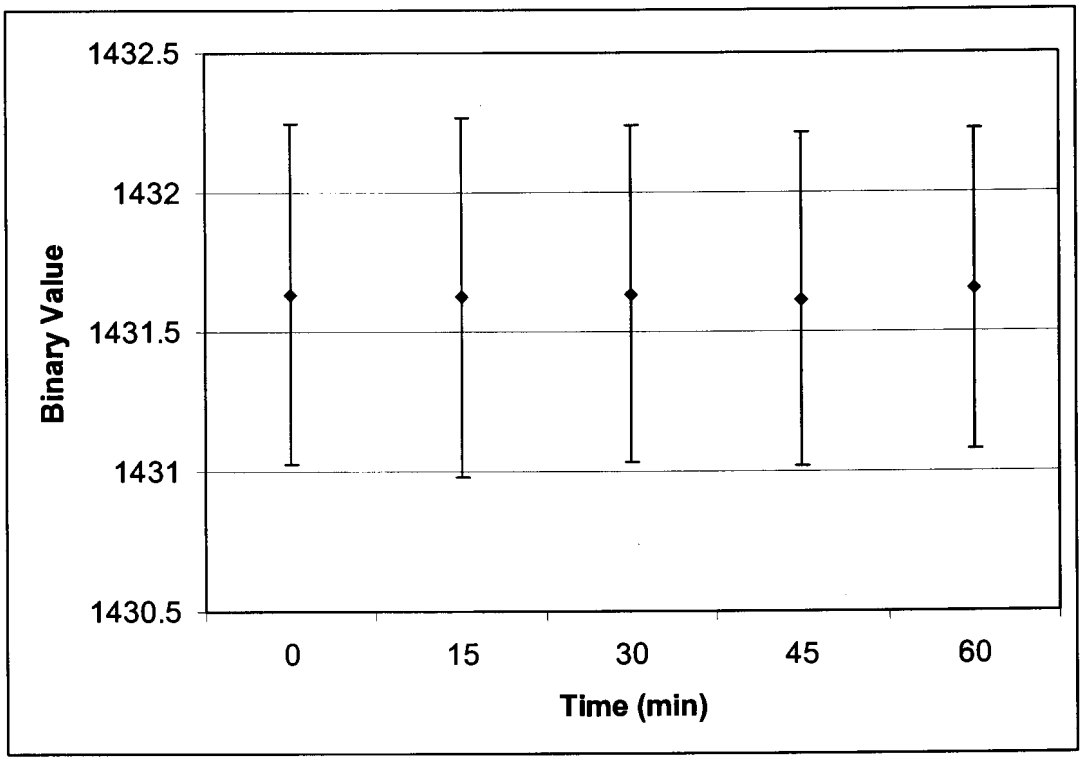

Fig 3.4 Mean and standard deviation of 1000 samples taken every 15 minutes .

3.4 Electrodes

The Ag/AgCl electrode approaches the characteristics of a perfectly nonpolarizable electrode [30], therefore all electrodes used in this study were of this type.

The reference electrode consisted of two large (each 10 cm^2) pregelled Ag/AgCl electrodes. These were placed on the skin on opposite sides of the body. The series resistance of the two electrodes and the body was measured using a DC voltage source (5V) and a sensing resistor. The skin beneath the electrodes was dermabraded until the combined resistance of the two electrodes was less than 1 kΩ. The two large electrodes

were then connected in parallel to form a single reference electrode with resistance less than 500 Ω. Each large electrode was manufactured from ten ECG tab electrodes (Ag/AgCl 1 cm diameter, ARBO, model H34SG) that had been removed from their adhesive strips and connected in parallel.

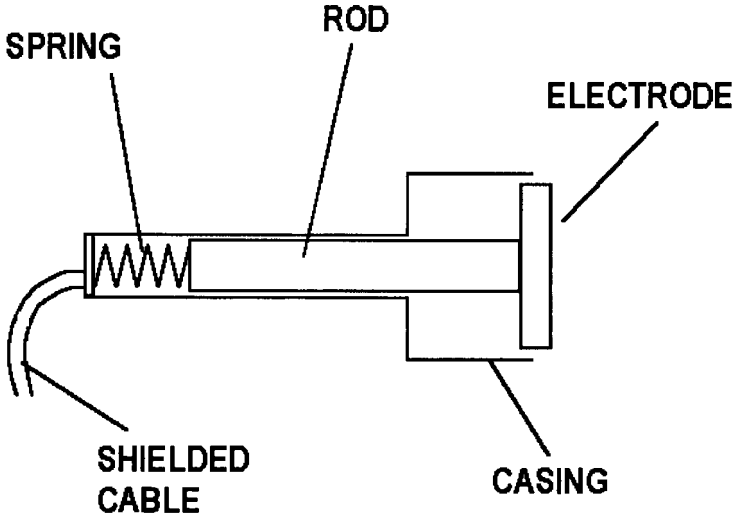

Fig. 3.3 Measuring electrode designed to apply constant pressure on the skin. A conductive rod and spring provides the electrical connection to the electrode. The casing is non-conductive.

The measuring electrode (Fig. 3.3) was designed to apply a specified constant pressure on the skin throughout the duration of the measurement, in order to ensure repeatability. A conductive rod was mounted on a spring inside a non-conductive cylindrical casing. A 1 cm diameter ECG electrode (ARBO, model H34SG) was mounted on the rod. The rod allows the electrode to move in and out of the casing. When the electrode is placed such that the casing makes contact with the skin, the pressure that the electrode exerts on the skin is 200 g/cm^2.

3.5 Environment

The environmental temperature was controlled using a 2400 W electric fan heater controlled by a thermistor based circuit. The fan heater was placed in the part of the room most distant from where experiments were carried out, approximately three meters from

the test subject. It did not blow directly in the direction of the test subject. A thermistor was placed in the vicinity of the test subject. The thermistor was connected to a Schmitt trigger circuit which controlled a relay that turned the fan heater on and off, to keep the ambient temperature at 25 ± 1°C. Measurements were done in winter and only when the environmental temperature was less than 25°C.

The thermistor was calibrated against a thermometer by performing a least squares fit at five environmental temperatures using the equation:

$$R_2 = R_1 \cdot e^{\left(\frac{B}{T_2} - \frac{B}{T_1}\right)} \qquad (3..1)$$

Where R1 and R2 is the resistance (ohm) of the thermistor at temperature (K) T1 and T2 respectively and B is the temperature coefficient.

3.6 Subjects

One subject was used for all experiments. Grimnes [9] experimented on four subjects, Panescu on two subjects [20] or one subject [7], and Yamamoto on one subject [15] or several subjects [6]. The low frequency skin impedance observed in this study, in experiment 1, was measured under similar conditions to the mentioned studies (using a dry electrode at ambient temperature 25°C) over a similar range of frequencies and amplitudes. The skin VCC phenomena (those described in section 2.3) observed in all previous studies were also observed in this study, therefore it is assumed that the skin of the test subject was representative of normal human skin.

3.7 Summary of Experiments

Table 3.2 Summary of Experimental Results

	AIM	RESULT	CONCLUSION
1	Verify that the VCC phenomena of asymmetry, non linearity and breakdown can be observed on the skin of the test subject using sinusoidal voltage stimulation. Obtain a complete data set for comparison with model.	Non-linearity, asymmetry and breakdown were observed in the expected voltage and frequency range.	The skin of the test subject is representative of normal human skin.
1a	Identify any phenomena related to the VCC of the skin other than asymmetry, non-linearity and breakdown.	At low voltages the skin conductance (G) and capacitance (C) both increase over time while the ratio G/C remains constant.	Trans-epidermal water loss increases the effective electrode area of a dry electrode over time.
2	Observe the VCC of the skin with square voltage pulses and find evidence of electroporation, electro-osmosis or thermal effects. The dry skin VCC was previously mainly studied with sinusoidal stimuli.	The skin conductance increases at a linear rate when a constant voltage is applied. This conductance increase is independent of the polarity of the applied voltage.	The linear skin conductance increase due to a constant voltage stimulus is more likely to be due to electroporation than to thermal effects or electro-osmosis.
3	Investigate the possible influence of electroporation on skin conductance in the 10-20V range by measuring the skin conductance and skin conductance rate of change as a function of voltage and comparing the measured data with the	The measured nonlinear relationship between skin resistance and voltage fits the theoretical description of electropore conductance in a multilamellar lipid bilayer system for 15 bilayers in series. The measured relationship	The conductance properties of the skin is consistent with the theoretical description of an electroporated multilamellar lipid bilayer system with 15 bilayers in series. Only a small area beneath

	theoretical description of electroporation.	between the rate of skin conductance increase and the applied voltage fits the theroretical relationship between electroporation rate and applied voltage if it is assumed that the skin is composed of 15 lipid bilayers in series.	electrode is involved in current conduction.
4	Qualitatively investigate electro-osmosis in a closed capillary.	Significant similarity exists for current curves obtained from skin and from a closed cappillary.containing electrolyte.	Electro-osmosis occurring within interbilayer spaces may be responsible for the asymmetry of the skin VCC.
5	Determine the current distribution under the electrode during breakdown.	Visible discoloration due to high current density are observed on the stimulating electrode surface after breakdown at highly localized sites.	Breakdown occurs at highly localized areas. The sweat glands are a possible area where such a highly localized breakdown could occur.
6	Determine whether appendages are involved in breakdown	Breakdown occurs on lips where there are no appendages	Appendages such as sweat glands do not play a role in the breakdown of the skin resistance.
7	Determine if activation level of sweat glands influence breakdown	Breakdown is unaffected by activation level of sweat glands	The activation of sweat glands is not the cause of skin breakdown. Active sweat glands provide parallel current paths
8	Measure energy dissipated before breakdown to determine whether a thermal trigger could be responsible	Average energy before breakdown stayed relatively constant	High variance meant result was inconclusive.
8a	Measure time to breakdown as a function of voltage	Linear relation between log (time to breakdown) and	Consistent with lipid membrane rupture

		voltage	
9	Measure recovery of skin after breakdown over 30 seconds	Significant recovery observed. Thirty seconds after breakdown skin resistance had increased by factor of 3. Indicates intact lipid bilayers remained after breakdown.	Suggests breakdown is not due to melting of lipid bilayers.
10	Measure recovery of skin after breakdown over 1 to 24 hours.	Skin recovery incomplete after 1 hour ($p < 0.001$) and probably incomplete after 24 hours ($p < 0.1$).	Indicates semi-permanent changes induced in the lipid bilayers, such as rupture or partial melting of the lipid membranes
11	Determine the influence of heating the skin directly beneath the electrode to about 35°C.	Rate of current increase due to constant applied voltage was greater at higher temperatures.	Indicates elevated temperature may have increased the electroporation rate.
12	Test hypothesis that breakdown occurs when the skin temperature exceeds a threshold value, using thermal-electrical model of the skin. It is assumed that electroporation is the primary phenomenon determining the dry skin resistance (conclusion of experiment 4).	The predicted relationship between time to breakdown and the applied voltage is not consistent with the experimentally observed relationship (experiment 8a).	Breakdown cannot be due to a thermal threshold being exceeded, if electroporation is the primary phenomenon determining the dry skin resistance.
13	Determine the extent of thermal changes in the skin due to joule heating, using an axisymmetric finite element model, for stimulus parameters used in previous experiments.	A worst case estimate yields a 10°C increase in skin temperature. The actual skin temperature increase would be significantly less.	The increase in skin temperature is unlikely to play a significant role in determining the voltage-current characteristic of the skin or cause breakdown.

4 VOLTAGE CURRENT CHARACTERISTIC OF THE SKIN

Experiments were conducted to determine the origins of the nonlinearities and asymmetries (see section 2.3) of the VCC of the human skin.

4.1 EXPERIMENT 1 - VCC measured with sinusoidal stimulation

The low frequency VCC of the dry human skin has been measured by previous authors over a range of frequencies and amplitudes (Table 3.1). The VCC is known to change from linear to nonlinear and symmetric to asymmetric as a function of stimulus duration, frequency and amplitude. These changes are known to occur in the frequency range 3-30 Hz and over the voltage range 20 - 40 Vpp [6]-[9]. The VCC was therefore measured at 3, 14 and 28 Hz, using amplitudes 20 and 40 Vpp, in order to verify that these changes occur on the skin of the test subject used and to obtain a complete and consistent data set. These data could then be used for quantification of electrical parameters of the test subject (e.g. capacitance), for presentation and for comparison with a future mathematical model of the skin.

The skin on the stomach was stimulated with a sinusoidal voltage stimulus and the current measured. The stimulus was applied for 9 seconds or until painful sensations were experienced due to the breakdown of the skin.

Fig 4.1 - 4.5 show the time course and Lissajous representation of the VCC. Lissajous loops are clockwise as voltage lags current. Graphs display traces at about 1, 5 and 9 seconds. In all cases the current through the skin increases with time. The applied voltage phase is displayed above the current traces in the current vs. time figures.

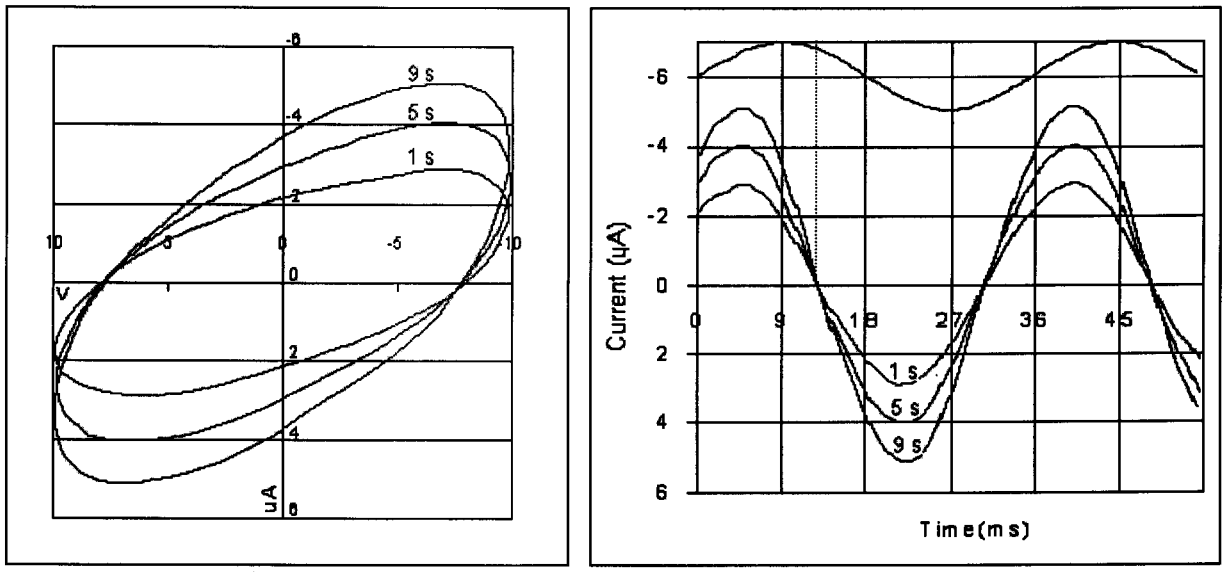

Fig. 4.1 Measured skin VCC at 20 Vpp, 28Hz. The voltage phase is shown above current curves.

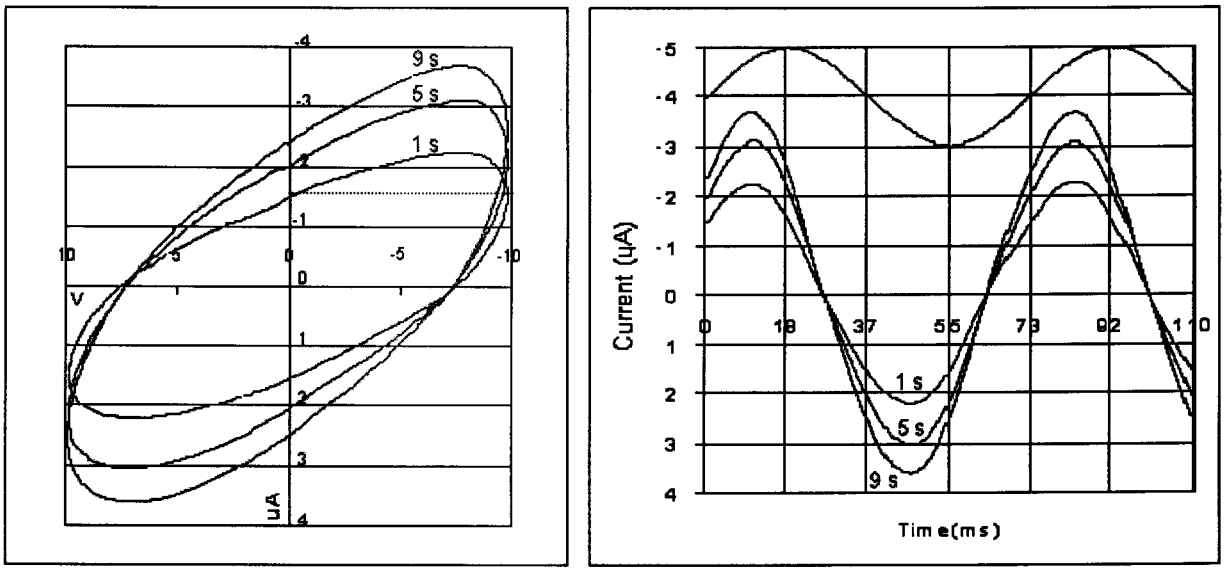

Fig. 4.2 Measured skin VCC at 20 Vpp, 14 Hz. The voltage phase is shown above current curves.

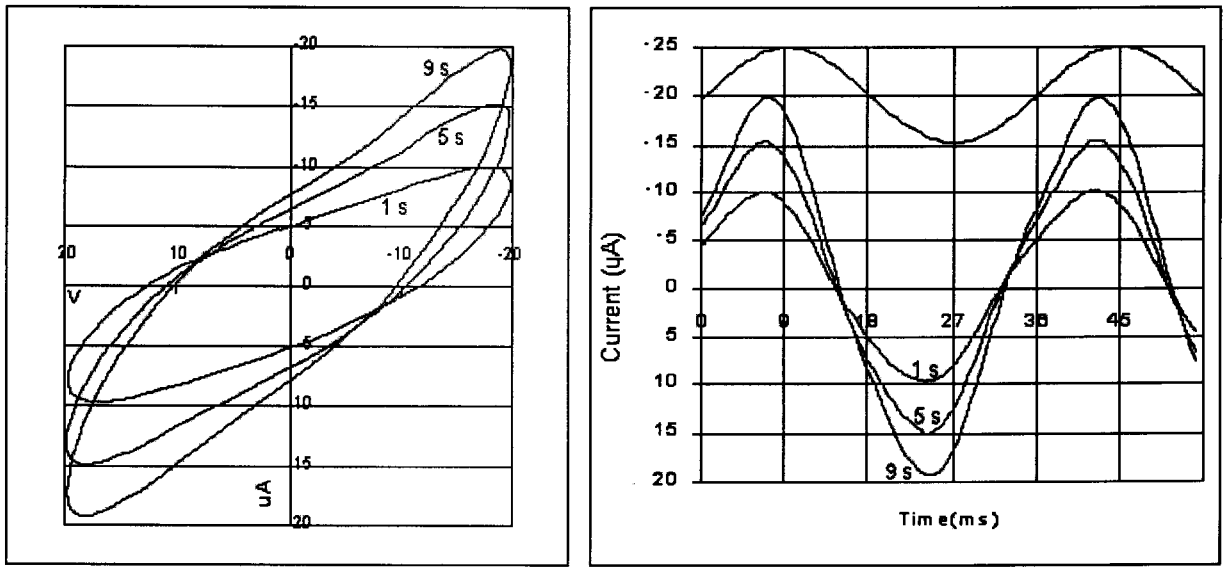

Fig 4.3 Measured skin VCC at 40 Vpp, 28Hz. The voltage phase is shown above current curves.

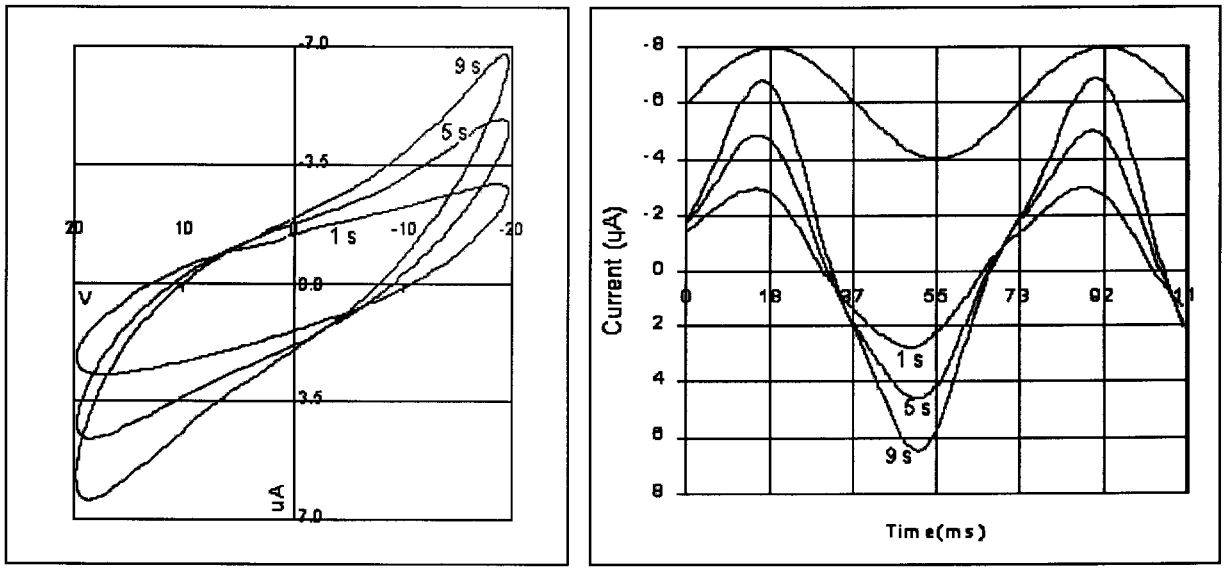

Fig. 4.4 Measured skin VCC at 40 Vpp, 14 Hz. The voltage phase is shown above current curves.

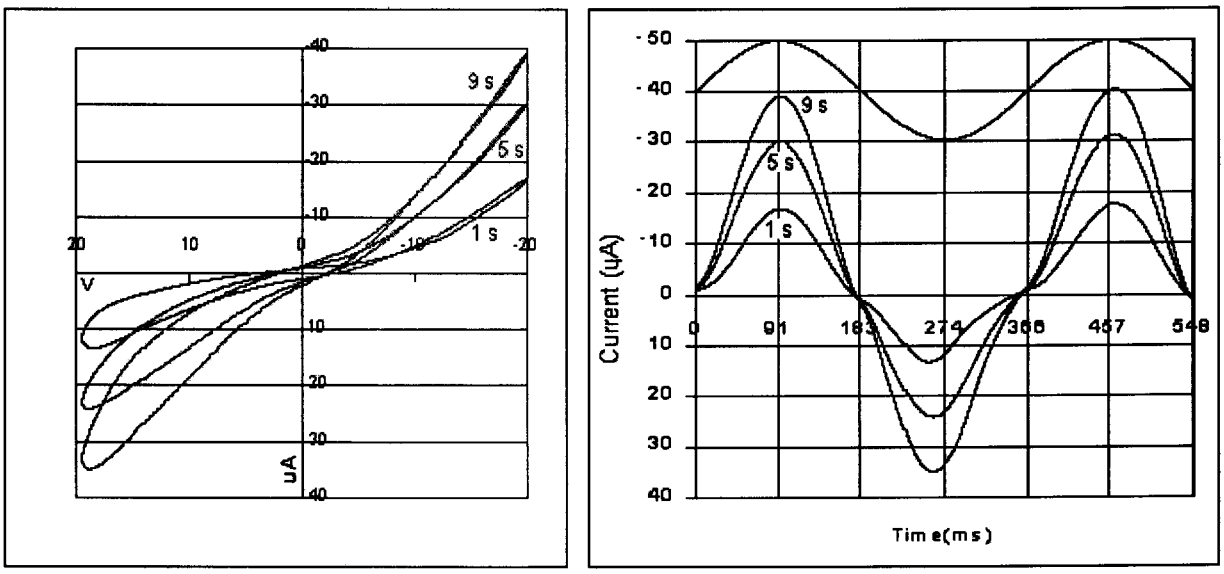

Fig. 4.5 Measured skin VCC at 40 Vpp, 3 Hz. The voltage phase is shown above current curves.

Fig. 4.1 and 4.2 show the skin VCC at 20 Vpp. The graphs are symmetrical and virtually linear and the skin impedance can be modeled, as is commonly done [1], using the circuit in Fig. 4.6 with G_e being much larger than G_i. Over time the Lissajous loop becomes wider and rotates towards the lower impedance region. On the Lissajous figure it can be seen that all three loops intersect the horizontal axis (I = 0) at the same point. This indicates that the ratio C_m/G_i must stay constant despite C_m and G_i increasing since

$$I_C + I_R = C_m \frac{dU_m}{dt} + U_m \cdot G_i \tag{4.1}$$

If $I_C + I_R = 0$ then

$$\frac{C_m}{G_i} = \frac{-U_m}{\frac{dU_m}{dt}} \tag{4.2}$$

From the time base graph on the right hand side of Fig. 4.1 and 4.2 it is clear that for all the curves I = 0 occurs at the same voltage level (dashed line in Fig. 4.1) and therefore $U_m/(dU_m/dt)$ when I = 0 remains constant over time . We have made the assumption that $U_m = V_s$ since G_e is more than 100 times greater than G_i or C_m.

Since the skin capacitance and conductance increase simultaneously while their ratio stays constant, they must be associated with a common origin. Electroporation is ruled out since it does not alter the skin capacitance [31]. The impedance decrease is consistent with an increase in the effective electrode area due to water, arising from trans-epidermal water loss (TEWL), being trapped underneath the electrode. TEWL is constantly occurring at a

rate of about 600 ml/day in humans [27]. Evidence exists for ohmic pathways through the skin. X-ray diffraction [23],[32] and IR spectroscopy [11] have shown that lipid phase separation occurs in the intact untreated stratum corneum. In other words a small fraction of the lipids in the skin exist in liquid phase. Highly permeable defects are thought to exist at the interfacial domain between the two phases [11].

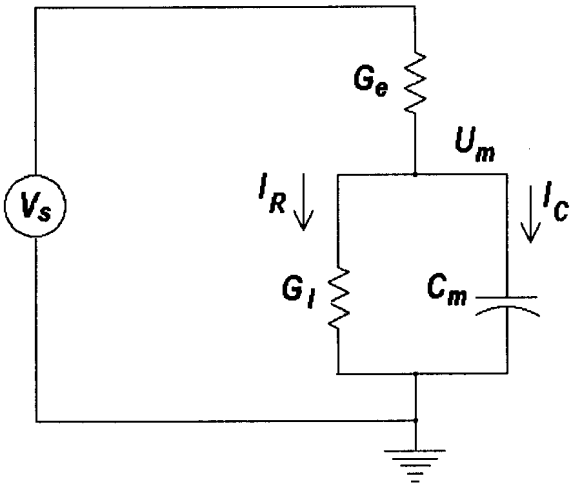

Fig 4.6 Electrical model of the skin [1]

From Fig. 4.1 or 4.2 G_i and C_m can estimated if we ignore G_e, since it is more than 100 times larger than G_i or C_m, therefore U_m=V_S. Referring to Fig. 4.2, at the intersection of the dashed line with $V = 0$, $I_R = 0$ and therefore I_C = 1.5uA. Since $dV/dt = 10 \cdot 2\pi \cdot 14$ and U_m = V = 0, at this point, we can estimate C_m from (4.1) to be 1.71 nF at t = 1 s. Using similar calculations we get C_m(t = 5) = 2.27 nF and C_m(t = 9) = 2.84 nF. In both cases the capacitance increase over 4 seconds is 0.57 nF. The process applied to Fig. 4.1 yields values for C_m of 1.25, 1.71 and 2.16 nF at t =1, 5 and 9 s. The capacitance increase is again linear and equates to 0.45 nF over 4 seconds.

G_i can be estimated by taking I_R = 1.5 uA at the intersection of the dashed line in Fig. 4.2 at V = 10, since I_C = 0 and dV/dt = 0. From (4.1) G_i = 150 nS with U_m = 10V. G_i increases to 200 nS and 250 nS at t = 5 and 9 s respectively. From (4.1) G_i = 220, 300 and 380 nS at t =1, 5 and 9 s.

Fig 4.3 shows the skin VCC at 40 Vpp, 28 Hz. At t = 1 s the graph is substantially linear. As time progresses, the non-linearity of the VCC becomes more apparent, with the current

rate of change suppressed at voltage minima and current peaks becoming more exaggerated. The VCC remains symmetric.

Fig 4.4 shows the skin VCC at 40 Vpp with the frequency reduced to 14 Hz. The non-linearity of the VCC is already apparent at t = 1 s. The VCC also starts to become asymmetric, with current peaks being higher and sharper during negative voltage cycles.

Fig 4.5 shows the skin VCC as 40 Vpp at 3 Hz. Both asymmetry and non-linearity is evident throughout the duration of the stimulus. The slowing rate of change of the current as the voltage approaches zero is more pronounced , as is the asymmetry.

The absolute value of the skin impedance, measured with a dry electrode, displays great variability. However at 10Vpp the variation is much lower than at 20 Vpp. The peak to peak current (Ipp) was measured after 1 s at 10 Vpp and at 20 Vpp. Three measurements were taken at 3, 14 and 28 Hz for a total of 9 measurements at each voltage level. The average Ipp at 10 Vpp was 3.7 ± 1.4 μA while at 20Vpp Ipp averaged 23 ± 15 μA. Doubling the voltage increased the current by a factor of about 7. It is therefore possible that higher voltages induce alternate current pathways that introduce a greater degree variation in the skin impedance and are responsible for the asymmetry and non-linearity of the skin VCC. The onset of non-linearity and asymmetry was consistently observed over the same voltage and frequency intervals. This study will therefore focus on qualitative rather than quantitative aspects of the skin VCC.

Electroporation could potentially provide an explanation for the non-linearity of the VCC observed in Fig 4.3 - 4.5. At 40 Vpp both asymmetry and non-linearity is observed the skin VCC, neither being present at 20 Vpp. In addition the average current level is significantly greater. The trigger for the dramatic differences in the VCC at 20 and 40 Vpp is clearly the increased voltage. It is hypothesized that the lower voltage was too low to create electropores and the resistance of existing electropores was too high to influence the overall impedance. At the higher voltage electropores are created. Due to the non-ohmic nature of electropore resistance, the conductivity per electropore is also much greater. This is clearly evident from the graphs. At 28 Hz (Fig. 4.3) the VCC is non-linear but virtually symmetric. On the Lissajous figure the current is exaggerated near the voltage peak, where the electropore conductance would be at it's maximum. The current rate of change slows as

the voltage approaches zero from either side, as the electropore conductance is decreases. Over time as electropores accumulate, this effect becomes more pronounced.

4.2 EXPERIMENT 2 - VCC measured with square wave stimulation

Other authors have attributed the skin impedance changes and the breakdown effect to electro-osmosis [6], [9], thermal effects [7] and sweat gland activation [7] (section 2.4). In these studies primarily low frequency sinusoidal stimulation was applied in the frequency range 0.01 - 200 Hz. Only Grimnes [9] briefly mentions square wave stimulation. Electroporation is known to be a voltage phenomenon, therefore it is usually studied using constant voltage pulse protocols [13],[14],[26]. A qualitative assessment of the skin resistance was therefore undertaken using square wave stimulation, at very low frequency (0.1 Hz) and low frequency (15Hz). The current curves thus obtained could then be assessed for evidence of electro-osmosis, thermal effects or electroporation.

The data was acquired from the inside forearm using the equipment described in section 3. Measurements were carried out at 25 °C.

Fig. 4.7 shows the current through the skin during unipolar stimulation. A negative polarity 18 V DC was applied to the skin until it broke down (at about 1300 ms).

Fig. 4.8 shows the current through the skin during bipolar stimulation. A 15 Hz bipolar square pulse train with amplitude ±18 V was applied until the skin broke down.

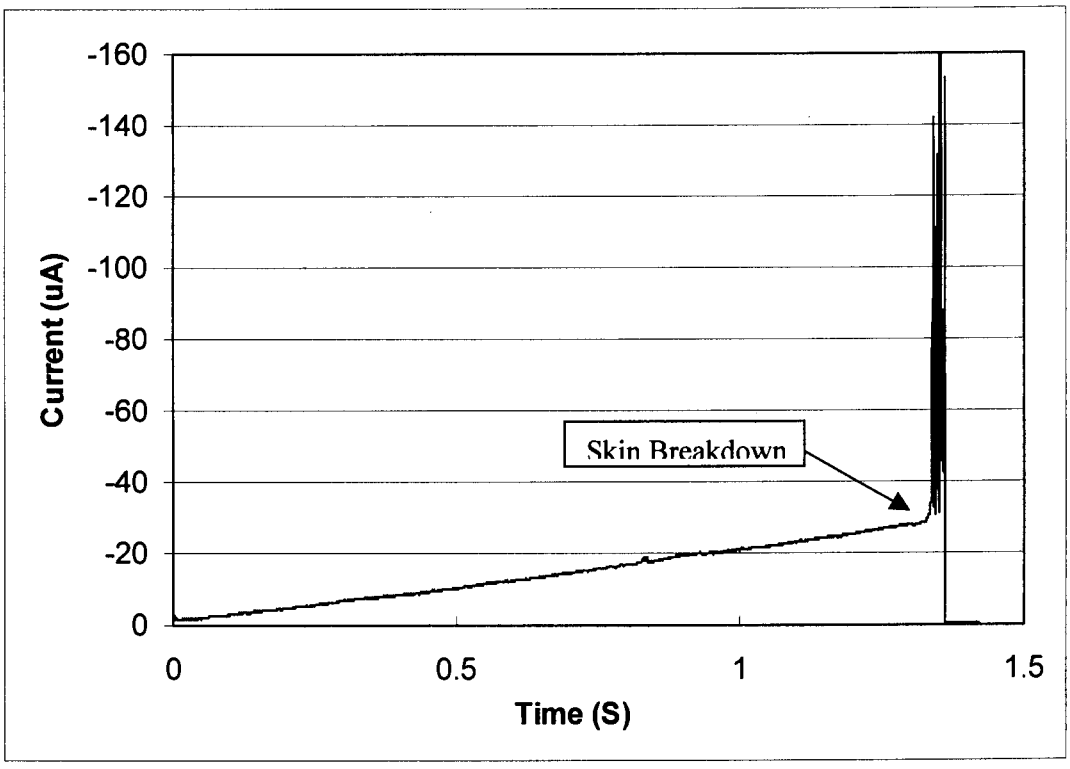

Fig. 4.7 Skin current due to a constant -18 V pulse.

The rate of change of current (which is proportional to skin conductance since a constant voltage is applied) before breakdown in both Fig. 4.7 and Fig. 4.8 is almost exactly linear. The data in Fig. 4.7 before breakdown yields a linear correlation coefficient of 0.9990. According to the electro-osmosis theory, for semi-filled capillaries, the change in conductance of a semi-filled capillary is proportional to the amount of water transported into it and the flow rate is directly proportional to the current through the capillary [9]. Therefore, the rate of change of conductance should be proportional to the flow rate and thus proportional to the square of the current. This implies that the rate of change of current should be greater at higher current levels. Both Fig. 4.7 and 4.8 show that the rate of change of current stays constant despite the current increasing by more than an order of magnitude.

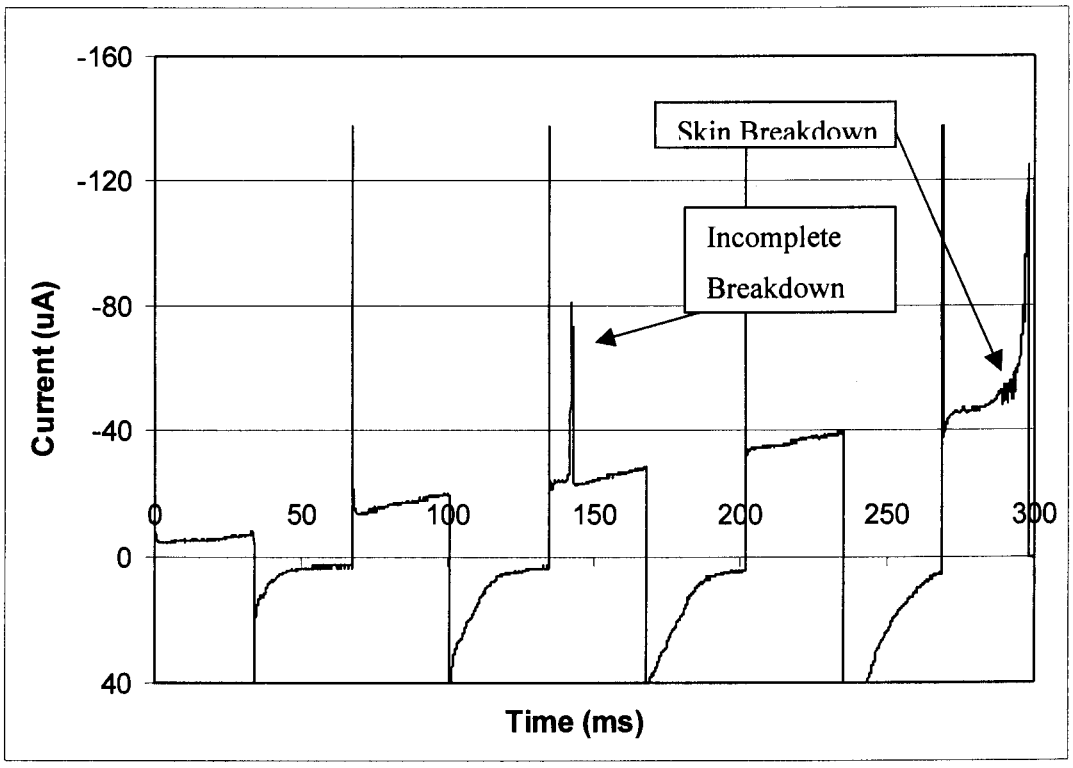

Fig. 4.8 Amperogram of skin stimulated with a 15 Hz, ±18 V pulse train, showing breakdown of the skin. The current spike labeled 'Incomplete Breakdown' will be discussed in section 5.10.

In Fig. 4.8 the current increases occur during negative cycles (axis inverted) and decreases during positive cycles. However the conductance at the beginning of any negative cycle is greater than the conductance at the end of the previous negative cycle. Furthermore, this increase in conductance is almost identical to the linear conductance increase observed during the negative cycle. Electro-osmosis therefore cannot be responsible for the conductance increase during negative cycles. If it were, the current at the beginning of a negative cycle should have been less than or equal to the current at the end of the previous negative cycle.

The linearity of initial conductance changes also casts doubt on a model of the skin that implies thermal effects are primarily responsible for skin impedance changes, since the power dissipated in the skin changes over time along with the skin current. In addition the relationship between the skin temperature and the skin conductance is known to be non-linear [7].

From the onset of stimulation until the moment of breakdown both the current and the power dissipated are changing, only the applied voltage (independent of polarity) stays constant. It is therefore reasonable to argue that the conductance rate of change is dependent on the applied voltage. Electroporation fits this description since the electroporation rate (and the subsequent conductance rate of change) is dependent on the applied voltage, rather than current. In addition electroporation is independent of the polarity of the stimulus.

These observations therefore suggest that certain aspects of the skin VCC are more likely to be due to electroporation than to thermal effects or electro-osmosis and provide a motivation for a more detailed investigation of this phenomenon.

4.3 EXPERIMENT 3 - Influence of electroporation on skin resistance

The high degree of linearity observed in the skin's conductance increase during constant voltage stimulation (Fig. 4.7) suggested that electroporation could be responsible for this conductance change. This kind of conductance change could be seen for stimulus voltages as low as 13 V. Most authors set a threshold for electroporation of the stratum corneum at between 30 and 50 V [13],[14]. However these studies were done using very short voltage pulses (<10 ms), while the skin impedance effects occur over much greater time scales. Therefore an experiment was designed to test whether evidence for electroporation could be seen during dry electrode stimulation in the range 10-20 V.

Lipid molecules in a bilayer membrane are in continuous thermal motion. When a gap between the molecules exceeds a critical radius a metastable pore is formed, its lifetime ranging from seconds to hours depending on the type of membrane [16]. The application of an electric field across the membrane increases the probability of such a pore being created. The conductance of these pores exhibit a non-linear dependence on the applied voltage due to electrostatic interaction of ions with the wall of the pore. Ions crossing the membrane through the narrow pore must overcome some energy barrier. The voltage applied reduces this barrier. When the applied voltage is sufficient to eliminate the barrier completely, pore conductivity becomes ohmic [26]. In experiment 3a the non-linear nature

of the skin conductance was investigated as a function of voltage and compared with the theoretical description of electropore conductance.

The intact skin of the human stomach was stimulated with an 18.5 V, 33 ms pulse (U1), directly followed by a 33 ms pulse (U2) with amplitude at either 20%, 40%, 60% or 80% of U1. The second measurement was taken 0.6 ms after the start of the second pulse, to avoid interference from transient effects (see Fig 4.9). The instantaneous conductance at the end of the first pulse (G1) and the instantaneous conductance at the start of the second pulse (G2) were measured to determine the ratio (G2/G1). Results were averaged over 10 measurements for each setting of U2.

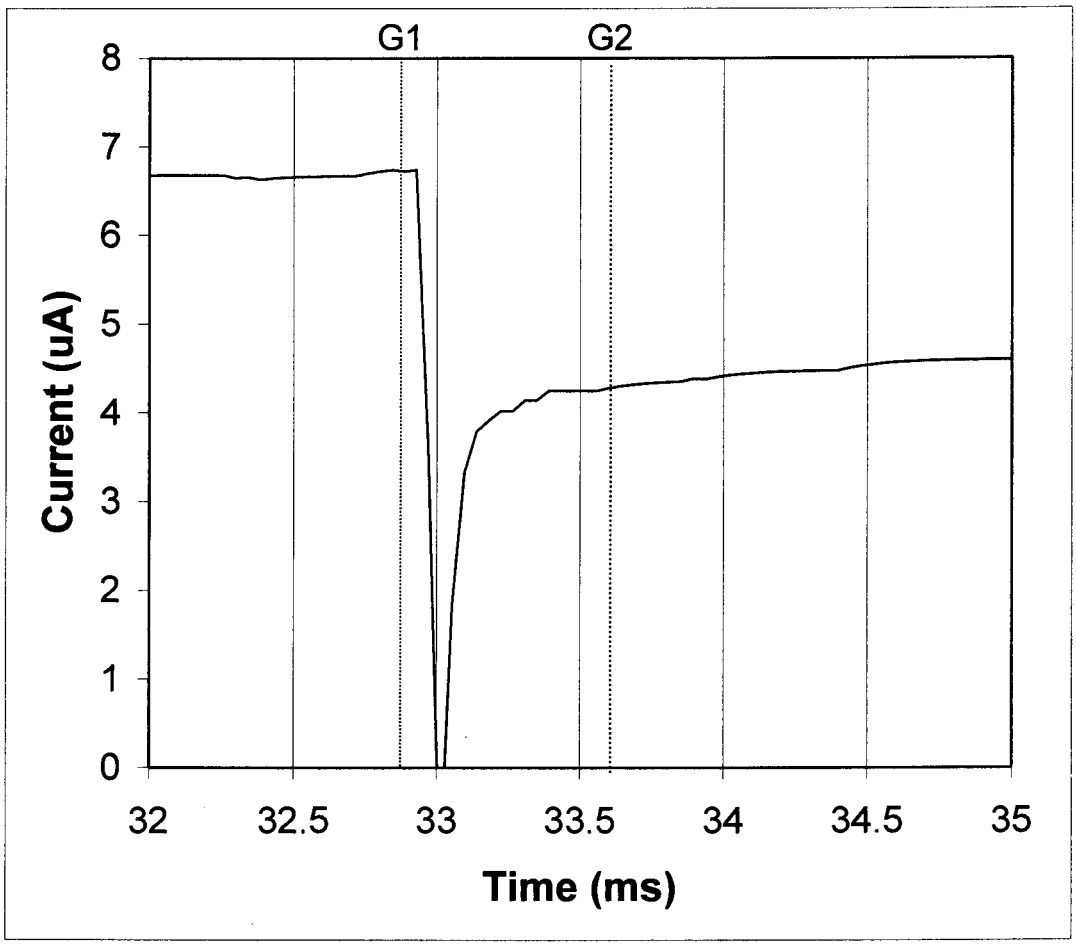

Fig. 4.9 Amperogram from experiment 1 showing the end of pulse 1 (33 ms, -18.5 V) and the start of pulse two (33ms, -7.4 V). The dotted lines indicate when G1 and G2 were measured. Positive current is taken to flow out of the skin.

Fig. 4.10 shows the skin resistance (1/G2), after the application of the 18.5 V pulse, as a function of voltage. This is compared with the voltage dependence of the resistance of an artificially created lipid bilayer observed by Glaser [16] using a similar experimental technique (i.e a test pulse followed by a measurement pulse). The shapes of the curves are very similar and in both cases are seen to be a non-linear function of voltage. The membrane resistance recovers to some degree on a timescale of milliseconds or less, after the application of the first pulse.

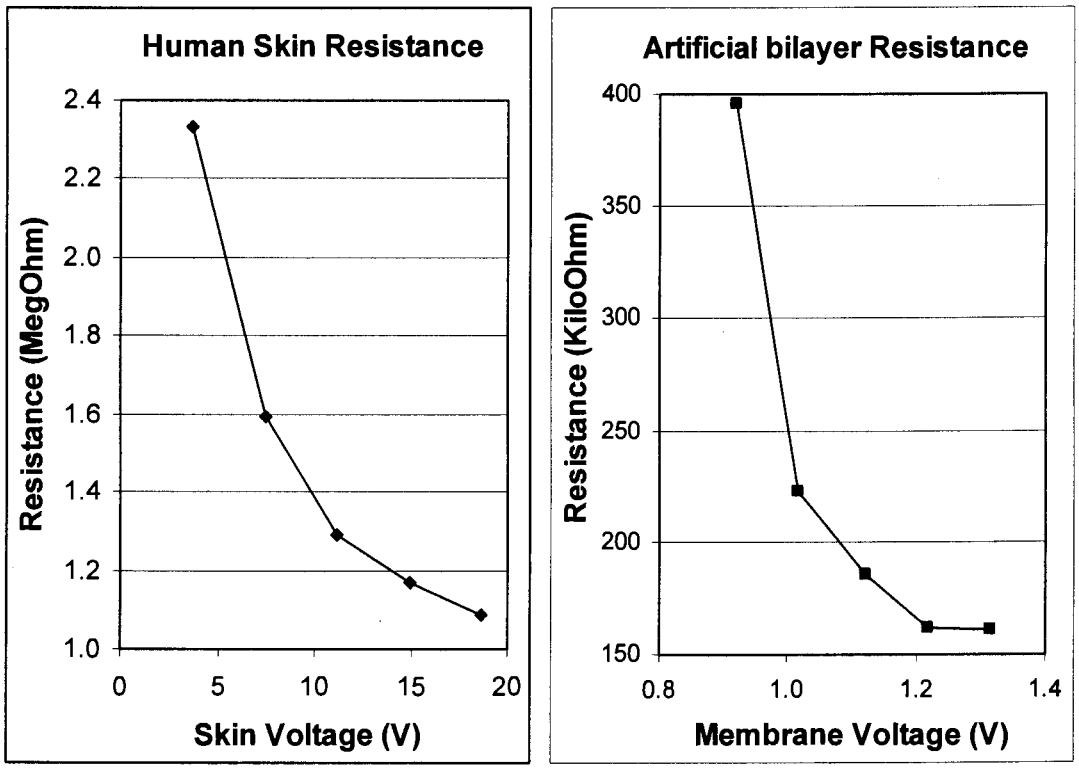

Fig. 4.10 Plot of human skin resistance versus voltage after the application of a 33ms, -18.5V pulse Comparison is made with plot obtained for artificial lipid bilayers by Glaser [16], using a similar experimental technique. The shapes of the graphs are qualitatively very similar.

The measured data (Fig. 3) was fitted to theoretical ratios determined from the relationship between electropore conductance (G) and voltage [16] using the MATLAB function NLINFIT:

$$\ln G = \ln\frac{\pi R^2 \mathrm{HN}}{h} - \ln\left[\left(1+\frac{n\beta U}{w_0 - n\beta U}\right)\cdot\exp(w_0 - n\beta U) - \frac{n\beta U}{w_0 - n\beta U}\right] \text{ with } U = \frac{U_{skin}}{m} \quad (4.3)$$

where U is the potential difference across a single lipid bilayer and U_{skin} the total voltage applied over the m layers of the stratum corneum. In (4.3) the known constants are [16]: h (=5 nm) the membrane thickness, R (=h/2) the external radius of the pore entrance, H (=1.3 S/m) the specific conductivity of the bulk solution, $\beta = e/(kT)$ (6.5×10^{-40}) with e the electron charge, n the relative size of the entrance region of the pore (=0.15), k Boltzman's constant and T the temperature (=293K). The fitted parameters are w_0 , the energy of an ion in the center of the pore expressed in units of kT, N the number of pores and m, the number of lipid bilayers in series. The parameters w_0 and N are dependent on the amplitude and duration of the first pulse and do not change significantly during the 0.6 ms delay after the end of the first pulse before the second measurement is taken [16]. By taking the ratio G2/G1, the parameter N is eliminated from the equation and therefore the fit can be done with only w_0 and m. The variability of the ratio G2/G1 is much less than the variability of G2 or G1 individually. The parameter N was estimated by taking the average of the 40 measurements of G1 and solving for N in (4.3) by substituting the fitted values of w_0 and m. The best fit was provided by w_0 = 1.8 kT, and m = 15. The value of N was estimated to be 3.2×10^3.

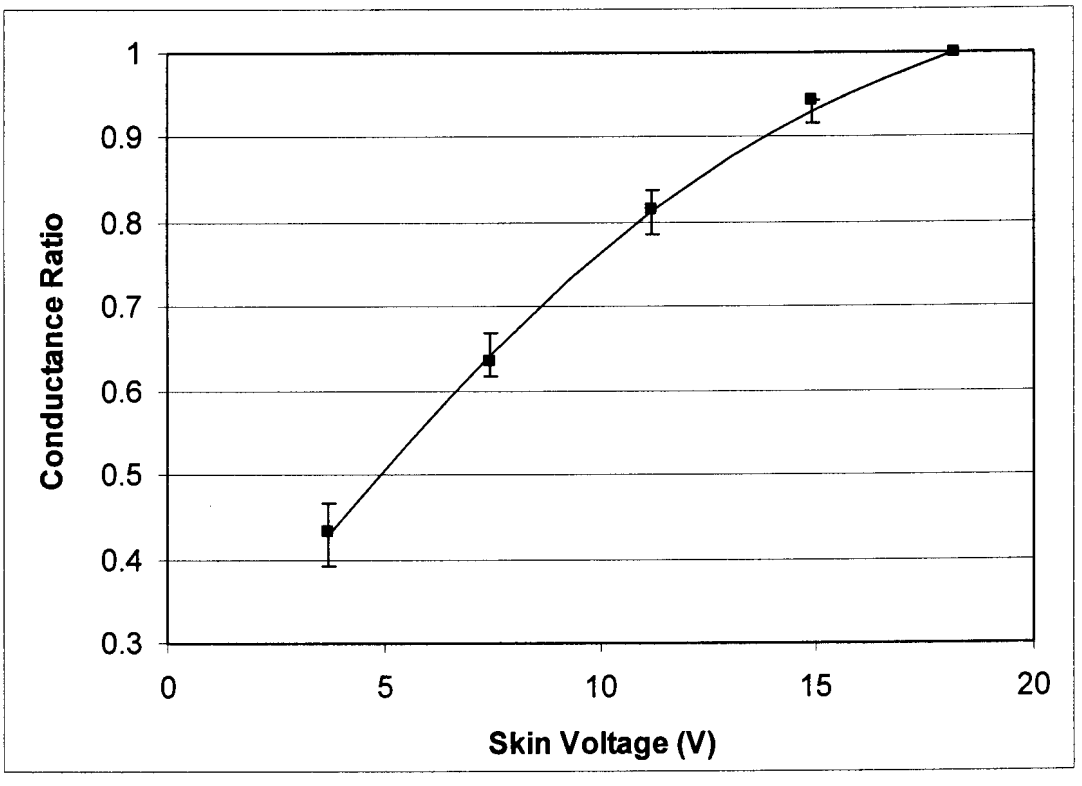

Fig 4.11 The ratio of the skin conductance at the start of pulse 2 to the skin conductance at the end of pulse 1 (Experiment 1) as a function of the amplitude of pulse 2, averaged over 10 measurements. Error bars indicate the standard deviation of the estimate.

The observed non-linearity can be explained from electroporation theory. The reduced voltage applied during the second pulse causes an instantaneous reduction in pore conductivity, without affecting the number of pores.

In experiment 3b the hypothetical electroporation rate in the skin was investigated. The rate of increase of the current through the skin was measured on the skin as a function of the applied voltage. In vivo, the current increases linearly as observed in Fig. 4.7 only beneath a negatively polarized electrode. Therefore a unipolar constant voltage pulses was applied to the skin. The stimulus was applied until the skin broke down, in order to also allow characterization of the breakdown phenomenon through measurement of parameters such as time to breakdown and energy dissipated before breakdown as a function of voltage, for use in experiment 8.

Using a felt tip marker, a grid containing 66 blocks, each 1.5 × 1.5 cm, was drawn on the skin of each forearm for a total of 132 blocks. Each block was stimulated with a constant voltage pulse with amplitude 12.5, 15, 18 or 21 V until the skin broke down. Below -12.5V breakdown cannot be consistently induced. Above -21V breakdown starts happening so quickly that measurements become inaccurate. Therefore four groups of 33 samples were obtained. Randomization was used to eliminate the possible influence of variations in skin parameters (thickness, number of sweat glands etc) over the area. The computer randomly changed the sequence in which the different voltage levels were applied for each group of four measurements. Blocks were tested sequentially along rows in the grid. The ambient temperature was controlled at 25°C. Measurements were done with the equipment described in section 3.

The measured data (Fig. 4.12) was fitted to the following theoretical relationship between the rate of change of current and the voltage across a lipid membrane [16] using the MATLAB linear regression function POLYFIT:

$$\ln\frac{\Delta I}{\Delta t} = A + \frac{BU^2}{m^2} \tag{4.4}$$

where

$$A = \ln\frac{U_m g(U_m)\nu S}{a_0} - \frac{\Delta W p(U=0)}{kT} \tag{4.5}$$

and

$$B = \frac{\pi R^2 (\varepsilon_w - \varepsilon_m)\varepsilon_0}{2hkT} \qquad (4.6)$$

over the range $0.5 < U < 1.45$. Here $U_m = U/m$, U is the potential over the lipid bilayers, m the number of lipid bilayers, $g(U_m)$ the electropore conductivity, v the frequency of lateral fluctuations of the lipid molecules, S the area of the membrane, a_0 the area per lipid molecule, $\Delta Wp(U=0)$ is the height of the energy barrier to be overcome for hydrophilic pore formation, ε_w is the relative permittivity of water, ε_m the relative permittivity of the membrane and ε_0 the dielectric constant of vacuum. The value of m was taken as 15, from experiment 3a. A linear least squares line fitted to the filled square data points in Fig. 4.12 yielded $A = -16.75$ and $B = 3.3$ V^{-2}.

Referring to experiment 3a, the value obtained for w_0 is close to the value 1.8 kT measured by Glaser [16] for pulses with similar amplitude and pulse width. The preexisting pore population under a 1 cm^2 electrode is estimated to be 10^6 [3]. The value of N therefore suggests that current conducts through about 0.35% of the electrode surface. It has been confirmed by several authors [7] that current is conducted through the skin at highly localized sites of relatively low resistance. The value of m is less than the general estimate of 70-100 bilayers in the stratum corneum. It follows that high conductivity regions would be associated with areas where the majority of lipid bilayers are bypassed by defects in the stratum corneum.

With respect to the parameters determined in experiment 3b, A = -16.75 provides a membrane area of about 1 mm^2, using an order of magnitude estimation by Glaser [16]. This compares well with the area calculated separately from N (0.32 mm^2). The value of B compares favourably with the value of 4.7 V^{-2} also derived by Glaser [16] from measurements on artificial bilayers. Chizmadzhev [3] estimated B/m^2 for skin to be 0.02, which equates to m between 13 and 15 if B lies between 3.3 and 4.7. The correspondence is good, considering that skin thickness varies between individuals and body locations.

In Fig. 4.12 the value predicted by the least squares line at V^2 = 2 (membrane voltage = 1.4 V) is a factor 1.5 greater than the unfilled square data point. This deviation is also observed experimentally for artificial bilayers at voltages greater than 1.45 V [16].

It may seem as if there are too many variables to allow their values to be determined with any certainty when fitted to the experimental data. However in equation (4.3) the value of

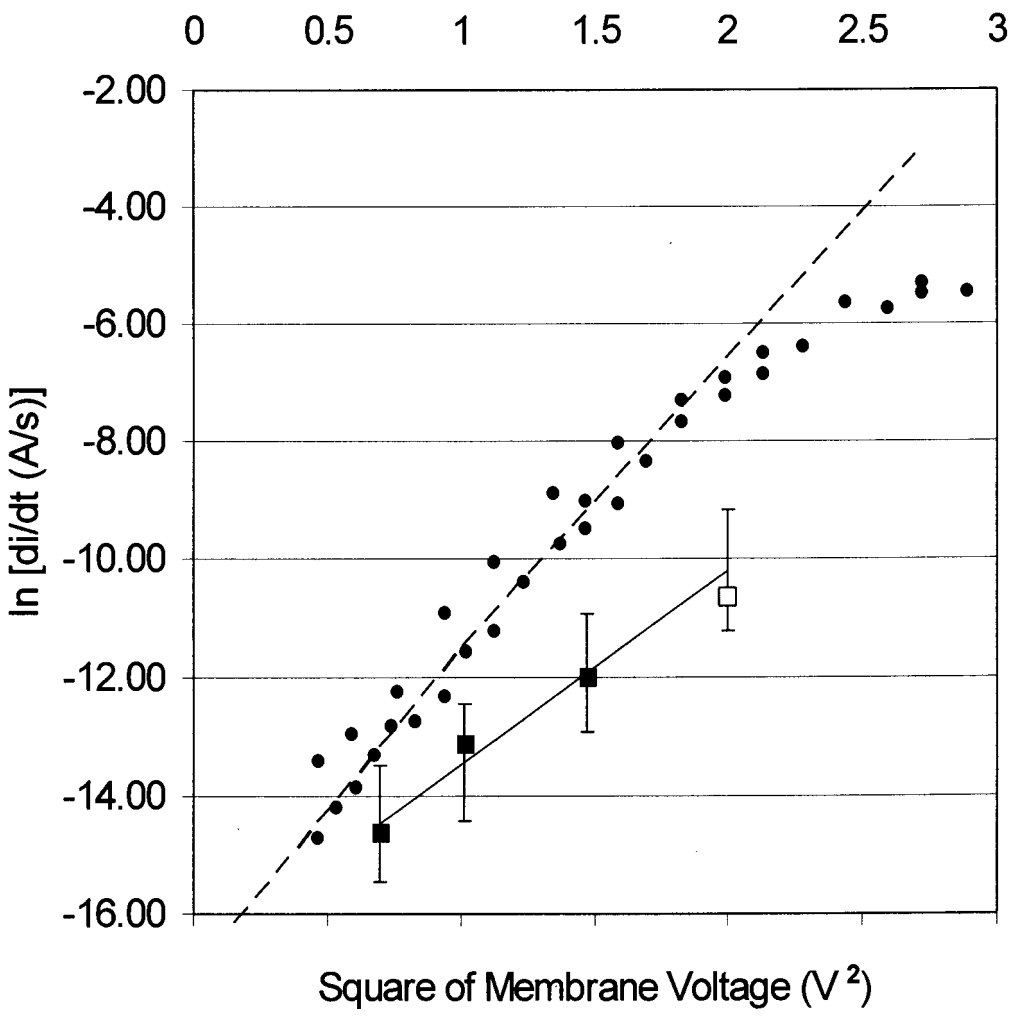

Fig. 4.12 Logarithms of the rate of current increase across a stratum corneum lipid bilayer vs. the square of the applied voltage, where the stratum corneum is assumed to consist of 15 bilayers in series for the calculation of the voltage per membrane from the total applied voltage. Squares indicate the averages of 33 measurements. Error bars indicate the standard deviation of the estimate. Dots are measured data reproduced from Glaser [16] which applies to an artificial lipid bilayer membrane. Note that saturation occurs in both cases at a membrane voltage of about 1.4 V.

w_0 is very close to the value expected from literature, only m is therefore truly variable. In (4.4), A only influences the y-intercept of the line, while B alone determines the slope, with m again the only real variable. In addition, the linear range of the data in Fig. 4.12 coincides closely with the expected range.

The use of a dry electrode for measurements allows the VCC of the stratum corneum to be observed in the low voltage range (<20V) without interference from alternative current pathways such as skin appendages (primarily sweat ducts). A wet electrode makes very good contact with the skin, making it difficult to distinguish between current conducted through the stratum corneum and current conducted through alternative pathways. Since the sweat ducts account for only 0.1% of the skin surface area, it is unlikely that they will be in direct contact with a dry electrode.

The changing shape of the VCC in Fig. 4.3 can be explained from electroporation theory. The VCC as exhibited by the Lissajous figures is flat near V=0 which can be explained by a higher electropore resistance in the low voltage region. The current peaks increase with time as electropores accumulate in the lipid membranes. The rate at which electropores are created depends on the applied voltage. With an applied sinusoidal voltage stimulus of fixed amplitude, the current peaks therefore increase at a constant rate.

The correspondence of the value determined for m from fundamentally different aspects of electroporation, namely the electropore conductance and the electroporation rate as functions of voltage is highly significant. Skin appendages have been identified by other authors as sites of high current density. Instead an alternative current path is hypothesized comprising defects in the lipid-corneocyte matrix, where the usual number of lipid bilayers (70-100) are reduced to about 15, thus providing low resistance sites. Electroporation at these sites accounts for the non-linearities of the VCC of the human skin, observed when the applied voltage exceeds about 10V.

4.4 EXPERIMENT 4 - Electro-osmosis

Electro-osmosis is defined by Edwards [17] as the flow of fluid accompanying an applied electric field, typically arising as a consequence of ionic motion within electrical double layers gathered near fixed charge surfaces within the medium.

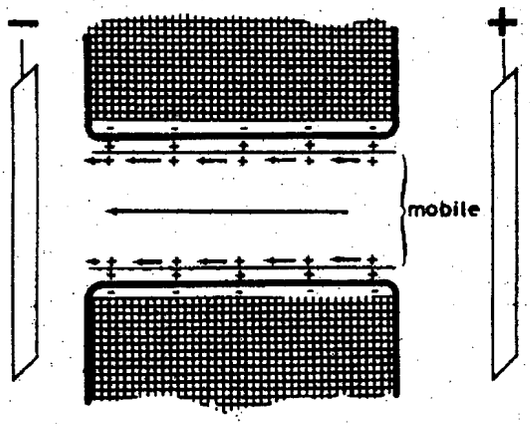

Fig 4.14 Figure reproduced from Grimnes [9] showing suitable conditions for electro-osmosis to occur

Fig. 4.14 is reproduced from Grimnes [9] and shows how water, bounded by a charged surface, is transported by an applied electric field. Previous studies have only investigated the possibility that electro-osmosis occurs within the capillaries formed by the sweat ducts. [7],[9],[6]. However suitable conditions for electro-osmosis to occur conceivably exists in four possible areas in the stratum corneum [17]. These are:

- inside the sweat ducts
- within the lipid phase separation sites
- within the corneocytes since they are bounded by lipid bilayers
- inside the bound water regions separating the lipid bilayers (interbilayer spaces) (Fig.2.2).

The asymmetry of the skin VCC, which is observed in Fig. 4.4 , 4.5, and 4.14, has been linked by several authors [6],[7],[9] to electro-osmosis, since the skin resistance is apparently increased during positive cycles.

The evidence presented in experiments 2 and 3 and later in experiments 6 and 7 indicates that under the experimental conditions used, current through the skin flows through defects in the stratum corneum lipid matrix rather than through the sweat glands. The current flowing through the ohmic lipid phase separation sites is too small to account for the reduction in current observed during positive cycles in Fig.4.14. Therefore it is proposed that if electro-osmosis does affect the skin VCC, it must occur in the latter two areas mentioned.

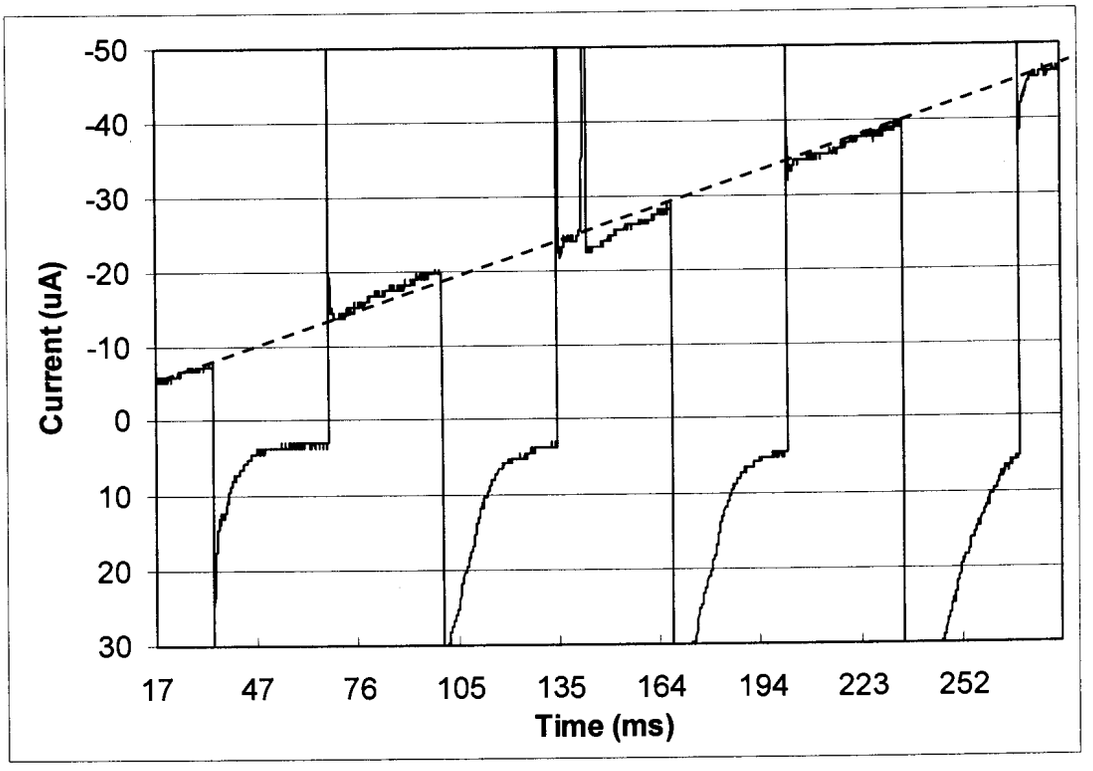

Fig 4.14 Detail of fig 4.8. Dashed line shows electroporation continuing during rectification phases

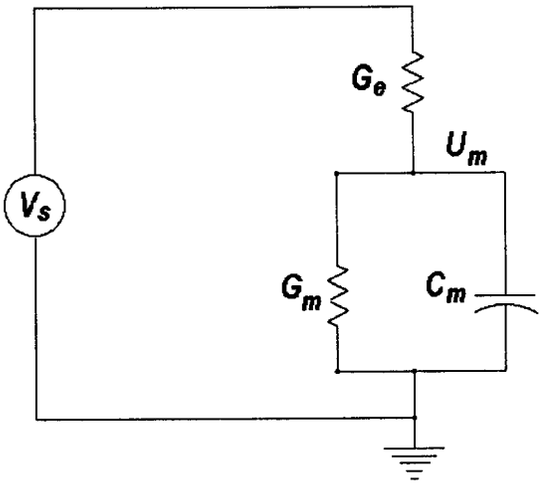

Fig 4.15 Electrical model of the skin [1]

The skin is frequently modeled as shown in Fig 4.15 [1]. G_m, represents the lipid membrane resistance and G_e, represents all other resistive elements in the skin, including the corneocyte resistance [10]. The resistance increase during positive cycles must occur in one of these two resistances. In Fig. 4.19 it is observed that the capacitive spikes are unaffected by the increase in resistance, implying that Re stayed constant. Therefore the resistance increase could only have occurred in Rm.

In addition Fig. 4.14 shows that electroporation continues to occur at the same rate during positive cycles (dashed line). This is only possible if the resistance increase occurs within the lipid bilayers themselves (i.e. in G_m), otherwise the voltage over the bilayers would have been reduced due to a voltage divider effect and the rate of electroporation would have slowed. These observations suggest that electro-osmosis probably occurs in the bound

water regions separating the lipid bilayers. It is well proven that the fluidity of the lipid membranes in the stratum corneum depends on their hydration level and that the resistance of these membranes is increased when the hydration level is reduced [33]. The interbilayer spaces are 0.7 nm wide. Therefore the amount of water contained in these spaces is orders of magnitude less than in the corneocytes. A much smaller amount of water would have to be transported within these spaces to significantly affect the skin resistance than through the corneocytes. It is therefore likely that electro-osmosis in these areas would have a much greater impact on skin conductance than through other pathways.

The equation used to describe electro-osmosis by previous authors [6],[9], is applicable to unrestricted electroosmotic flow through a filled capillary in a situation where a water reservoir exists on either side of the capillary and the water pressure is the same on either side [35]. This situation does not exist within the interbilayer spaces. The lipid bilayers create an enclosed volume, therefore the net movement of water out of these spaces must create a water pressure gradient. An attempt was therefore made to design an experiment that recreates such a situation, where electro-osmosis takes place within a restricted area.

Fig. 4.16 shows the experimental setup. Ag/AgCl electrodes (1 cm^2) were placed on opposite sides in a chamber filled with saline (0.9% NaCl). The saline was kept at 35°C by heating pads placed below the chamber. A thermistor in contact with the saline measured the temperature. One electrode was covered with Eurocel adhesive plastic tape, through which a hole had been punctured with a thin heated wire. Holes with radii between 50 μm and 200 μm were created in this fashion. The punctured tape was placed on an Acer Vuegoscan scanner and an image of the surface was taken at 19200 dpi. The size of the hole could then be estimated from the image. Fig. 4.17 shows an example of a hole, imaged in this fashion, with a radius of about 80 μm. Layers of tape were stuck onto each other until a measurable thickness was obtained. The average thickness

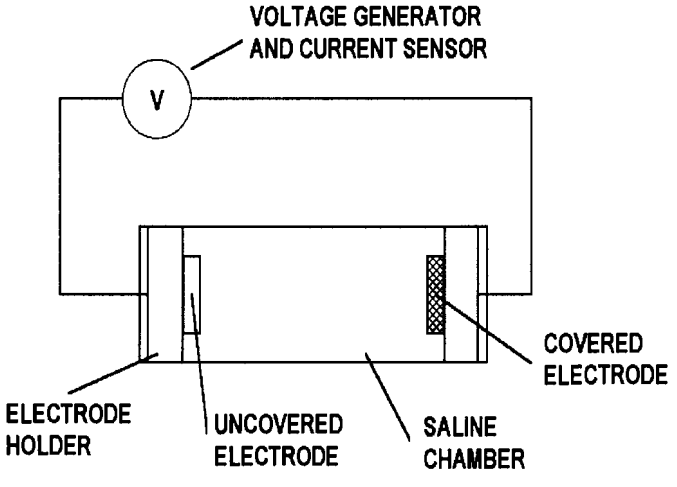

Fig 4.16 Equipment used for experiment 4.

of the tape was determined to be 40 μm. A limiting resistor was placed in series with the saline chamber. Control experiments were done with both electrodes uncovered yielded the expected output for a pure resistor.

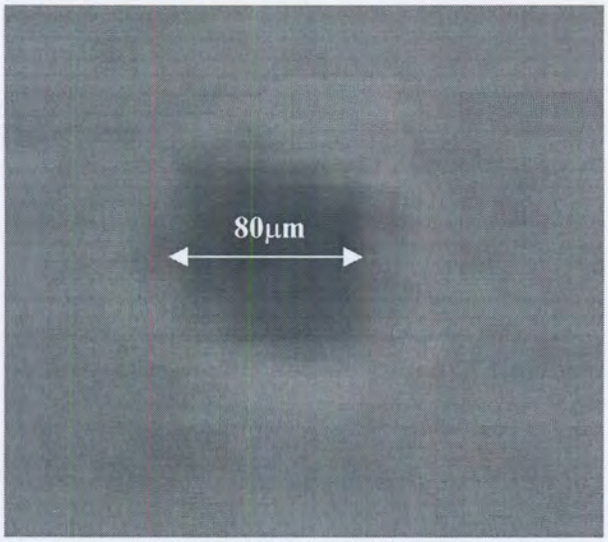

Fig. 4.17 Scan at 19200 dpi showing hole with radius 80 μm in tape.

Fig. 4.18 shows positive current rectification observed when the Ag/AgCl electrode is covered with tape, through which a 50 μm radius hole was punctured, and a 1.5 Hz bipolar square voltage wave was applied. Fig. 4.19 shows a similar phenomenon observed on the skin. The shapes of the graphs are qualitatively very similar, except for the capacitive spike at the beginning of each pulse in Fig. 4.19.

The similarity between the two graphs suggests that similar mechanisms could be responsible. It could be argued that the increasing resistance during positive in Fig. 4.18 is due to a concentration overpotential. The conductance at the start of positive cycles is initially high and then decreases. During negative cycles the conductance is initially low then increases (this is also evident in Fig. 4.19, ignoring the capacitive spikes). It therefore appears that the conductance does not change immediately after the voltage polarity is reversed. This observation suggests that the changing conductance is probably not due to a concentration overpotential. In such a case the conductance would have recovered immediately after the voltage polarity was inverted.

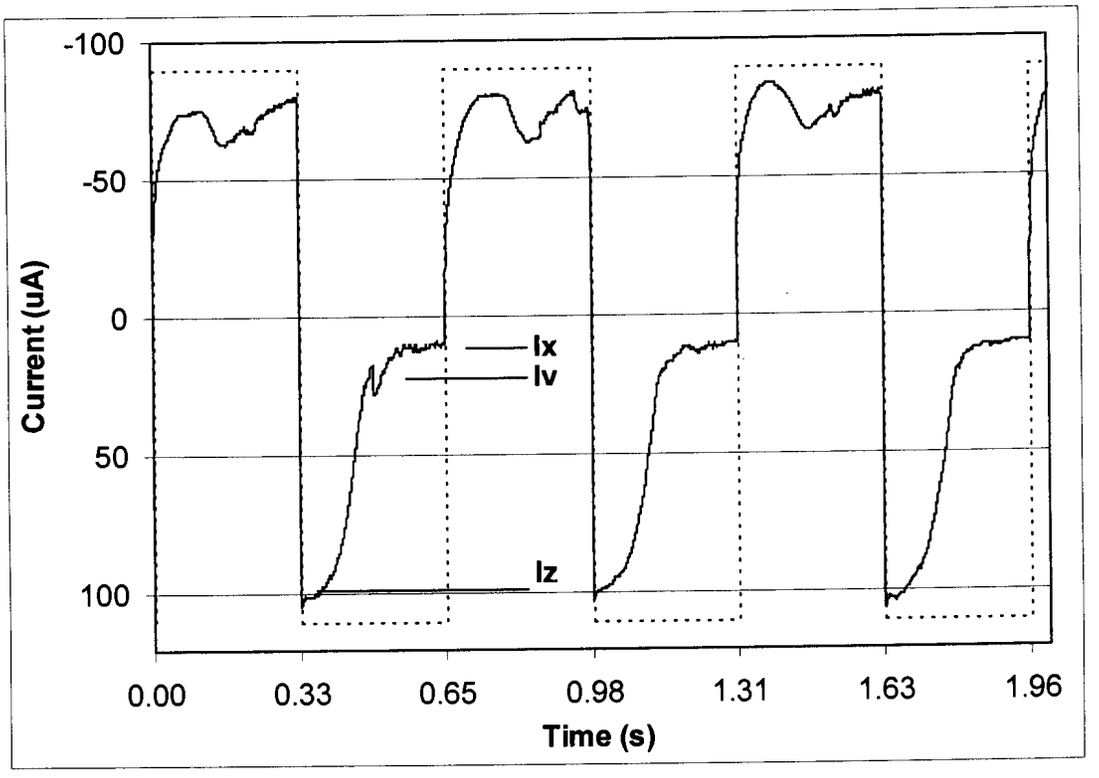

Fig. 4.18 Amperogram showing rectification observed with Ag/AgCl electrodes in saline solution. One electrode was covered with tape through which a hole had been punctured. Dotted line indicates phase of applied voltage.

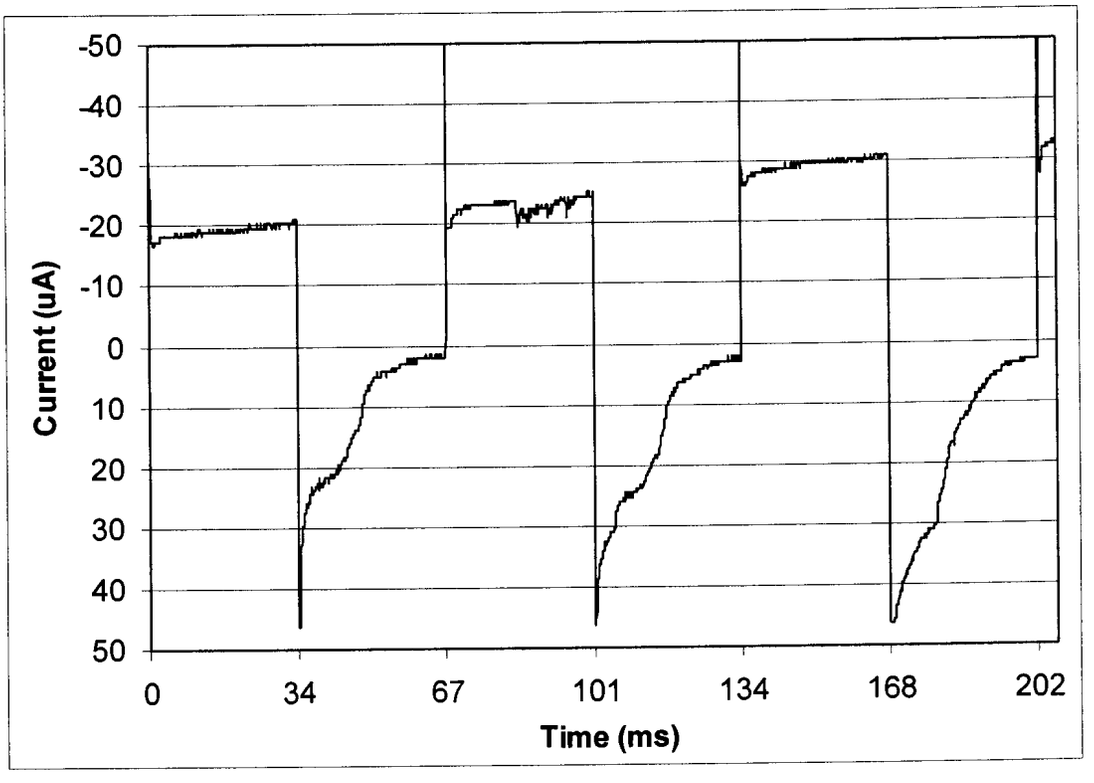

Fig. 4.19 Amperogram of bipolar voltage pulse applied to skin showing rectification.

The observed current curve is consistent with electro-osmosis. Since thickness of the tape is comparable to the radius of the hole through it, the geometry is suitable for electro-osmosis. The time constant of the system could be much greater during positive cycles because the electroosmotic force is transporting the liquid against the pressure applied by the water outside the capillary, whereas during negative cycles both forces are acting in the same direction.

The conductance increase in Fig. 4.18 and 4.19 after application of a positive potential is slow initially and then accelerates. According to Grimnes [9] the acceleration of bulk liquid, as an inert mass, due to electro-osmosis is not rate determining. It would therefore appear that a certain amount of water must first be transported before the resistance is significantly affected. This may explain why asymmetry is not observed at lower voltages or higher frequencies in the skin. The amount of water that can be transported against the pressure gradient by the lower potential or over a shorter period, could be insufficient to significantly decrease the skin resistance.

The time scale in Fig. 4.18 is about 10 times shorter than in Fig. 4.19. The relationship between the area of the hole and current decay time was investigated, by observing the graphs acquired with different hole sizes at the same current density. In Fig. 4.18, Iz is the peak current. Ix is minimum current and Iy = Ix + 0.1*(Iz-Ix). TD is the decay time measured from the onset of the positive pulse until the current level equals Iy. Fig. 4.20 shows TD versus the electrode area on a logarithmic scale for a current density of 4600 A/m^2. A clear tendency is seen, with TD decreasing as the hole size is reduced. The volume of water involved in electro-osmosis was lower when smaller hole sizes were used. In the interbilayer spaces, the volume of water involved would be orders of magnitude lower still. This could account for the difference in the time constants observed in Fig. 4.18 and Fig. 4.19.

The smallest hole size that could be created had a 50 μm radius. The measurement circuit also had a limited output voltage/current range. These factors limited the range of electrode areas and current densities that could be tested.

Asymmetry of the VCC was observed during sinusoidal stimulation (Fig. 4.4 and 4.5).The rectification observed during square wave stimulation in (Fig. 4.18 and 4.19) appears to be due to the same underlying cause for two reasons:

1. In both cases the phenomenon is due to increased resistance during positive voltage cycles. In Fig. 4.5 it can be seen that during positive cycles the current is lower at the voltage peak (when IC = 0) than during negative cycles. In Fig. 4.18 and 4.19 square voltage pulses were used and rectification was observed long after the capacitive spikes have died out.
2. The time delay before onset of rectification for square wave stimulation is consistent with the frequency range over which asymmetry is observed with sinusoidal stimulation. In experiment 1, the VCC asymmetry was very slight at 28 Hz (Fig 4.3) but appears at 14 Hz (Fig. 4.4) and becomes more prominent at 3 Hz (Fig. 4.5) as the frequency decreases. In Fig. 4.19 a delay period of 16 ms occurs before the current starts to fall during positive cycles. The period of a positive cycle at 28 Hz is 17 ms, insufficient time for rectification to manifest. At 14 Hz and 3 Hz the positive cycle period increases to 35 ms and 167 ms respectively, allowing rectification to play a more significant role.

These data suggest that electro-osmosis is responsible for the asymmetrical current waveform.

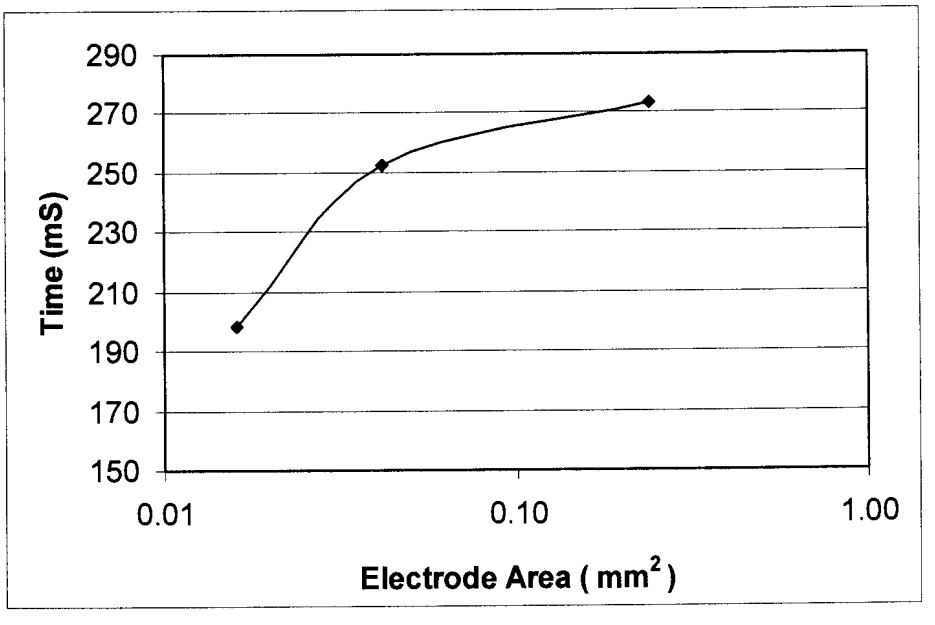

Fig. 4.20 Delay before rectification after onset of positive voltage pulse versus electrode area.

5 REVERSIBLE RESISTANCE BREAKDOWN

In literature the partially reversible resistance breakdown has been attributed to sweat gland activation [7] and to electro-osmosis through the sweat ducts [9] (see Section 2.4). Other mechanisms are also conceivable. An increase in skin temperature could increase the rate of electroporation. No studies have been reported relating the electroporation rate to temperature. However in (4.5), an increase in the parameter ν (the frequency of lateral thermal fluctuations of lipid molecules), would increase the electroporation rate. A differential confocal microscopy study [34] has shown that the amplitude of these fluctuations in artificially created lipid bilayers stays constant upto 40°C (the first lipid thermal transition, where a change in the geometric packing of the lipids occurs, see section 2.2.1.2) and then rises sharply. Thus it is speculated that an increase in skin temperature above 40°C could trigger a change in the thermal fluctuations of the lipid molecules, which could influence the electroporation rate. Alternatively a rapid and sufficient skin resistance decrease is known to occur at 65°C due to the second lipid thermal transition [10],[11],[25], where lipids in the gel phase melt into a liquid phase. Pliquett et.al. [25] have demonstrated that during high voltage pulsing (60-300 V), the skin temperature can exceed 65°C, resulting the creation of highly conductive pathways through the skin.

The current curves obtained in experiment 2 were analyzed for evidence of these four possible mechanisms. Fig. 5.1 shows voltage pulses that were applied after breakdown had been induced as shown in Fig 4.8. The current decays exponentially (i.e. the skin resistance increases) when stimulation is stopped after the breakdown effect, but appears to stabilize at a value that is lower than the initial resistance. This could conceivably be due to sweat gland activation. After stimulation is stopped, the local skin temperature falls, increasing the resistance. However, sweat trapped under the electrode maintains a high conductivity pathway through the skin and the skin resistance does not return to initial value.

Fig. 5.2 is a detailed view of the breakdown effect in Fig. 4.7. The current oscillates wildly while rapidly increasing. This behavior is not consistent with an electro-osmosis model. Any increase in current could only increase the rate of fluid flow towards the electrode, increasing the conductivity and leading to further current increases. A similar argument seems valid against the breakdown phenomenon being thermal in nature, since the power dissipated in the skin increases, rapidly increasing the skin temperature. If the breakdown

is due to sweat gland activation it could be argued that fluid filling the sweat duct rapidly cools the skin down, increasing the surrounding resistance and temporarily diminishing the current through the skin.

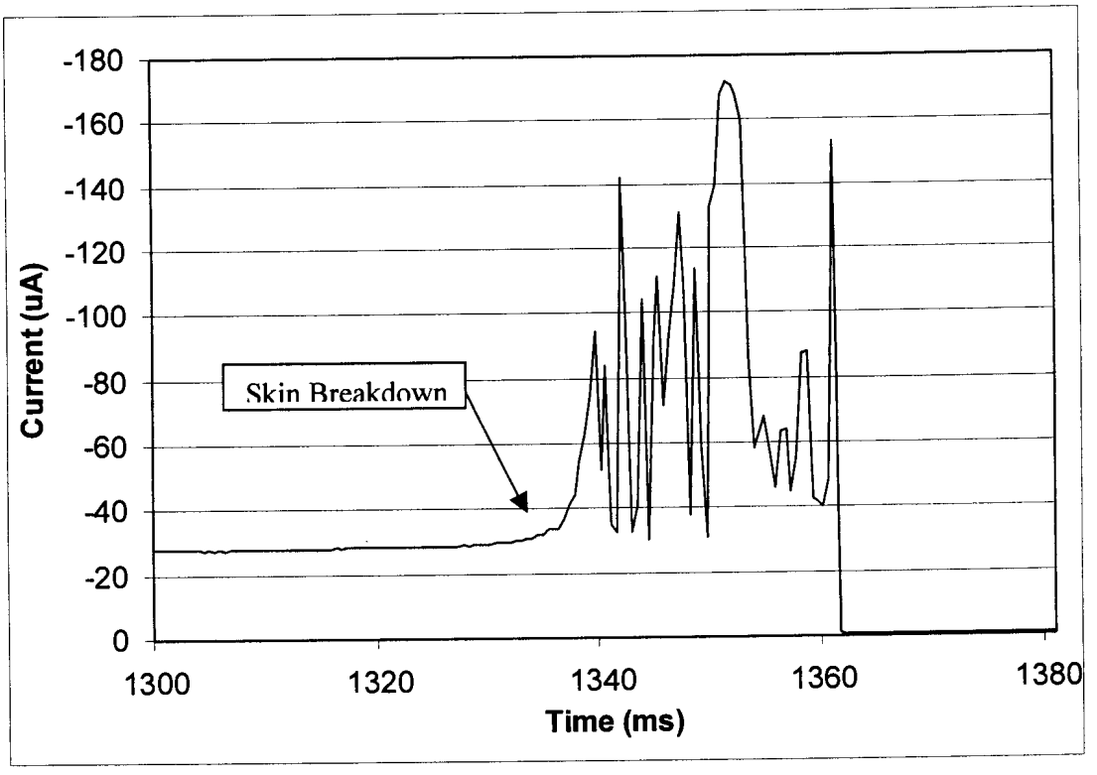

Fig. 5.2 Detailed view of skin breakdown in Fig 4.7

Fig. 5.3 compares the capacitive charging current observed before breakdown (Fig 5.3a) and after breakdown (Fig 5.3b). The amplitude of the pulse on the left is greater because the applied voltage was higher for the first pulse. The first pulse has a flat top due to saturation of the input amplifier. However it is apparent that the time constant in the second amperogram (Fig 5.3b) is not significantly longer than in the first amperogram (Fig 5.3a). At the onset of stimulation, the sweat ducts are empty [9]. If breakdown is due to sweat gland activation, the sweat ducts should be filled after breakdown occurs. According to Indenbom [13] the charging time of the sweat ducts are 100 times greater than the charging time of the stratum corneum. Therefore we would expect the time constant to increase significantly if the sweat ducts became involved after breakdown. Fig. 5.3c shows a measurement taken with the ambient temperature sufficient to activate the sweat glands, the time constant is visibly greater. The absence of an increase in the charging time constant of the skin after breakdown is inconsistent with a sweat gland activation model of breakdown. In addition, it could not be confirmed from literature that selective local sweat gland activation is possible. Most references indicate that the CNS integrates information

from dermal and internal thermoceptors to activate sweat glands, primarily to stabilize the body's core temperature [12],[27],[36]. Therefore more evidence is needed to determine conclusively whether sweat gland activation is responsible for the breakdown effect.

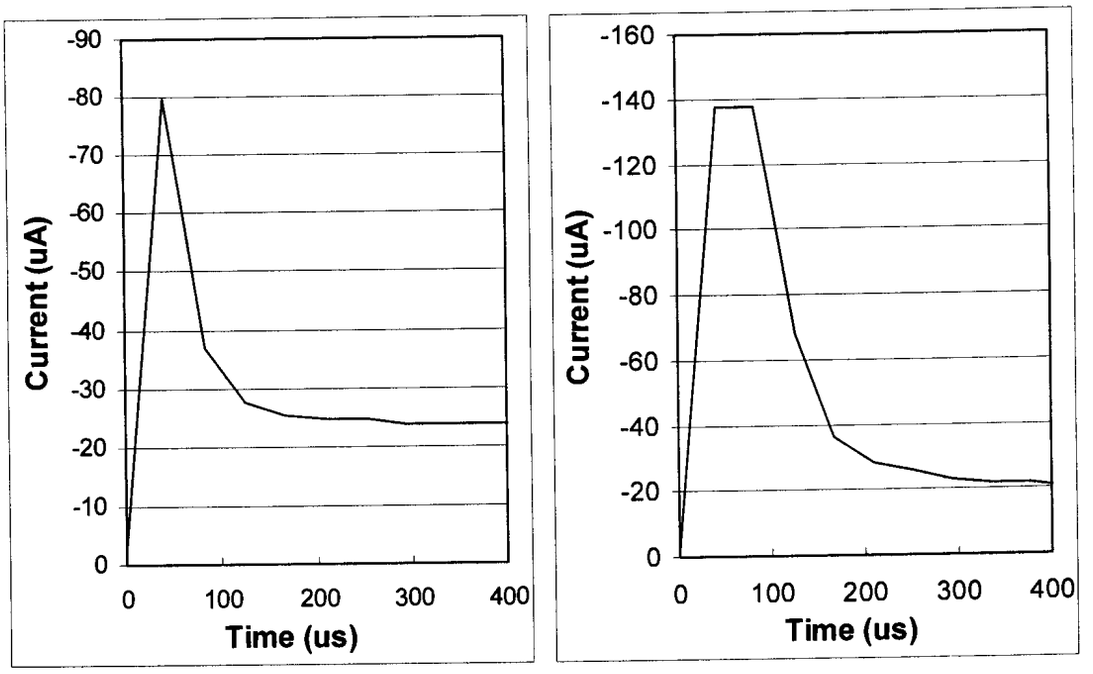

Fig 5.3. a and b. Amperogram of square voltage pulse applied to skin before breakdown (a) and after breakdown (b) from Fig. 4.8 and Fig. 5.1 respectively.

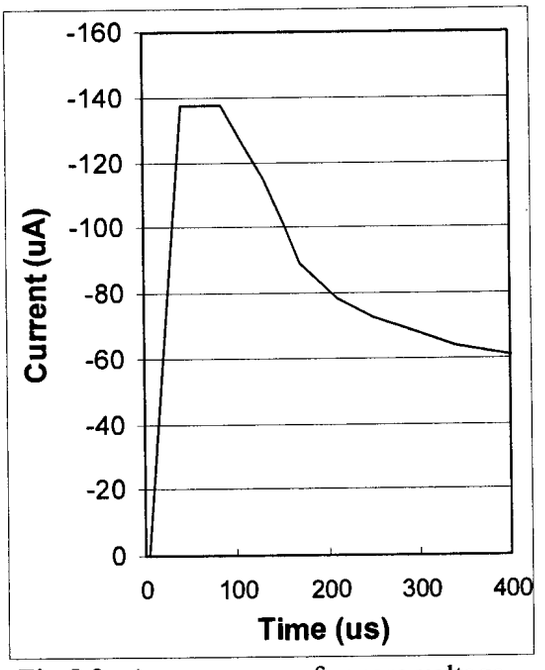

Fig 5.3c Amperogram of square voltage pulse applied to skin at high ambient temperature during active sweating.

5.1 EXPERIMENT 5 - Current distribution during breakdown

Evidence suggests that the breakdown phenomenon is highly localized and is associated with large current densities at sites of low resistance [1],[6],[7],[20]. These low resistance sites are believed to be the sweat glands [18],[20]. A reference point was marked on an electrode. An image of the electrode surface was then taken using an Acer Vuegoscan scanner, with the reference mark in an arbitrary position. The skin was then stimulated using the electrode with a unipolar negative voltage pulse at 21 V for 500 ms. A stinging sensation was felt under the electrode. The electrode was then removed and the surface scanned again with the reference mark in the same position. The two images were then compared. Fig. 5.4 shows the surface of the electrode after the experiment. The dark spots pointed to by the arrows were created during stimulation due to the high current density. The diameter of the large spot was estimated at 200 μm (calculated from the scanner resolution). This confirms that breakdown occurs only at a small fraction of the total stimulated skin area. It would therefore appear possible that the high current density could increase the skin temperature, supporting to the hypothesis that breakdown is a thermally triggered phenomenon.

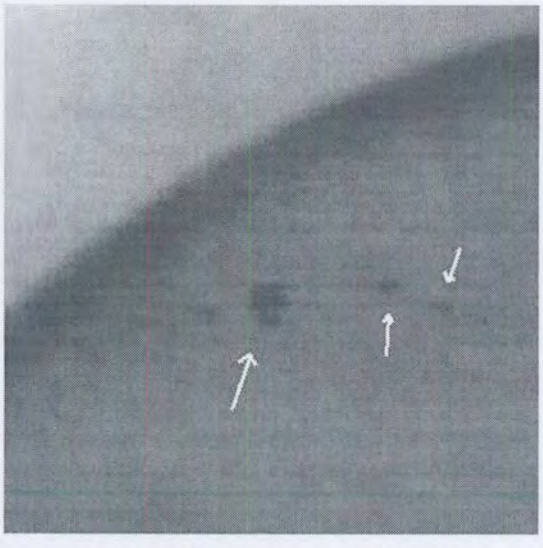

Fig 5.4 Electrode surface degradation due to high local current density after skin breakdown.

5.2 EXPERIMENT 6 - Role of appendages in breakdown

The conflicting evidence regarding the possible role of the sweat glands in skin breakdown, presented in previous sections of the chapter, suggested that further investigation was needed. It is known that the vermilion region of the lips is devoid of any sweat glands [12]. Therefore measurements were done on the lips to see if breakdown could be induced.

A 7 cm by 7 cm piece of cardboard was placed between the lips to prevent moist air from being blown onto the bottom lip during breathing. To ensure that the lip surface was dry, a delay of 10 minutes was introduced before proceeding with measurements. The equipment described in section 3 was used to take measurements. A constant 12 V stimulus was applied. Stimulation was stopped when the current exceeded 150 μA.

Fig. 5.5 shows an example of breakdown occurring on the lips. The shape of the graph is qualitatively very similar to Fig. 4.7. This strongly suggests that breakdown on the lips and elsewhere occurs due to the same mechanisms, which does not include sweat gland activation.

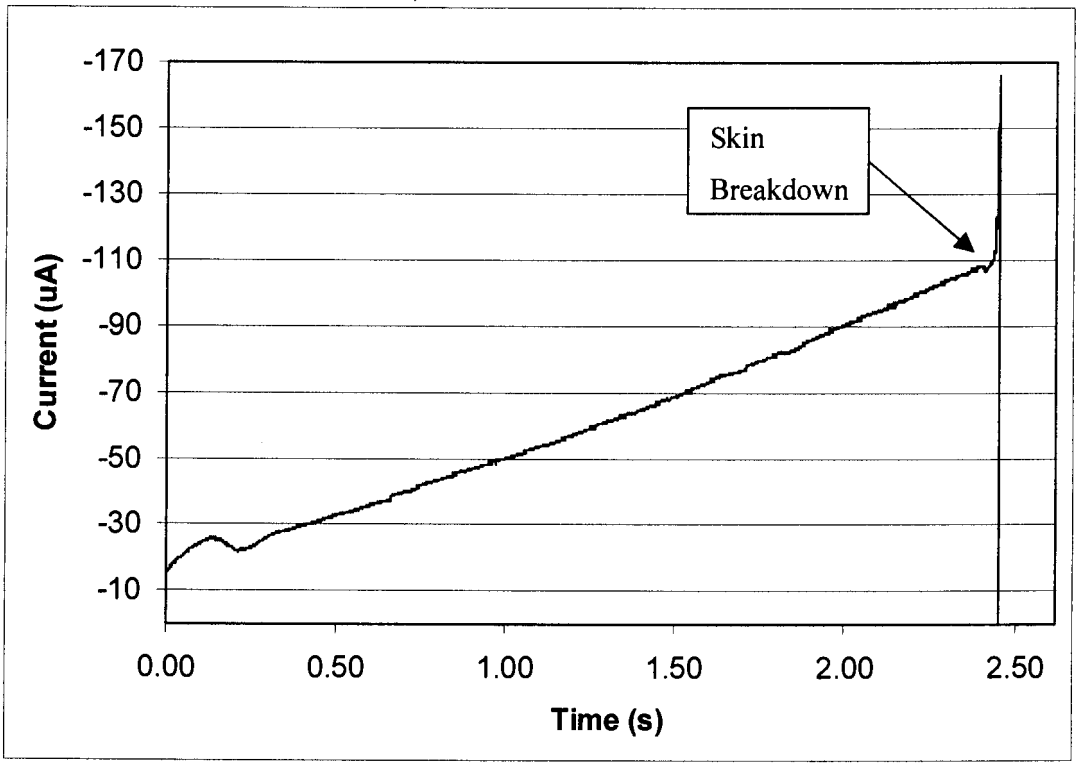

Fig 5.5 Amperogram of constant voltage pulse applied to lips.

Breakdown on the lips often occurred immediately with onset of stimulation. A possible explanation for this could be that the stratum corneum on the lips is thinner than on the rest of the body.

5.3 EXPERIMENT 7 - Influence of ambient temperature on breakdown

The observation that breakdown occurs on the lips, where sweat glands are not present, is strong evidence that sweat glands are not involved. However, it has been argued that different mechanisms are responsible for breakdown on body locations with differing types of skin [6]. Therefore, breakdown was investigated under environmental conditions above and below the thermoneutral zone (25°C - 32°C) in order to determine the influence of active sweating on the breakdown effect.

The room temperature was set to 20°C. Sixty sites were marked on the stomach Thirty of the marked sites were stimulated with an 18.5 V pulse (V1) until the skin broke down, using the equipment described in section 3. The room temperature was then increased to 32°C and the skin was given 30 minutes to acclimatize. The thirty unused sites were then stimulated with the same parameters.

The initial current (at onset of stimulation after capacitive spike), time to breakdown and energy dissipated was calculated for each sample. Table 5.1 shows the average and standard deviation for each group.

Table 5.1 Influence of ambient temperature on skin breakdown parameters

Ambient Temperature	20°C	32°C
Initial Current	6.7 ± 8.5 μA	23.2 ± 25.7 μA
Energy Dissipated	148 ± 121 μW	243 ± 178 μW
Time to Breakdown	3.39 ± 2.40 s	3.20 ± 2.74 s

The data sets were compared using a two tailed t-test assuming unequal variances. Statistically significant differences ($p<0.02$) were observed for the initial current and the energy dissipated. No difference could be detected in time to breakdown.

The graphs observed at 20°C in general, had a different form compared to the graphs observed at 32°C (Fig. 5.6.). Measurements at 20°C yielded graphs similar to Fig. 5.6.a while measurements at 32°C resulted in the form shown in Fig. 5.6.b. In 5.6.b the initial capacitive spike is almost completely obscured by the sharp initial current rise, which then slows to a more linear increase until the breakdown point.

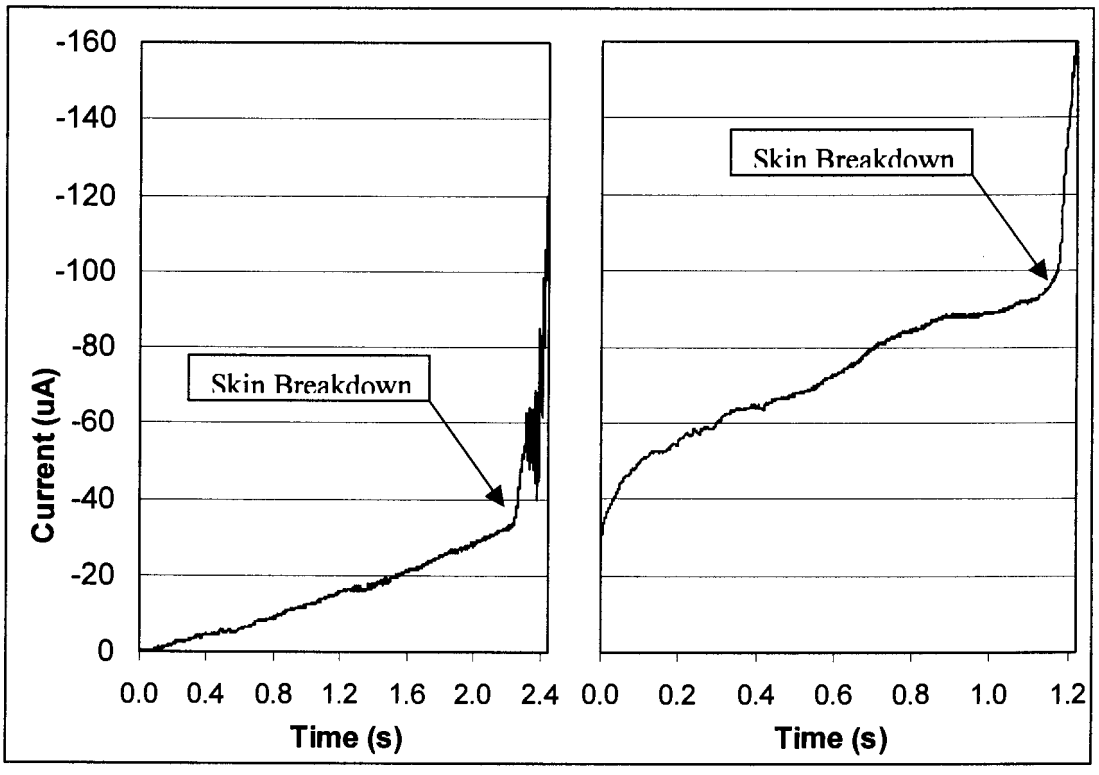

Fig. 5.6. a and b. Amperograms of skin breakdown due to a constant voltage pulse at ambient temperature 25°C (left hand graph) and 32°C (right hand graph).

Increasing the ambient temperature above thermoneutral zone where sweating is strongly stimulated increased the initial skin current and the energy dissipated before breakdown, while time to breakdown remained virtually unchanged. This leads to the conclusion that active sweat glands provided additional current pathways, which resulted in additional current flow and energy dissipation. In support of this, it is observed that Fig 5.6.b looks like Fig 5.6.a with a constant current offset. Time to breakdown was unaffected by the state of the sweat glands. It can therefore be concluded that breakdown is not related to the presence of sweat glands, neither through sweat gland activation nor through electroosmotic filling of sweat glands.

5.4 EXPERIMENT 8 - Influence of applied voltage on breakdown

The breakdown phenomenon has been linked by several authors to thermal changes in the skin [7],[8],[20],[29]. A thermal trigger was identified as a possible cause of breakdown in the introduction to this chapter. Panescu and Webster [20] observed that the energy dissipated in the skin before breakdown stays almost constant, independent of the applied voltage. However their observation was based on very limited data. Since skin measurements with a dry electrode display a great deal of variability, an experiment was designed to investigate this claim statistically. Such a study has not yet been reported and could provide information which could be potential useful in explaining the breakdown phenomenon (e.g. time to breakdown as a function of applied voltage).

In vivo, breakdown is known to occur only beneath a dry negatively polarized electrode. To allow accurate measurement of breakdown parameters (such as time to breakdown and energy dissipated before breakdown) as a function of voltage, breakdown will be induced with a unipolar constant voltage stimulus.

The energy required to break down the skin was measured using the data from experiment 3. In experiment 3, a constant voltage pulse was applied at one four different voltage levels (-12.5, -15, -18 and -21 V) until the skin broke down. At each voltage level 33 samples had been obtained.

Graphs similar to Fig. 4.7 were obtained. The moment of breakdown was defined as the moment when the rate of change of current with respect to time exceeded a set threshold. The computer displayed each trial on the screen, with an indication of where the skin was deemed to have broken down. Each trial was checked visually to make sure that the breakdown point was correctly determined. . The results of the 132 trials were combined and then analyzed using the Data Analysis Toolpak in Microsoft Excel. The energy dissipated was calculated as the integral of the product of measured current, applied voltage and sample period, from the start of the trial until the moment of breakdown. For each voltage setting used the average and standard deviation of the energy dissipated during relevant trials were calculated. Student's t-test was used to determine if differences in the dissipated energy were statistically significant.

Fig. 5.7 shows the mean energy dissipated and the standard deviation versus applied voltage. The mean value remains fairly constant, tending lower at higher pulse amplitudes. The hypothesis of equal means could not be rejected at a 0.1 level of significance between any two groups. Table 5.2 shows p-values obtained for a Student's two tailed t-test assuming unequal variances. The large standard deviation reflects the skin's mosaic electrical characteristics described by Panescu et al [20]. They showed that the skin resistance measured with a 10 μm diameter electrode varies by a factor of 10 over a 1 cm^2 area. Since a dry electrode makes poor contact with the skin, only a small percentage of the total area under the skin makes contact with the electrode, making a large number of samples necessary to obtain a meaningful average. It is not clear why the standard deviation decreases at higher voltages.

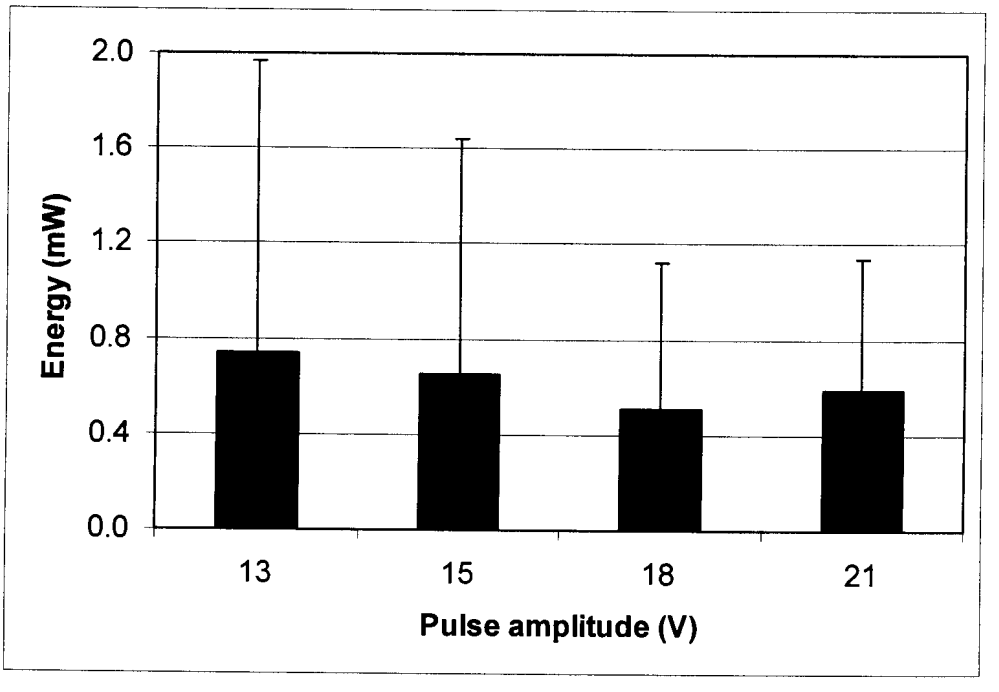

Fig. 5.7 Total energy dissipated before breakdown versus applied voltage using 33 samples per group

Table 5.2 Statistical significance in terms of p-values obtained with a Student's two tailed t- test assuming unequal variances indicating that hypothesis of equal means cannot be rejected between any two groups.

	15 V	18 V	21 V
12.5 V	0.76	0.36	0.61
15 V		0.69	0.76
18 V			0.58

The sample size was increased to test the possibility that the energy required for breakdown was lower at higher voltage levels. We must decide between the hypotheses

H0 : u13 > u21

H1: u13 <= u21

where u13 is the average breakdown energy at 13 V and u21 is the average breakdown energy at 21 V.

Each group contained 66 samples. Samples were taken using the same technique from the skin of the forearms. The skin was given 72 hours to recover from the first part of the experiment. Fig. 5.8 shows the mean and standard deviation obtained. The p-value calculated using a one tailed t test assuming unequal variances was 0.034. The mean value difference result was therefore significant at a level $p < 0.05$

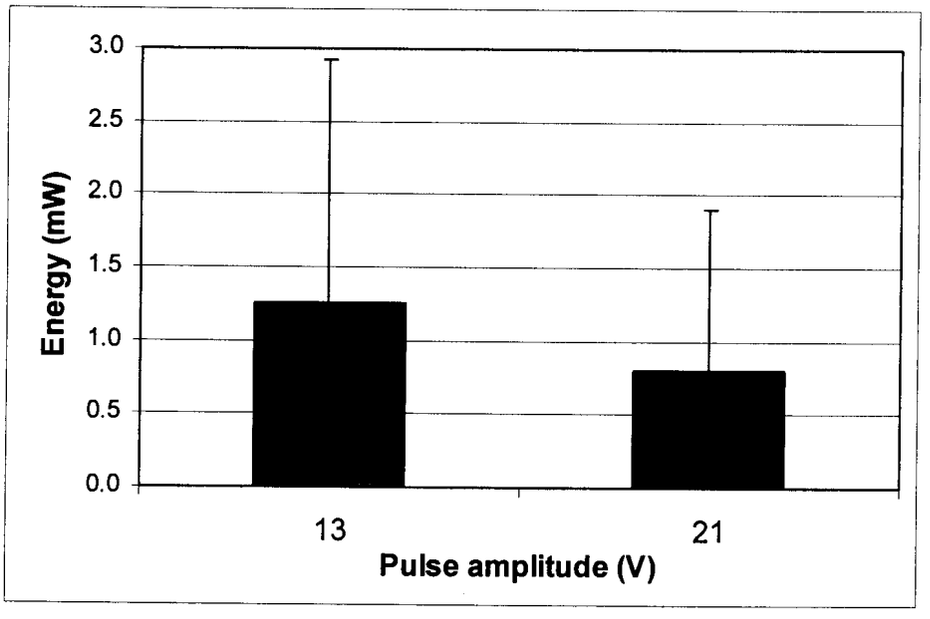

Fig 5.8 Total energy dissipated before breakdown versus applied voltage using 66 samples per group

A large sample size of 66 samples per group was required to observe a difference in the energy applied before breakdown, despite a large difference in the applied voltage, and the result was of low statistical significance. This could suggest that breakdown occurs when the dissipated energy exceeds a particular threshold and that breakdown is only weakly dependent on the applied voltage. However, the high variance of the data makes interpretation of the result speculative. It could reflect large variations in the size and resistance of highly localized low resistance pathways through the skin. Alternatively it may mean that there is no link between the breakdown effect and the applied energy,

5.5 EXPERIMENT 9- Short term recovery of skin after breakdown

The recovery of the skin after breakdown was investigated over a timeframe of 30 seconds. If breakdown is due to melting of the lipid membranes at 65°C, no (or very minimal) resistance recovery should be observed over 30 seconds [10],[11],[25], since the liquid lipids do not recrystallize into their orginal bilayer formations. Measurements were done at two voltage levels to determine whether the applied voltage influenced the recovery rate.

The skin was stimulated with a unipolar voltage pulse with amplitude 13 V or 18 V until it broke down. Ten -4.5 V 20 ms pulses were applied with inter pulse pauses of 260 ms. A further ten -4.5 V 20 ms pulses were applied with pauses of 2.6 seconds.

The skin resistance at the onset of each pulse after breakdown is plotted against time in Fig. 5.9. The result is averaged over 32 measurements for each breakdown voltage. The line labeled ratio is the resistance values measured at 18 V divided by those measured at 13 V at each time interval.

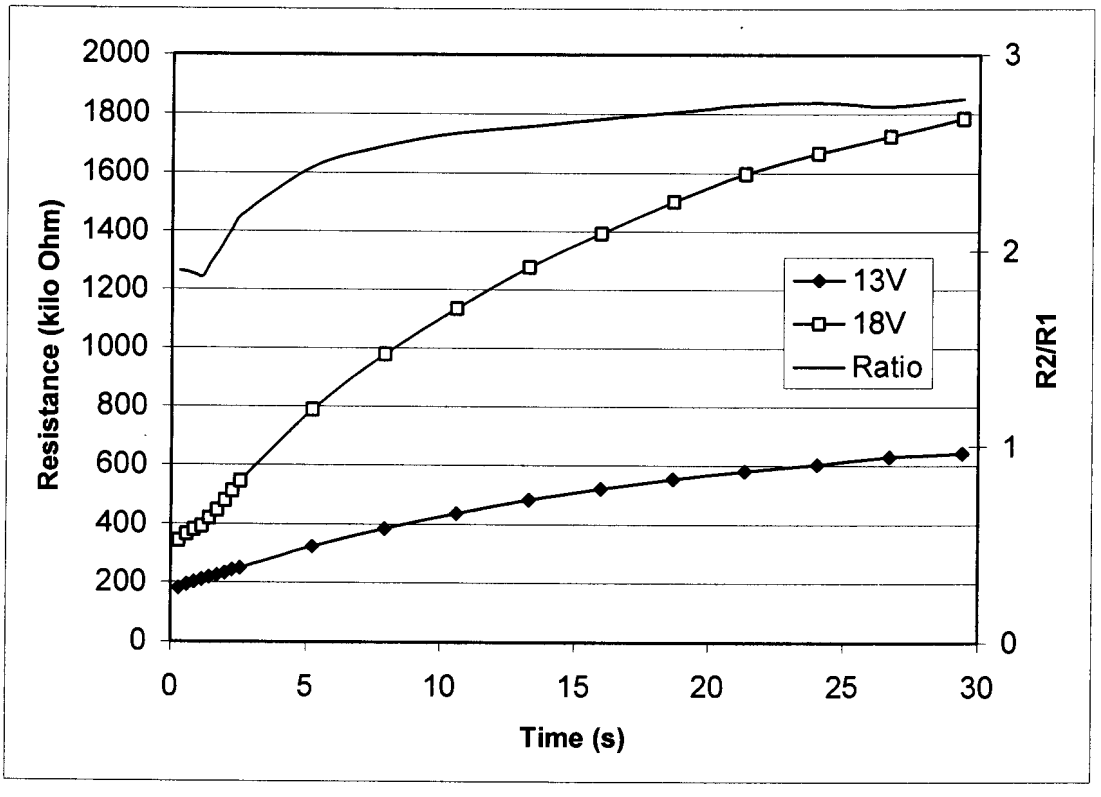

Fig. 5.9 Skin resistance recovery after breakdown.

At the moment of breakdown, the skin resistance was 107 kΩ and 151 kΩ for 13 V and 18 V stimulus respectively, since stimulation was stopped when the current reached 120 μA in both cases. The 13 V stimulus therefore created a greater defect in the skin. As a result the skin recovers both more quickly and to a greater degree after the 18 V stimulus, as is evidenced by the "Ratio" line rising from 2 to 3 over the time period.

An exponential decay curve was fitted to the current vs. time plots. It was assumed that the same process or processes were responsible for the current decay over time both at 13 V and at 18 V and therefore that the same time constant or constants would be involved. Using the Solver in Microsoft Excel, the RMS error was minimized simultaneously for the two data sets. The RMS error was an order of magnitude lower when biexponential curve (5.1) was used than for a single exponential. Therefore the curves of (5.1) and (5.2) was fitted to the 13 V and 18 V data respectively.

$$I13(t) = I_1 \cdot \exp(-\frac{t}{\tau_1}) + I_2 \cdot \exp(-\frac{t}{\tau_2}) + b1 \qquad (5.1)$$

$$I18(t) = I_3 \cdot \exp(-\frac{t}{\tau_1}) + I_4 \cdot \exp(-\frac{t}{\tau_2}) + b2 \qquad (5.2)$$

Least squares fitting yielded the following parameter values:

$I_1 = 40$ μA, $I_2 = 40$ μA, $b1 = 25$ μA

$I_3 = 34.6$ μA, $I_4 = 14.5$ μA, $b2 = 9.5$ μA

$\tau_1 = 2.8$ s, $\tau_2 = 11.4$ s

The biexponential fit suggests two processes with different time constants. The faster time constant could be associated with the falling skin temperature. The agreement between *I13* and *I18* would suggest that the local temperature had reached approximately the same value at the time stimulation was stopped.

The slower time constant of 11 seconds is of the expected order for the natural destruction of electropores [2]. *I2* and *I4* could therefore represent a measure of the number of electropores present immediately after breakdown. *I2* is much larger than *I4*. Since stimulation was stopped at the same current level for both stimuli, the membrane conductance at that instant would have been lower for the 18 V stimulus, implying fewer electropores. Hence the difference between *I4* and *I2*.

The resistance increased by more than a factor of three at both applied voltage levels. This indicates that the skin temperature did not increase sufficiently to melt the lipid membranes.

5.6 EXPERIMENT 10 - Long term recovery of skin after breakdown

In vitro measurements of the recovery of the skin resistance after electroporation indicates that the complete recovery of the insulating properties of the skin takes less than 1 hour [3],[13]. Therefore, if breakdown is due to accelerated electroporation, it is expected that breakdown should not induce measurable changes in the skin that last longer than 1 hour.

With dry electrode stimulation it is known that only a very small percentage of the total surface area under the electrode is involved during breakdown (<1% according to Yamamoto [6] and experiment 5). Therefore even if semi-permanent changes (with a life span of days) are induced at these sites, a dry electrode may not come into contact with the same high conductivity regions during successive measurements at the same skin site. It could therefore be incorrectly concluded that the skin is recovering completely. The degree of recovery of the skin after the breakdown effect was therefore investigated statistically.

One hundred and twenty sites were marked with a permanent marker on the skin of the stomach. This was done by placing an electrode on the skin at each site and drawing a ring along its border. The marked areas were clustered together in groups of four. The sites in each group were designated S1-S4. For each group, S1 was stimulated with a constant 18 V pulse and S2 with a constant 13 V pulse until the skin broke down. After 20 minutes, S1 was again stimulated with an 18 V pulse and S2 with a 13 V pulse until breakdown occurred. As a control S3 was stimulated with an 18 V pulse. After a further 60 minutes, S3 and S4 were stimulated with 18 V, with S4 serving as the control. All measurements for a particular cluster were taken before moving on to the next cluster. During each delay the electrode was replaced. Measurements were done at 25°C with the equipment described in section 3.

From each measurement the initial skin resistance (at t=0) and the time to breakdown was determined. Changes in these parameters at site S1 and S2 were investigated after a twenty

minute interval. For convenience S1-1 refers to the first measurement taken at site S1 etc. If environmental factors were constant there should be no statistical difference between S1-1, S3-1 and S4-1. If this is true then a statistically significant difference between S1-1 and S1-2 or S2-1, and 2-2 would show induced physical changes occurring in the skin that last longer than 20 minutes. A statistical difference between S3-1 and S3 -2 would show an induced change lasting longer than 60 minutes.

Table 5.3 Skin breakdown parameters measured at the same sites with a 20 minute delay.

		0 min	20 min	Control
18V	Initial Resistance	8.57 ± 6.76 MΩ	4.62 ± 4.26 MΩ	9.42 ± 11.5 MΩ
	Time to Breakdown	3.47 ± 2.92 s	1.23 ± 1.5 s	3.42 ± 2.85 s
13V	Initial Resistance	14.5 ± 14.1 MΩ	11.4 ± 11.7 MΩ	
	Time to Breakdown	14.97 ± 9.38 s	6.97 ± 9.2 s	

Table 5.4 Skin breakdown parameters measured at the same sites with a 60 minute delay.

18V	0 min	60 min	Control
Initial Resistance	9.42 ± 11.5 MΩ	7.95 ± 6.69 MΩ	8.47 ± 7.68 MΩ
Time to Breakdown	3.24 ± 2.85 s	1.25 ± 0.9 s	3.62 ± 2.58 s

Results are shown in Table 5.3 and 5.4. No statistical difference was observed between initial measurements and any control group. It is therefore assumed that there were no other factors influencing the measured skin parameters. At 18 V the average value of the initial skin resistance first measured 8.6MΩ. When the initial skin resistance was measured again after 20 minutes at the same skin sites, the average value fell to 50% of the first value. After 60 minutes the initial skin resistance recovered to 84% of the first. Only the difference after 20 minutes was statistically significant ($p < 0.01$). At 13 V the value of the initial skin resistance fell to 78% of its first measured value after 20 minutes but the result was not statistically significant.

Statistically significant differences ($p < 0.001$) in time to breakdown was observed at all time intervals. Time to breakdown fell to about 30% of its initial value, with similar results being obtained after 20 and 60 minutes.

The results confirm that skin recovery is still taking place after 20 minutes and that the changes in the skin impedance induced by the breakdown effect persist after 60 minutes.

A similar experiment was conducted over 24 hours. 50 sites on the left forearm were marked. Breakdown was induced at each site with an 18 V pulse as described previously. After 24 hours the 50 marked sites were again measured with the same parameters. Immediately after, 50 sites on the right forearm were measured as control sites.

Table 5.5 Skin breakdown parameters measured at the same sites with a 24 hour delay.

Time to Breakdown	Left Forearm day 1	Left Forearm day 2	Right Forearm day 2
Mean	0.64 s	0.50 s	0.66 s
Standard Deviation	0.60 s	0.56 s	0.85 s

No statistical difference was observed with a two tailed t-test assuming unequal variances between the left forearm day 1 and the right forearm day 2 ($p>0.80$). The mean time to breakdown measured on day 2 on the left forearm was about 20% lower than the other measurements. Since the time to breakdown was expected to fall a one tailed t-test assuming unequal variances was used for comparison with the other measurements. The result is almost significant with $p=0.10$ that Mean Left Forearm day 2 < Mean Left Forearm day 1 and $p=0.12$ that Mean Left Forearm day 2 < Mean Right Forearm day 1

The result is not conclusive but suggests that differences in breakdown time could still be observable after 24 hours. This result was not according to expectation. A possible explanation could be that lipid phase changes were induced at a fraction of the area where breakdown occurred, such that both reversible and irreversible changes were induced. Hence the recovery observed over 30 seconds in experiment 9.

5.7 *EXPERIMENT 11 - Influence of local temperature on breakdown*

A phenomenon observed while evaluating the data from experiment 10 gave further credence to the idea that temperature can affect the electroporation rate. Fig. 5.6 shows the

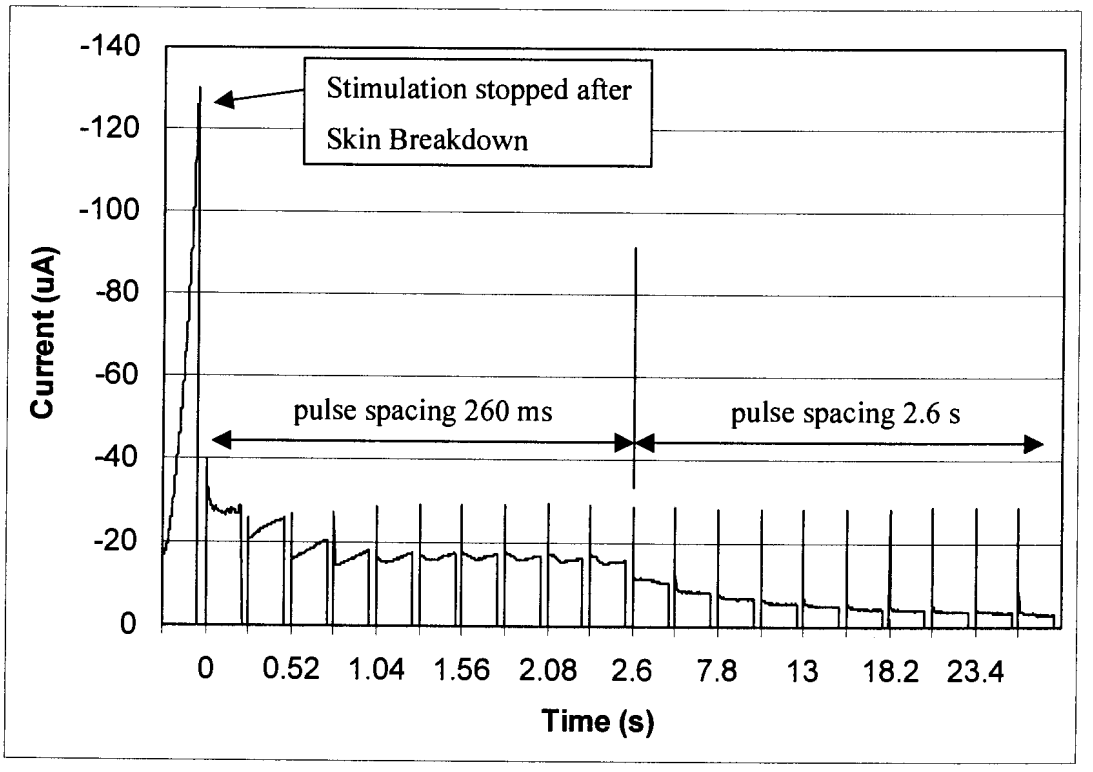

Fig. 5.6 Amperogram of voltage pulses applied after skin breakdown. A constant -18 V was applied until breakdown occurred. From time 0, square voltage pulses with amplitude -4.5 V and width 20 ms were applied. The first ten pulses are spaced 260 ms apart, the remaining pulses are 2.6 s apart. Periods between pulses are not drawn to scale, to make the graph more compact. The horizontal axis indicates the time of onset of each pulse after breakdown.

result of applying low voltage pulses with amplitude -4.5 V and width 20 ms, as the skin recovers after breakdown was induced using a high voltage pulse. The first low voltage pulse was applied 10 ms after the high voltage pulse ended, followed by pulses every 260 ms. The remaining pulses were spaced 2.6 seconds apart. Intervals between pulses are not drawn to scale. During the skin breakdown, the skin temperature is likely to rise due to increased power dissipated in the skin. When stimulation is stopped (indicated on Fig 5.6) the elevated skin temperature must fall to its equilibrium value. During the initial low voltage pulses the conductivity is seen to increase quite linearly during the pulse. It is hypothesized that this increase is due to electroporation, which is accelerated due to increased skin temperature. For each subsequent pulse the rate of change of conductivity decreases, as the skin temperature falls. Since the pulse width was only 20 ms the skin temperature during each pulse except the first pulse would be quite constant. The first pulse was applied only 10 ms after breakdown therefore the effect of the exponentially

decaying skin temperature during the pulse was probably greater than that of electroporation, hence the conductivity falls during the pulse.

To test whether increased skin temperature could affect the rate of electroporation a heating element was fixed to the back of the electrode. High resistance wire was wrapped around thin pieces of cardboard. Either side of the cardboard was covered with paper to insulate the wire. The heating element was then mounted on back of the electrode. Fig. 5.7 shows an expanded view of the probe assembly. The electrode plugs into the electrode connector. A constant current source heated the wire to a constant temperature. Temperatures sufficient to mechanically distort the electrode could be generated in this way. The surface temperature of the electrode was estimated at 40°C by taping a thermistor to it. The actual skin temperature would have been less since the electrode temperature falls when it comes into contact with the skin, nevertheless the skin temperature reached during each trial was likely to be very similar since the power output of the heating element is constant. The electrode was placed on the skin for 15 seconds before taking a

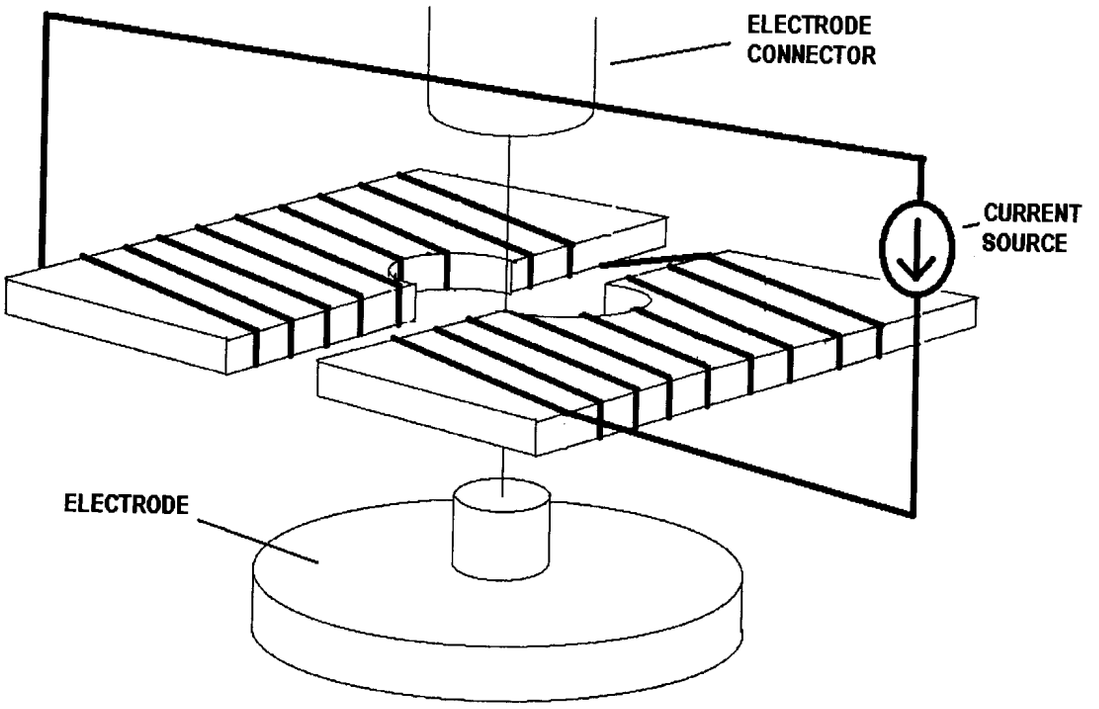

Fig. 5.7 Electrode designed to heat the skin during stimulation. The extrusion at the back of the electrode plugs into the electrode connector and makes electrical contact with wires inside. The heating elements, which are electrically insulated, are mounted on the back of the electrode.

measurement to allow the skin temperature to stabilize. The skin beneath the heated electrode remained red for several minutes after the electrode was removed. This suggests that the skin temperature in this experiment was significantly greater than the skin temperature reached when the ambient temperature was 32°C (experiment 7).

Sixty sites were marked on the skin of the stomach to ensure that no area is stimulated more than once. Thirty sites were stimulated with a heated electrode, the other thirty sites with an electrode at ambient temperature (25°C).

Parameters were extracted from the data. The average and standard deviation are shown in Table 5.6.

Table 5.6 Influence of local skin temperature on skin breakdown parameters

	Heated Electrode	Cold Electrode
Initial Resistance	5.2 ± 4.4 MΩ	23.4 ± 38.0 MΩ
Energy Dissipated before Breakdown	73 ± 51 μW	82 ± 55 μW
Time to Breakdown	1.1 ± 1.0 s	2.8 ± 2.6 s
Rate of Change of Current	87 ± 160 μA/s	29 ± 47 μA/s

Data was analyzed using the one tailed t-test assuming unequal variances. The initial conductance was significantly greater for heated skin ($p < 0.01$). This is consistent with the known resistance - temperature relationship of the skin [10]. Heated skin broke down more quickly than unheated skin ($p < 0.01$). The rate of change of conductivity was higher for heated skin ($p < 0.05$). The energy dissipated before breakdown was about 10% less for heated skin than unheated skin but the result was not statistically significant ($p=0.25$).

The increase in rate of change of current and the reduction in time to breakdown at higher skin temperatures suggest that the electroporation rate increases with increased skin temperature. This raises the possibility that electrical heating of the skin due to high local current density could increase the electroporation rate and create a positive feedback loop, leading to the resistance breakdown.

Higher ambient temperatures in experiment 7 did not reduce the time to breakdown. This could mean that the skin has to be heated above a threshold value, greater than 32°C before an effect is observed. The increase in energy dissipated before breakdown at the higher

ambient temperature (experiment 7) pointed to parallel current pathways being present, due to activation of the sweat glands. Since the energy dissipated before breakdown in this experiment remained relatively constant, it appears that increased local temperature did not activate the sweat glands, which suggests that sweating is controlled by the CNS and triggered globally. This supports the conclusion of experiments 6 and 7 that sweat gland activation is not responsible for the resistance breakdown of the skin.

5.8 EXPERIMENT 12 - Linked heat transfer / electroporation model

A two dimensional (2D) finite element model was created to test the hypothesis that the skin breaks down when a thermal threshold is exceeded. This idea was supported by the following observations:

1. All other known possible causes of breakdown had been eliminated (experiment 5 - 9).
2. In literature breakdown is most commonly attributed to joule heating of the skin as a result of high local current densities [1],[7].
3. The energy dissipated in the skin before breakdown did not appear to be strongly related to the applied voltage (experiment 8).
4. Evidence was found that electroporation occurs at the applied voltage range, in a small percentage of the skin surface area where the stratum corneum only consists of about 15-20 lipid bilayers (experiment 3).
5. Evidence was found that the electroporation rate could be influenced by an increase in skin temperature (experiment 11).

As an initial experiment a one dimensional (1D) axisymmetric finite element heat transfer model of the skin surface linked to an electrical model was created with the intention of expanding the model to three dimensions depending on the results obtained.

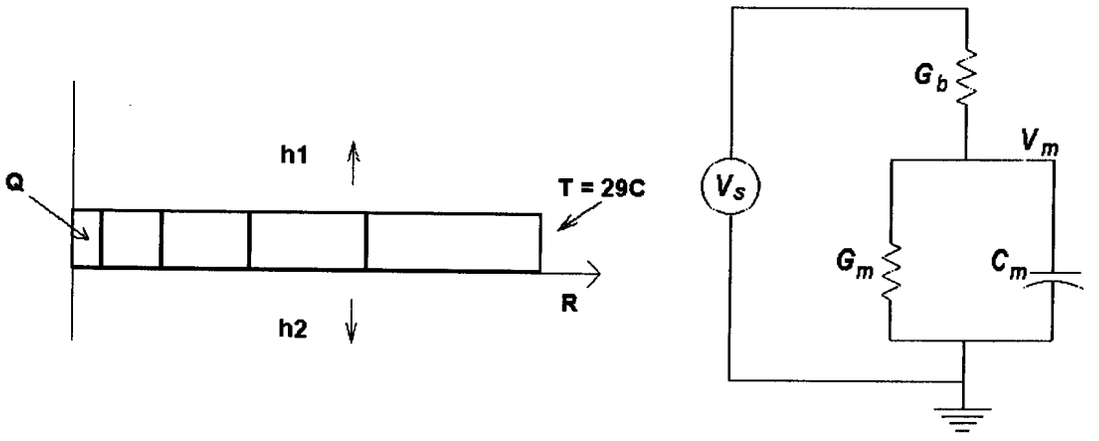

Fig. 5.12. Combined 1D axisymmetric finite element heat transfer - electrical model of the skin. The vertical line next to the center element marked Q is the symmetry axis.

The model is shown in Fig. 5.12. A small low resistance defect in the stratum corneum is modeled. The heat flow in the stratum corneum is simulated by an axisymmetric finite element model. In the figure, R indicates the radial axis. It is assumed that all current passes through the stratum corneum via a small cylindrical defect represented by the center element. The heat generated by the current flow is represented by heat source Q. The electrical characteristics of the skin are modeled according to the electroporation model of Chizmadzhev [20]. Conductance element G_b represents the combined conductance of the corneocytes and the bulk region. G_m and C_m are the lumped conductance and capacitance of the lipid bilayers. V_s is the voltage applied across the skin. The energy released by heat source Q is equal to the energy dissipated in conductance G_m.

The equations used to model the electrical behavior of the skin are:

$$\frac{dV_m}{dt} = \frac{-V_m \cdot (G_m + G_b) + V_s \cdot G_b}{C_m} \tag{5.3}$$

$$G_m = \frac{g \cdot N}{m} \tag{5.4}$$

$$\frac{dN}{dt} = K \cdot (\exp\left[\alpha\left(\frac{V_m}{m}\right)^2 - \frac{N}{N_0}\right] \tag{5.5}$$

if $T < Tcritical$

$$K = K1$$

else

$$K = K1 \cdot (1 + T - T_{critical}) \tag{5.6}$$

$$\frac{dP}{dt} = V_m^{\,2} \cdot G_m \tag{5.7}$$

$$\frac{dT}{dt} = \Delta T \tag{5.8}$$

where N is the number of electropores in the membrane, g is the conductance of one electropore, m is the number of bilayers in series, K and α are experimentally determined constants. T is the temperature in the center finite element and ΔT is the temperature rate of change calculated by the FEM (see below). $T_{critical}$ is the lipid phase change temperature.

(5.3) describes the circuit shown in Fig 5.12.
(5.4) describes the conductance of the electroporated stratum corneum [3].
(5.5) describes the rate of change in the electropore population [3].
(5.6) models the dependence of the electroporation rate on temperature. In accordance with Lee [34], it is assumed that K rises linearly after the critical temperature is exceeded. No attempt was made at this stage to model the complexity of phase change kinetics.
(5.7) calculates the energy dissipated in Gm during a particular time interval, used to calculate the volume heat flux (Q) in the finite element model.
(5.8) calculates the skin temperature at a particular instant from parameter ΔT, determined in the finite element model.
The differential system was coded in MATLAB and solved using fourth and fifth order Runge-Kutta formulas.

The finite element model was created in MATLAB using CALFEM. The axisymmetric element equations were derived using the technique described by Fenner [37]. The axisymmetric heat transfer model was verified separately against MARC Mentat, a commercial finite element application. The boundary conditions stipulated the temperature at the edge of the disk (the skin temperature was assumed to be 29°C), heat convection to the air above the disk, heat convection to the body below the disk and internal volume heat source Q at the center element. Heat flow constants for the skin were calculated from Rideout [38].

The coupled system was solved as follows:

1. The time t was set to zero.
2. The differential equations were solved over a time step dt, starting at time t, using ΔT as the predicted rate of temperature change (initially ΔT was set to zero).
3. The energy dissipated in R_m was integrated over this period.
4. The average volume heat flux (Q) over the period was calculated from the total delivered energy.
5. The finite element equations were solved over the period dt using the calculated Q.
6. The change in temperature of the center element (dT_{ce}) was compared with ΔT. If the difference was within a specified tolerance then t was incremented by dt.
7. ΔT was set equal to dT_{ce}.
8. If $t < t_{final}$ then return to step 2.

The MATLAB code and values of constants are in appendix 1

Results of the model for a constant applied voltage are shown in Fig. 5.13 . As expected the membrane conductance initially increases linearly. When the temperature rises above the critical temperature, the electroporation rate increases. The current therefore starts to

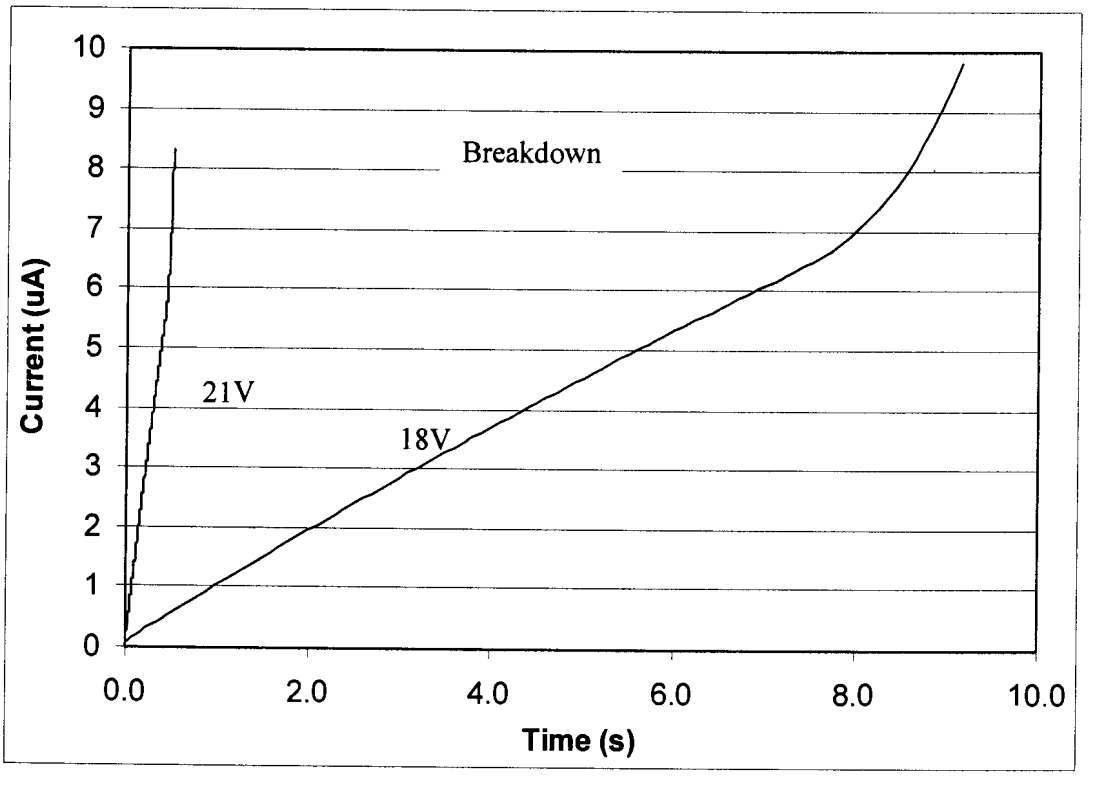

Fig. 5.13 Simulated electrical breakdown of the skin due to constant voltage stimulus with amplitude 21 V and 18 V.

increase more rapidly generating more heat and creating a positive feedback effect, or "thermal runaway" as termed by other authors.

The time required to break down the skin at different applied voltages was compared with experimentally measured values. The average time to breakdown was calculated as a function of voltage from the data measured in experiment 8. The mean and standard deviation is shown in table 5.7. Fig. 5.14 plots the logarithm of the mean time to breakdown against the applied voltage.

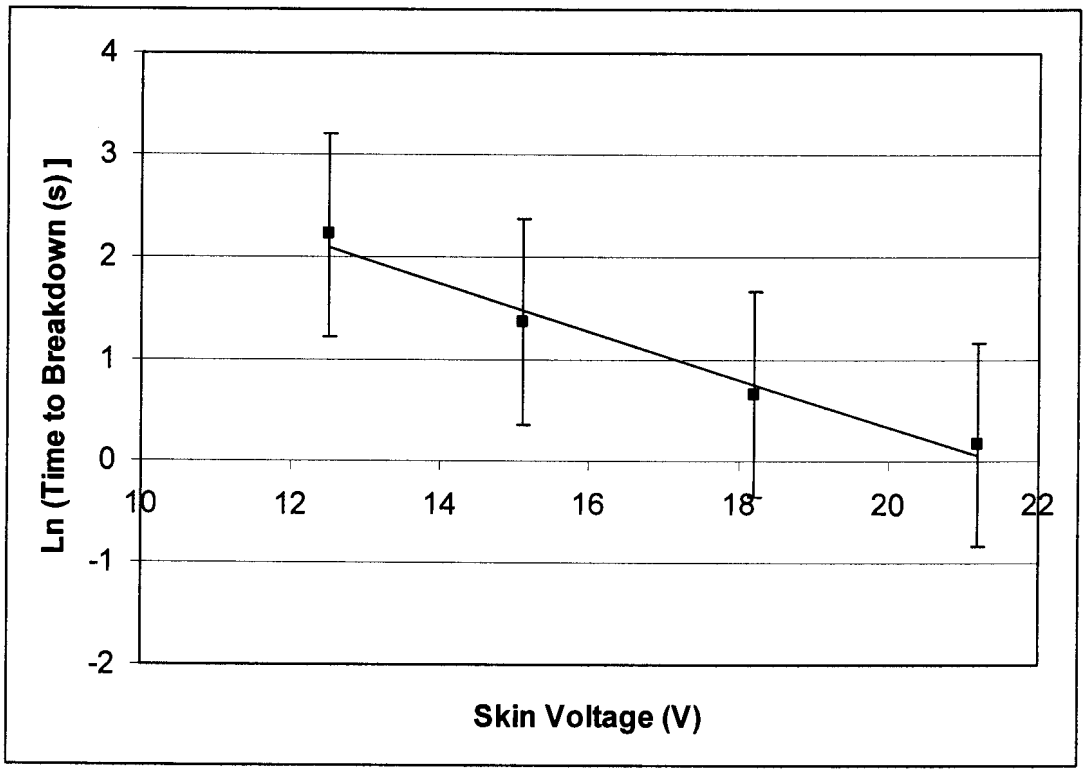

Fig. 5.14 Linear relation between the logarithm of mean time to breakdown versus applied voltage. Error bars indicate standard error of the estimate.

Table 5.7.Time to breakdown versus applied voltage for skin on the stomach.

	12.5 V	15 V	18 V	21 V
Mean (s)	15.6	6.8	3.1	1.5
Standard Deviation (s)	16.4	6.7	2.7	0.9

Comparison of the simulation with the experimentally observed data pointed out fundamental flaws in the model. The time required to break down the skin increases by more than an order of magnitude when the applied voltage is lowered from 21 V to 18 V.

This is much greater than observed experimentally and is due to two assumptions inherent in the model:

1. the electroporation rate is exponentially related to the square of the applied voltage
2. the power dissipated is the product of the current through the hypothetical defect in the stratum corneum and the applied voltage, therefore the lower the voltage the higher the required current to obtain the same power output.

In this scenario it is impossible to reconcile the observed relationship between time to breakdown and the applied voltage. In experiment 8, Fig. 5.14 the logarithm of the mean time to breakdown was plotted against the applied voltage. The relationship is clearly linear.

An approximate expression can be derived for the time to breakdown predicted by the model. From (5.4) and (5.5) we have that

$$G_{BREAKDOWN} \approx k \cdot \exp(\alpha V^2) \cdot \Delta t \tag{5.9}$$

where $G_{BREAKDOWN}$ is the skin conductance just before breakdown, k an α are constants and Δt is the time to breakdown. The assumption is made that dG/dt is linear and G is initially close to zero. Since

$$P_{BREAKDOWN} = V^2 \cdot G_{BREAKDOWN} \tag{5.10}$$

then if we ignore the heat capacity of the skin and assume the skin temperature is proportional to the energy dissipated at the moment of breakdown then

$$\log(\Delta t) = \log(P) - \log(kV^2) + \alpha V^2 \tag{5.11}$$

which indicates that $log(\Delta t)$ should be a function of the square of the applied voltage. Neglecting the heat capacitance of the skin is valid since including it would only increase the discrepancy between the simulated and experimental results.

Additional problems were encountered with this model. The current density required to raise the skin temperature to 40°C implies a very high electropore density, in the order of 10^{10} pores/cm^2. This exceeds the maximum electropore density (10^8 pores/cm^2) where (5.5) is valid [3] and approaches the theoretical maximum electropore density [31]. Below 18 V the electropore density saturates at levels that are too low to achieve the required current density.

5.9 EXPERIMENT 13 - 2D heat transfer model

The failure of the thermal model to explain the electrical breakdown of the skin, coupled with the observation (experiment 2) that joule heating probably did not influence the skin resistance before breakdown, suggested that joule heating may not play a significant role in determining the non-linear VCC of the skin. This is contrary to the assertions of other authors [16],[24]. The heat distribution under the skin due to joule heating was therefore investigated using the commercial finite element package MARC Mentat.

Investigations were carried out using a 2D axisymmetric steady state model, since the steady state would be a worst case condition where maximum temperatures would be reached. The magnitude of the volume heat flux applied to the model was estimated from the experimental observations of power dissipated in the skin before breakdown.

The axisymmetric finite element model used to model the skin is shown partially in Fig. 5.15 . The axis of symmetry is normal to the skin surface and located on the left hand side of the figure. The epidermis was modeled upto a depth of 2000 μm. The model consists of three regions with different thermal properties at increasing depth. The greatest uncertainty about the values for thermal capacitance and conductance are in the stratum corneum region. However, since the skin consists of fats, proteins (mainly keratin) and water, it's thermal conductivity cannot be lower than that of it's least thermally conductive component namely keratin. Values for these constants were taken from Knox [28], assuming the stratum corneum consists of 5% water by weight, such that the thermal conductivity would be near the lower theoretical limit and highest temperatures would be reached.

The temperature at the deepest boundary was specified at 37°C, the core body temperature. The outer surface convects freely to the air at ambient temperature 25°C. The convection coefficient was chosen such that the skin surface temperature was 30°C. Along the symmetry axis, the boundary condition specified zero heat flow in the radial direction. Along the boundary at the outer edge of the disk the boundary condition also specified zero heat flow in the radial direction since the radial temperature gradient was expected to approach zero as the radius increases.

The data obtained in experiment 8 was analyzed to estimate the skin current at breakdown and the electropore density. The initial current (Iinitial) after capacitive currents had died

out, and the current just before breakdown (Ifinal) was measured for the four data sets and is shown in table 5.8.

Table 5.8. Comparison of initial current, measured after capacitive effects disappeared, with current level measured just prior to breakdown at various applied voltage levels, using data from experiment 8.

	12.5 V	15 V	18 V	21 V
Iinitial (uA)	0.46	0.61	1.1	2.1
Ifinal (uA)	6.0	10.1	17.1	35.1
Ratio	13.0	16.4	15.5	16.7

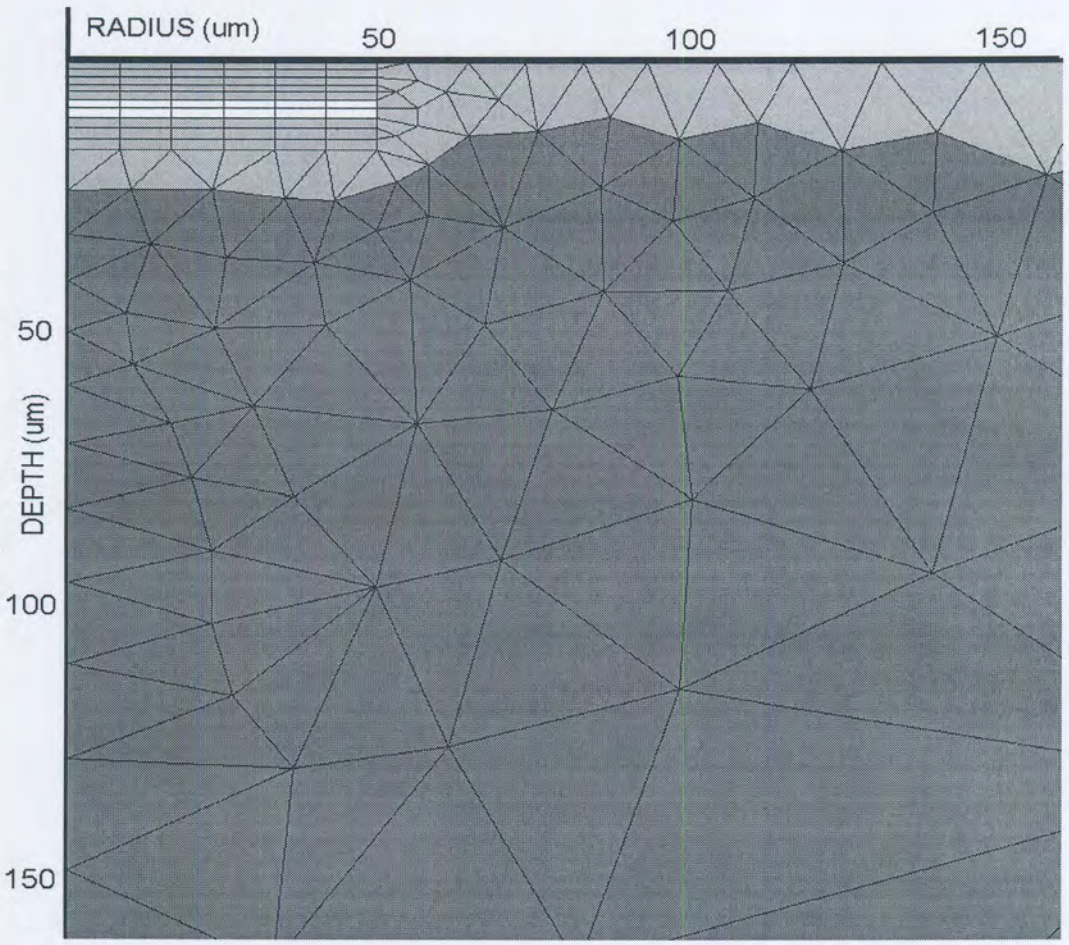

Fig. 5.15 2D axisymmetric finite element heat transfer model of the skin. A cylindrical 50 μm radius high conductivity defect in the stratum corneum is simulated. Joule heating of the skin is simulated by a volume heat flux applied to the white elements in the top left hand corner. Different shaded elements have different thermal properties. The left hand edge marked depth is axis of symmetry.

A high conductivity cylindrical defect through the skin is assumed. From Table 5.8. the mean current at breakdown for an applied potential of 21 V was 35 μA. We will estimate the temperature change in this condition, to obtain a worst case estimate of the temperature change. To calculate the radius of the defect the electropore density must be estimated. The ratio Ifinal/Iinitial (Table 5.8.) is about 15. Therefore the electropore density should have increased about 15 fold. The equilibrium electropore density is estimated at 10^6 cm^{-2} [3], therefore 10^8 cm^{-2} is an acceptable maximum guess. The membrane conductance at the defect is Gm = gN/m. In experiment 3, g and m were estimated to be 3×10^{-9} Ω^{-1} and 15 respectively. Therefore G is about 20×10^{-3} $\Omega^{-1}cm^{-2}$. Since the total resistance is 21 V / 35 μA ≐ 600 kΩ the area is 8300 μm^2 yielding a defect radius r=51 μm. With m=15 the height of the defect would be about 3 μm from which the volume is calculated. The value of the heat flux is calculated from $P = V^2/R/Volume = 30e\text{-}9$ J/s/μm^3. It is assumed that all power is dissipated in the defect.

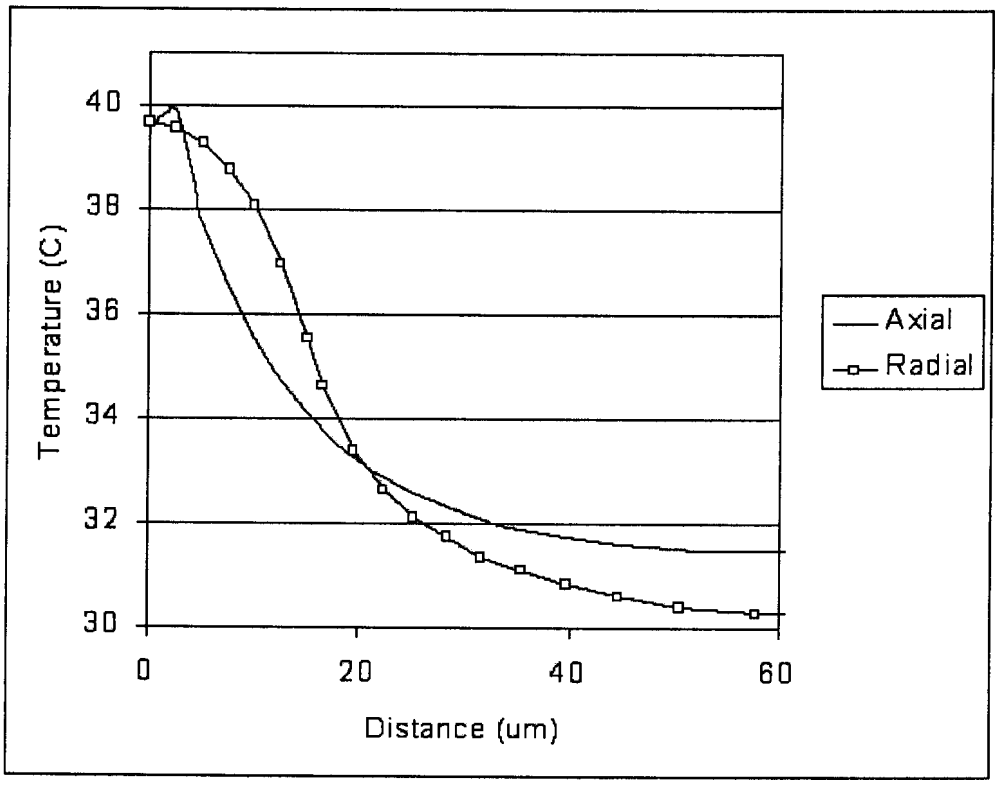

Fig. 5.16 Axial and radial heat distribution in the skin estimated with finite element model.

The result of the simulation is shown in Fig. 5.16. The temperature distribution along the symmetry axis is labeled "Axial". The model estimates the temperature increase at about

10°C. The actual temperature rise could easily be an order of magnitude lower, for the following reasons:

1. All estimates values are worst case estimates.
2. The effect of the metal electrode as heat sink was not included in the model.
3. The assumption that all current passes through a single defect is clearly unreasonable.

The model therefore supports the conclusion from experimental observations that heating was not the cause of the non-linear VCC of the skin, or of the breakdown effect. However, it does not rule out the possibility that joule heating of the skin can become significant after breakdown has occurred.

5.10 BREAKDOWN HYPOTHESIS

Experiments 6 and 7 disproved hypotheses regarding the cause of electrical breakdown of the dry skin found in literature, namely sweat gland activation [7] and electroosmotic filling of sweat ducts [9]. Experiments 12 and 13 disproved the hypothesis that breakdown occurs due to a thermal threshold being exceeded.

However, one possibility exists that could fit the observed data, although no direct experimental proof exists and several assumptions are necessary. The linear relation between the logarithm of time to breakdown and the applied voltage (Fig. 5.14) is also observed for the mean time to irreversible rupture of lipid bilayers, subject to an applied electric field [26]. Irreversible rupture of lipid membranes occurs when an electropore exceeds a certain critical radius at which point it's continued expansion becomes energetically favorable. This has been shown to be a stochastic process, with the mean time to failure at a particular voltage level distributed over an order of magnitude. This could account for the high variance of parameters related to the breakdown effect such as in Fig. 5.7. In a multi-lamellar system consisting of 15 bilayers in series, the failure of one bilayer, would increase the electroporation rate by a factor of 2 to 4 in the voltage range 13 V to 20 V. However in the stratum corneum bilayers occur in groups of five. The lipid bilayers are about 5.8 nm thick and are separated by water layers with a thickness of about 0.7 nm. It is conceivable therefore that the mechanical shock caused by the rupture of a membrane may induce the failure of neighboring membranes, already stressed by the electric field. In

addition the increased potential over the remaining membranes will shorten their lifetimes. A mechanical event could also be the cause of the unstable current curve (Fig. 5.2) frequently observed during breakdown. It is also notable that the ratio of initial current to current at the point of breakdown (Table 5.8.) stays relatively constant over the measured voltage range, which suggests that the degree of electroporation (i.e. number of defects in the membrane) at breakdown is independent of voltage.

Fig 4.8 shows an example of incomplete breakdown. It is hypothesized that the mechanical shock of membrane rupture disturbs the microscopic aqueous conductive pathway through the particular defect where rupture occurs. Occasionally, the pathway is disrupted sufficiently to break the connection, and the skin appears to recover instantaneously. After the incomplete breakdown, the current level is slightly lower than immediately before it, the curve appears to be shifted downwards. This could be due to one out of several parallel conductive pathways being eliminated.

The breakdown phenomenon does not occur during wet electrode stimulation [7],[9]. The hydration level of the lipid lamellae, especially the outer lamellae, are likely to be higher when the skin surface is wet. It is known that increased hydration increases the fluidity of the lipid membranes [33]. Hydration therefore affects the mechanical properties of the membrane, and they may become less likely to fail. Failure is most likely to occur in the outer membranes, since their hydration level is lowest and consequently their resistance would be the higher than deeper lipid bilayers. The voltage drop over them would therefore be greater. Under a wet electrode the total current is much higher than for a dry electrode, and the sensation quickly becomes unbearable, so that duration of the stimulus that can be applied may be too short at an adequate voltage level to induce membrane rupture.

The hypothesis of irreversible membrane rupture may seem contrary to the concept of reversible skin breakdown. However if the duration of the stimulus is not too long, some bilayers survive and partial recovery is possible. The recovery of the skin observed in experiment 9 and 10 therefore does not argue against this hypothesis. The lipid bilayers in the skin are known to be traversed by protein molecules that mechanically stabilize the membrane [13]. These would help to limit the extent of a defect caused by membrane rupture. It has been also shown that lipid bilayers are repaired if the right composition of lipids are present [25], as is likely to be the case in the skin. This could potentially account for the apparent healing of the skin over a 24 hour period observed in experiment 10.

6 EXPERIMENTAL CONCLUSIONS

6.1 Thermal effects

Evidence was found that thermal effects are not responsible for the skin breakdown or non-linearities of the VCC:

- An applied constant negative voltage results in a constant di/dt through the skin over a current range of more than an order of magnitude. Since the power dissipated in the skin is changing and the dependence of skin resistance on temperature is known to be non-linear, it appears unlikely that thermal changes are responsible for this constant di/dt (experiment 2).
- Heating was shown to increase di/dt (experiment 11), therefore since di/dt stays constant during constant voltage stimulation, joule heating was insufficient over the measured voltage range to cause thermally induced conductance changes in the skin.
- The theoretical skin temperature increase calculated with a finite element model is minimal over the measured voltage range (experiment 13). Worst case calculations showed a 10°C increase in skin temperature, with 1°C a more realistic value.
- The relationship between applied voltage and time to breakdown is not consistent with a thermal model of the skin (experiment 12)
- Heating could have affected the skin resistance after breakdown since the current density and consequent power dissipation increases significantly

6.2 Appendages

Evidence suggests that appendages are not involved to any significant degree during stimulation of the dry skin unless active sweating is taking place.

- The amperograms measured with a constant voltage stimulus during active sweating are similar in shape to those taken at lower ambient temperatures, with a constant offset (Fig. 5.6.) suggesting that the appendages act as shunt routes only when active. (Experiment 7)
- At ambient temperatures in the thermoneutral zone, the sweat ducts are empty [9]. It is logical therefore that they cannot act as low resistance sites in this condition.

- The constant di/dt observed is not consistent with electro-osmosis through the appendages (experiment 2)

The electrical breakdown of skin is not due to activation of sweat glands

- The time to breakdown measured statistically does not change when the sweat glands are activated by environmental conditions (experiment 7).
- Increasing the local skin temperature has a different effect on the skin VCC than the increasing ambient temperature (experiment 7 and 11). It is therefore unlikely sweat glands are activated by highly localized increases in skin temperature.
- The capacitive current decay time constant for square pulses does not increase after breakdown as would be expected if sweat glands were activated. Instead it appears to decrease, which is here postulated to be due to the lower stratum corneum resistance after breakdown (Fig. 5.3).
- Breakdown was observed on the human lips, which are devoid of sweat glands (experiment 3)

6.3 Electroporation

Strong evidence was found that electroporation occurs on the dry stratum corneum in the range between 10-20 V.

- Electroporation appears to be the only known phenomenon consistent with the constant di/dt observed during constant voltage pulsing (Experiment 2).
- The hypothesis that electroporation occurs in a small percentage of the stratum corneum where the usual 70-100 lipid bilayers are reduced to around 15, is supported by experimental data from unrelated aspects of electroporation.
- The theoretical non-linear dependence of electropore conductance on voltage fits the experimentally observed data for parameters close to those measured on artificial bilayer membranes (experiment 3).
- The theoretical dependence of the rate of electroporation on the square of the applied voltage fits the experimentally observed data for parameters close to those measured on artificial bilayer membranes (experiment 3).
- The recovery rate after breakdown is consistent with the natural rate of electropore destruction (experiment 9).
- Non-uniform current distribution was observed experimentally (experiment 5) and is supported in literature [1],[6],[7],[20].

- The high variability of the data (experiment 3 and 8) is consistent with the hypothesis that a few localized sites are responsible for current conduction and that the conductivity of these sites depend on the number of bilayers in series which varies from site to site.
- The distortions observed during sinusoidal stimulation (experiment 1) appear to be consistent with an electroporation model. The current is exaggerated at voltage peaks and depressed at voltage minima as expected from the theoretical electropore voltage-current relation. The gradual increase in current amplitude at higher voltages follows from a gradual increase in the electropore population.

6.4 Electro-osmosis

Circumstantial evidence was found that electro-osmosis plays a role in determining skin impedance (experiment 4).

- The shape of amperograms for positive voltage pulses observed for skin are qualitatively similar to those observed for Ag/AgCl electrodes in saline solution when conditions suitable for electro-osmosis are present.
- The rectification observed cannot be due to different electro-chemical reactions during positive and negative cycles or to a concentration overpotential, since there is a gradual shift from the high to low conductance states and vice versa after the voltage polarity is inverted. This observation can be explained by electro-osmosis.
- Evidence suggests that the resistance increase during positive cycles probably occurs in the lipid membranes. The only factor found in literature that could affect the lipid bilayer resistance, except for electroporation, is the level of hydration of the inter-bilayer spaces [33].

6.5 Trans-epidermal water loss (TEWL)

In order to observe all the skin impedance phenomena, the required duration of stimulation is in the order of seconds. Over this period, accumulation of moisture under the electrode due to insensible water loss was found to influence the skin impedance (experiment 1)

7 MODEL OF THE SKIN

7.1 INTRODUCTION

In accordance with the described experimental observations, it is hypothesized that the VCC of the skin is primarily due to three phenomena, namely electroporation, electro-osmosis and TEWL. Electric current is conducted through the skin either through the stratum corneum lipid-corneocyte matrix or through appendages such as sweat glands [3,7]. It is hypothesized that in the dry stratum corneum, when active sweating is not taking place, the appendages do not act as current conductors. In the stratum corneum, the lipid bilayers act as the primary current barrier and the primary contributor to charge storage. Therefore the electric circuit used to model the skin consists of those components that represent the lipid bilayers. According to Chizmadzhev [3] Fig 4.15 is suitable. G_m and C_m represents the conductance and capacitance of the lipid bilayers and G_e the conductance of the rest of the body and the electrode-skin interface.

Fig 7.1 shows the final model. This is the same circuit shown in Fig 4.15 with the addition of a single conductance G_i. G_i is included to model the effect of moisture accumulating under a dry electrode due to TEWL. In models that are generally derived for wet skin, G_i does not play a role. Previous dry electrode models have not attempted to model the effect of TEWL. Strictly speaking, a second capacitance C_i should also be introduced to model the corresponding increase in capacitance. However C_i has been lumped with C_m. C_m therefore has a constant component related to the lipid bilayers and a time varying component related to the effect of TEWL. G_i was not lumped with G_m since G_m is already a function of voltage and time.

The theoretical description of electroporation by Indenbom [13] and Chizmadzhev [14] was used to describe the effect of electroporation on the skin lipid bilayers (G_m) using experimentally derived parameters applicable to the dry skin condition.

Since it was found experimentally that electro-osmosis occurs within the lipid bilayers and therefore influences the lipid bilayer resistance directly, the theoretical description of G_m according to Chizmadzhev [14] was modified to include the hypothetical effect of electro-osmosis. Since the existing theoretical description of electro-osmosis is not applicable to this situation, equations were introduced to model the effect of electro-osmosis that would

describe the rectification observed in experiment 4 and be consistent with the current dependence of electro-osmotic transport from Grimnes [9].

The resulting system of ordinary differential equations were solved simultaneously using MATLAB.

7.2 MATHEMATICAL MODEL

The voltage U_m over the lipid bilayers is calculated for the circuit in Fig 7.1 using the differential equation:

$$\frac{dU_m}{dt} = \frac{(V_s - U_m)\cdot G_e - U_m \cdot (G_m + G_i \cdot A_i)}{C_m \cdot A_i} \tag{7.1}$$

where Vs is the voltage applied over the skin. Ai is the effective electrode due to TEWL (insensible perspiration). Ge is the combined conductance of the electrode-skin interface and the rest of the body. A value of 40 kΩ was assigned. The actual value (estimated using two large pregelled electrodes) was less than 1 kΩ. However since the values of the other elements were in the order of megohms, the larger Ge value used in simulation had a minimal effect on the result and promoted numerical stability of the model. Cm was assigned 1nF and Gi 200 nS, approximating the values of Cm and Gi calculated in experiment 1.

Ai has an initial non-zero value and increases linearly according to

$$A_i = A_0 + K_i \cdot t \tag{7.2}$$

A0 was chosen as 1 and Ki to be 0.125 such that the area doubles after 8 seconds, to approximate the behavior in Fig. 4.1.

Gm was calculated according to Chizmadzhev [3], modified by the factor $1/K_{osmosis}$ to simulate the effect of electro-osmosis.

$$G_m = \frac{1}{K_{osmosis}} \cdot \frac{g \cdot N \cdot A}{m} \tag{7.3}$$

$K_{osmosis}$ is calculated in (7.7). N the number of electropores per lipid bilayer, calculated in (7.4). The number of lipid bilayers in series.in the stratum corneum, m was determined to be 15 in experiment 3. A is the combined area of the defects where current is conducted

through the stratum corneum. An order of magnitude estimation was made for this parameter by taking the initial skin conductance (V/Iinitial) from table 5.8. and dividing by the expected conductance per cm^2 assuming the equilibrium electropore concentration to be 10^6 cm^{-2} [3] and estimating the electropore conductance at 3×10^{-9} from experiment 3. The value used was 100×10^{-6} cm^2, however since the defect size primarily influences the amplitude of the current when the voltage is sufficient to cause electroporation and electro-osmosis, a wide range of values would be valid for this parameter, considering the wide variation in the measured skin resistance.

The rate of change in the electropore population N was determined according to Chizmadzhev [3].

$$\frac{dN}{dt} = K \cdot \left[\exp(\alpha \cdot \left(\frac{U_m}{m} \right)^2 - \frac{N}{N_0} \right] \tag{7.4}$$

N_0 is estimated at 10^6 [3]. According to the values derived in experiment 3, $m = 15$, $\alpha = 4.8V^{-2}$, $K = 10^3$ $s^{-1}cm^{-2}$.

The electropore conductance was calculated according to Chernomordik [26]

$$g = \frac{M_g \cdot (w_0 - z)}{w_0 \cdot \exp(w_0 - z) - z} \quad \text{where} \quad z = \frac{n \cdot \beta \cdot |U_m|}{m}, \; M_g = \frac{R^2 HN}{h} \tag{7.5}$$

where h (=5 nm) the membrane thickness, R (=h/2) the external radius of the pore entrance, H (=1.3 S/m) the specific conductivity of the bulk solution, $\beta = e/(kT)$ (6.5×10^{-40}) with e the electron charge, n the relative size of the entrance region of the pore (=0.15), k Boltzman's constant and T the temperature (=293 K) [16]. The parameters $w_0 = 1.8\ kT$, and $m = 15$.

It was hypothesized based on experiment 4 that electro-osmosis occurs within the lipid bilayers of the skin, however the description of electro-osmosis in the literature would not adequately describe this situation. Equations were therefore determined to describe the observed behavior. Grimnes [9] described the electro-osmotic flow rate as proportional to the current through the relevant area. In accordance with this equations were determined for the flow rate

if Um > 0

$$\frac{dH}{dt} = k_1 \cdot U_m \cdot G_m \tag{7.6}$$

else

$$\frac{dH}{dt} = -k_2 \cdot U_m \cdot G_m \cdot H \tag{7.7}$$

(7.6) describes the flow rate *dH/dt* as proportional to the current through G_m during positive cycles, in accordance with Grimnes [9]. H therefore is a measure of the amount of water transported away from the area under the electrode. The parameter k_1 was empirically determined to be 10^9.

(7.7) describes how water transported away from the electrode (H), returns during negative cycles. It was observed experimentally (Fig. 4.19) that at the onset of negative pulses the conductance decrease, due to the previous positive cycle, is quickly negated, after which further conductance increases are due to electroporation rather than electro-osmosis. Therefore it was assumed that H returns to zero during negative cycles at a rate determined by the current through G_m. Parameter k_2 equalled -10^{11}. According to (7.7), H cannot become negative, implying that negative potentials cannot increase the hydration level beyond its original value. This is clearly not consistent with the hypothesis that electro-osmosis occurs. In reality a non-linear relationship probably exists between the conductance of the lipid bilayers and their percentage hydration. The lipid bilayer conductance may only be strongly dependant on the hydration level at low levels of hydration, such that at normal hydration, a quantity of water must first be transported away before the bilayer conductance is affected. This would also explain the delay after onset of a positive pulse, before the skin conductance decreases.

H affects G_m through the parameter $K_{osmosis}$.

$$K_{osmosis} = 1 + k_3 \cdot H \tag{7.8}$$

$K_{osmosis}$ increases linearly from one as H increases. G_m is proportional to $1/K_{osmosis}$, such that the impact of a particular increase in $K_{osmosis}$ becomes less as $K_{osmosis}$ increases and G_m can never reach zero. The parameter k_3 was empirically determined to be 0.02.

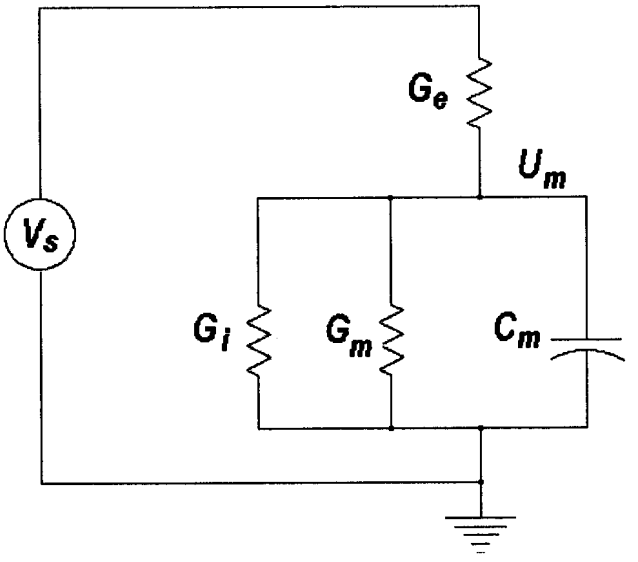

Fig 7.1 Electrical model of the skin

The dry skin is therefore modeled through the simultaneous solution of (7.1) - (7.8).

7.3 SIMULATION RESULTS

The results of simulation with the model are shown together with skin measurements taken at the same frequency and amplitude. It is important to emphasize that the magnitude of the skin impedance at the same applied voltage amplitude and frequency varies widely from sample to sample. Nevertheless the phenomena that are being modeled, namely non-linearity and asymmetry were observed to manifest consistently over the same voltage and frequency ranges, for measurements done on the same type of skin (e.g. skin of the stomach of a particular individual). Therefore the shapes of the current curves remain compatible, despite large variations in amplitude. This is hypothesized to be due to large variations in the sizes or number of local defects in the stratum corneum. For this reason it is more important to compare simulated and measured graphs qualitatively rather than quantitatively. All simulations were done assuming the same defect size. Quantitative similarity with a particular measured graph could be achieved by adjusting the defect size on the simulation.

On the following pages measured results shown in Fig 4.1 - 4.5 are reproduced alongside the simulated results for easy comparison.

7.3.1 20 Vpp 28 Hz

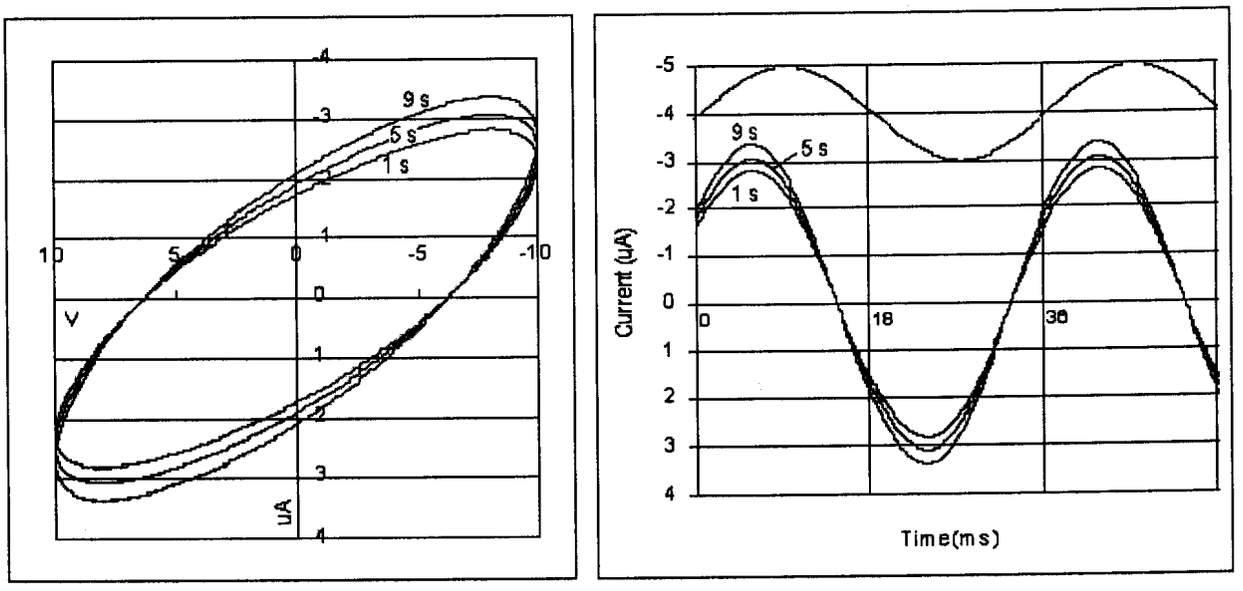

Fig. 7.2 Simulated VCC at 20 Vpp, 28 Hz. The voltage phase is shown above current curves.

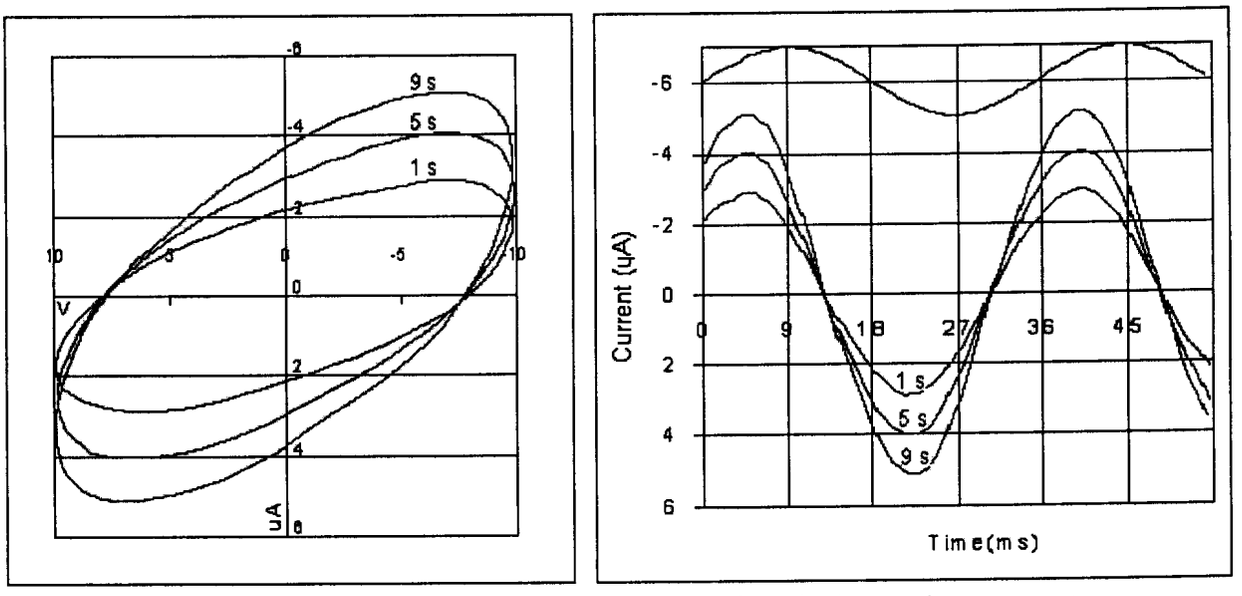

Fig. 7.3 Measured skin VCC at 20 Vpp, 28Hz. The voltage phase is shown above current curves.

As in the measured result (Fig 7.3), no asymmetry or non-linearity is observed on the simulated graph (Fig 7.2). The current curves intersect at the horizontal axis on the Lissajous plots and the time based graphs. In both figures the current increases linearly with time. In the measured example the capacitance is larger relative to the conductance than used in the simulation, therefore the intersection of the simulated Lissajous loops with the V = 0 axis (Fig 7.2) is relatively lower than in Fig 7.3. The rate at which the area increases (K_i in (7.2)) is lower in the simulation than for this particular comparative measurement.

7.3.2 20 Vpp 14 Hz

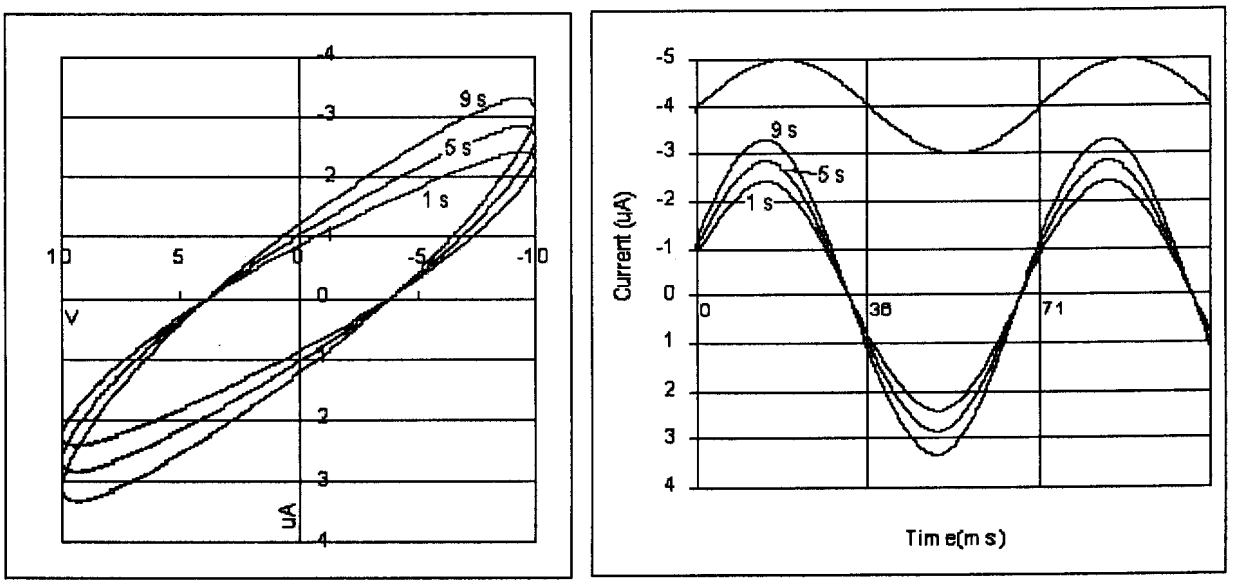

Fig. 7.4 Simulated VCC at 20 Vpp, 14 Hz. The voltage phase is shown above current curves.

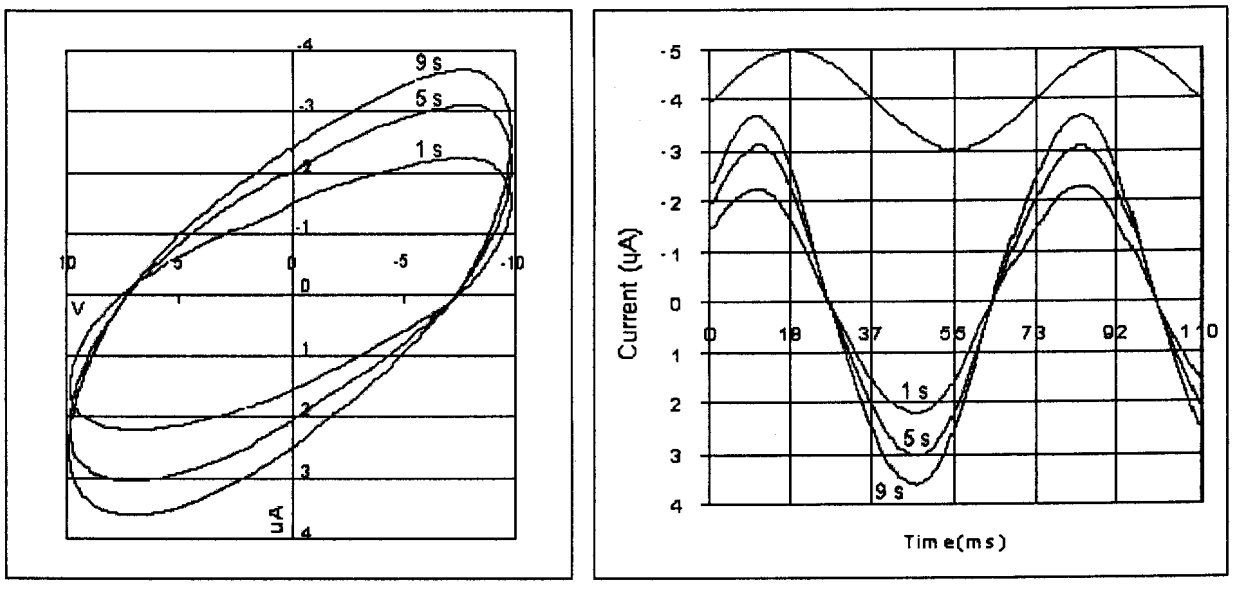

Fig. 7.5 Measured skin VCC at 20 Vpp, 14 Hz. The voltage phase is shown above current curves.

As in the measured result (Fig 7.5), no asymmetry or non-linearity is observed on the simulated graph (Fig 7.4). The current curves intersect at the horizontal axis on the Lissajous plots and the time based graphs. In both figures the rate of current increase is nearly lineary with time. In the measured example the capacitance is larger relative to the conductance than used in the simulation, therefore the intersection of the simulated Lissajous loops with the V = 0 axis (Fig 7.4) is relatively lower than in Fig 7.5. The rate at which the area increases (K_i in (7.2)) is lower in the simulation than for this particular comparative measurement.

7.3.3 40 Vpp 28 Hz

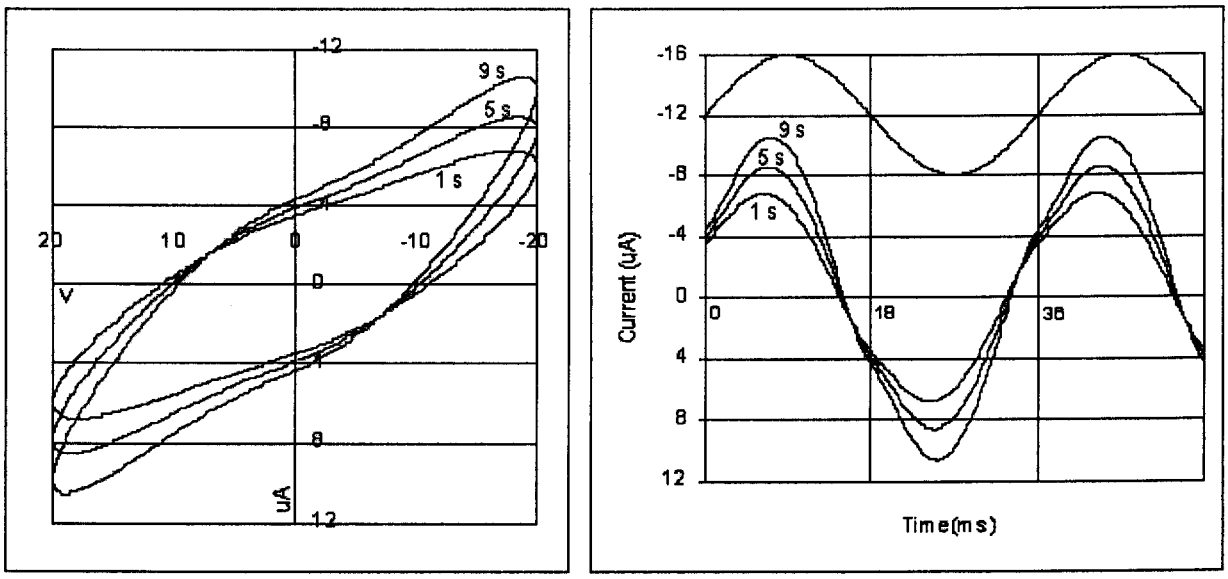

Fig. 7.6 Simulated VCC at 40 Vpp, 28 Hz. The voltage phase is shown above current curves.

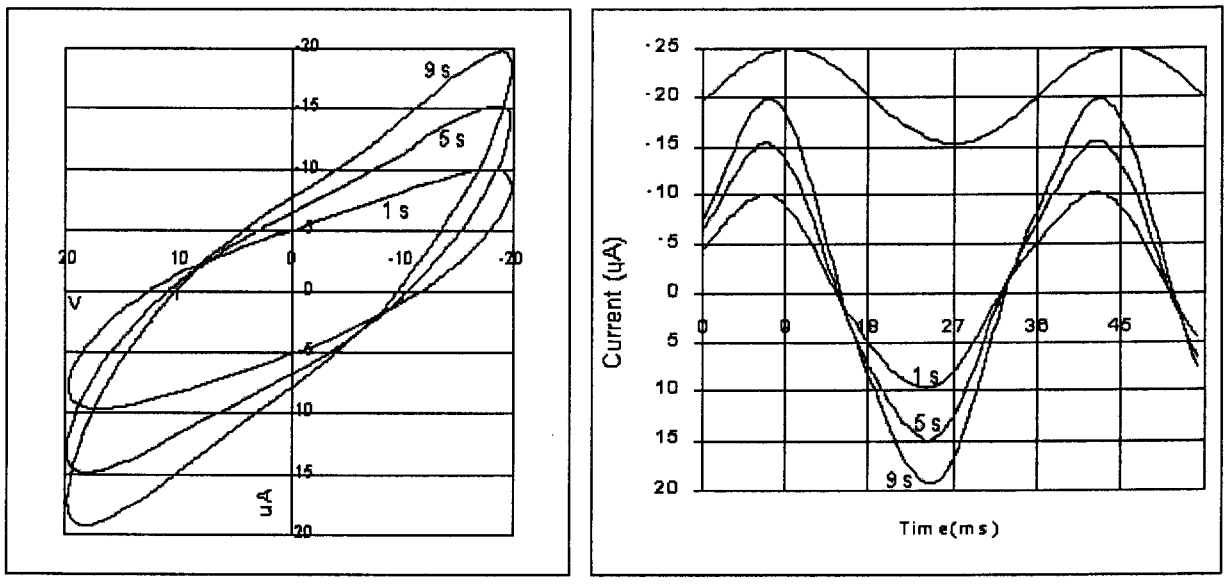

Fig 7.7 Measured skin VCC at 40 Vpp, 28Hz. The voltage phase is shown above current curves.

When the stimulus amplitude is increased to 40 Vpp, non-linearity becomes prominent while the graphs remain virtually symmetrical. In both the simulation and the measured graphs the VCC is initially nearly linear (t = 1 s). With increasing time the current peaks become exaggerated, with the increment being linear over time.

7.3.4 40 Vpp 14 Hz

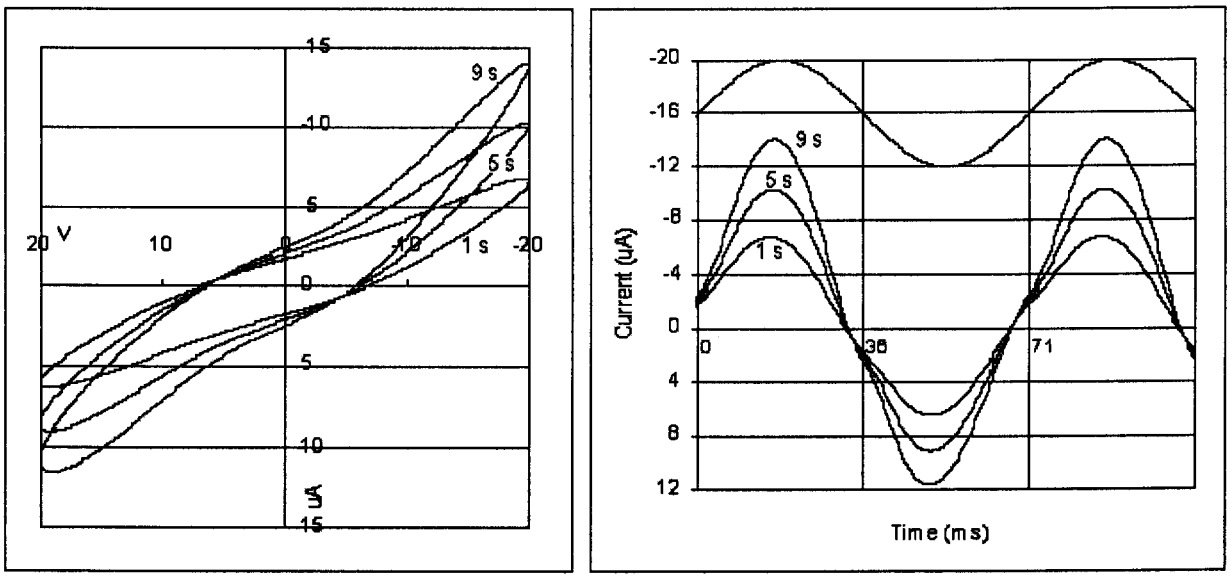

Fig. 7.8 Simulated VCC at 40 Vpp, 14 Hz. The voltage phase is shown above current curves.

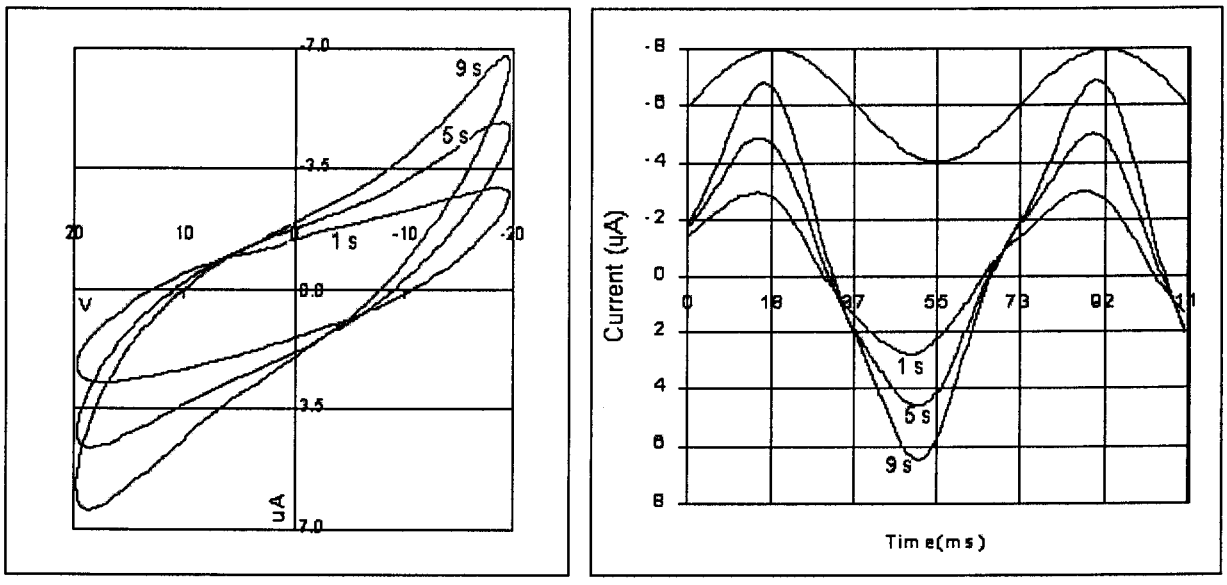

Fig.7.9 Measured skin VCC at 40 Vpp, 14 Hz. The voltage phase is shown above current curves.

As the frequency is reduced from 28 Hz to 14 Hz, the simulated and the measured figures start to become asymmetrical. Both figures are initially (t = 1 s) non-linear but almost symmetrical. With increasing time, the current peaks during negative cycles (upper peaks) become sharper and higher than during positive cycles (lower peaks). In the simulated graph (Fig 7.8) the current peaks during positive cycles is lower relative to current peaks during negative cycles than in the measured result (Fig 7.9) for t > 1 s. The model therefore overestimates the degree of rectification at extended simulation times.

7.3.5 40 Vpp 3 Hz

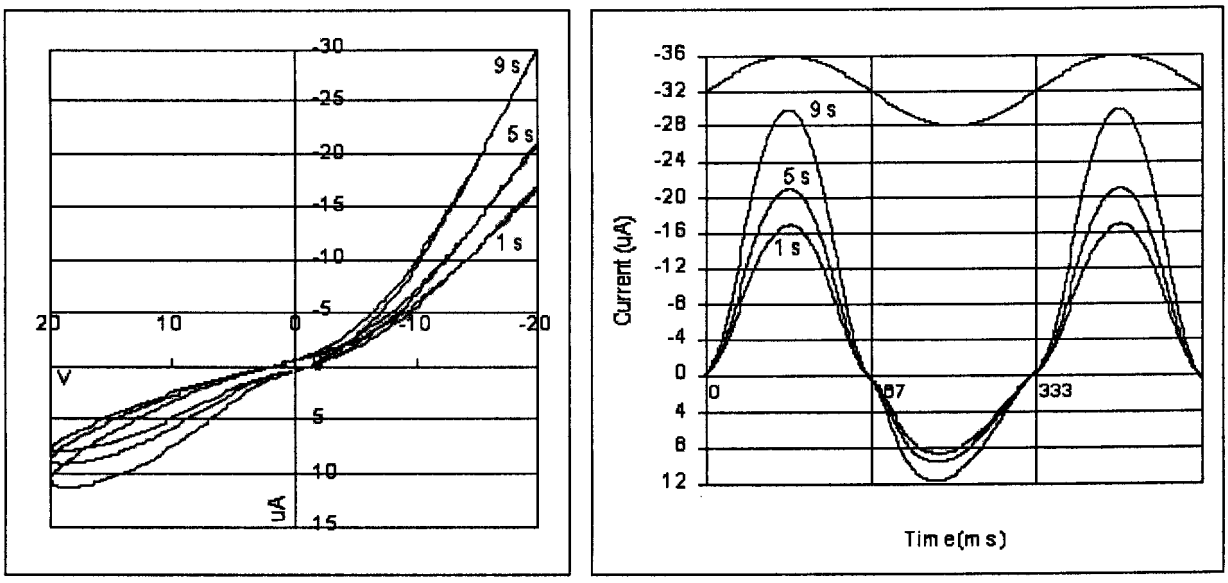

Fig 7.10 Simulated VCC at 40Vpp, 3Hz. The voltage phase is shown above current curves.

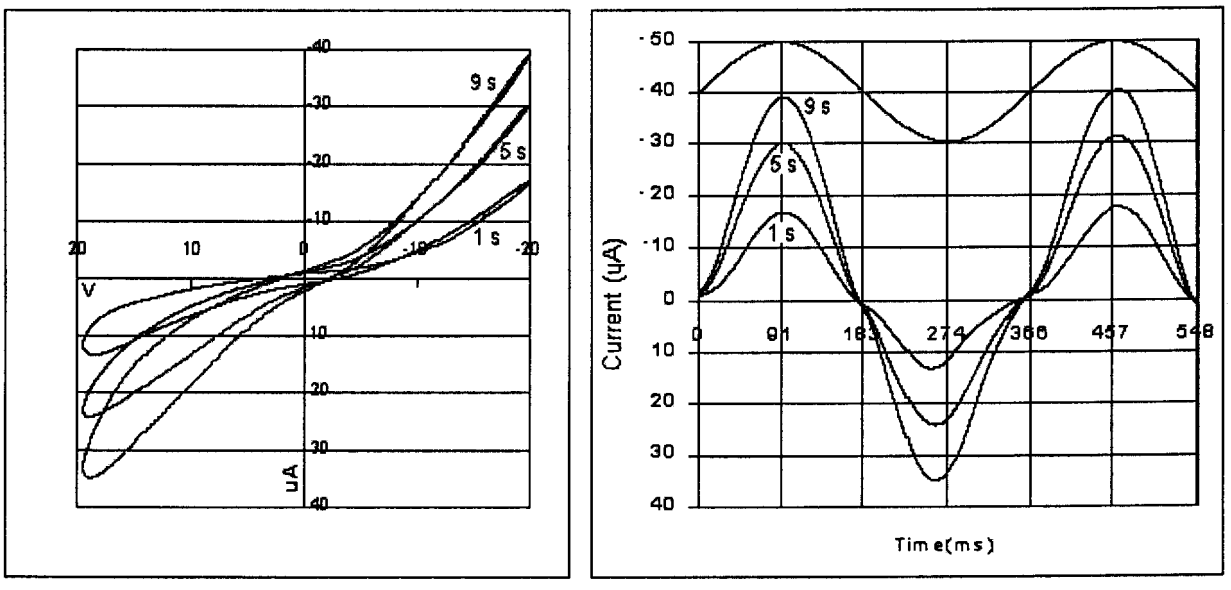

Fig. 7.11 Measured skin VCC at 40 Vpp, 3 Hz. The voltage phase is shown above current curves.

At 3 Hz both asymmetry and non-linearity is evident from the onset of stimulation on both the measured and simulated figures. In the simulated graph (Fig 7.10) the current peaks during positive cycles is lower relative to current peaks during negative cycles than in the measured result (Fig 7.11). The model therefore overestimates the degree of rectification. The rate of current increase in the measured graph (Fig 7.11) appears to slow down after 5 seconds. This could be due to the electropore density reaching a saturation point.

7.3.6 Square Wave

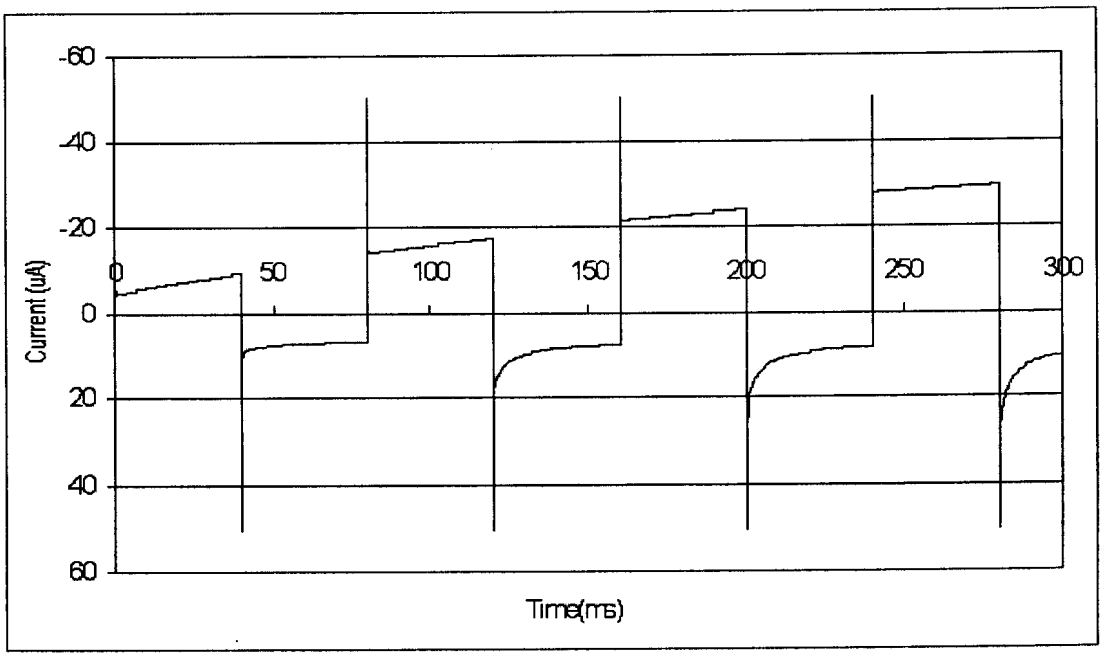

Fig. 7.12 Simulated skin current due to bipolar square wave stimulation.

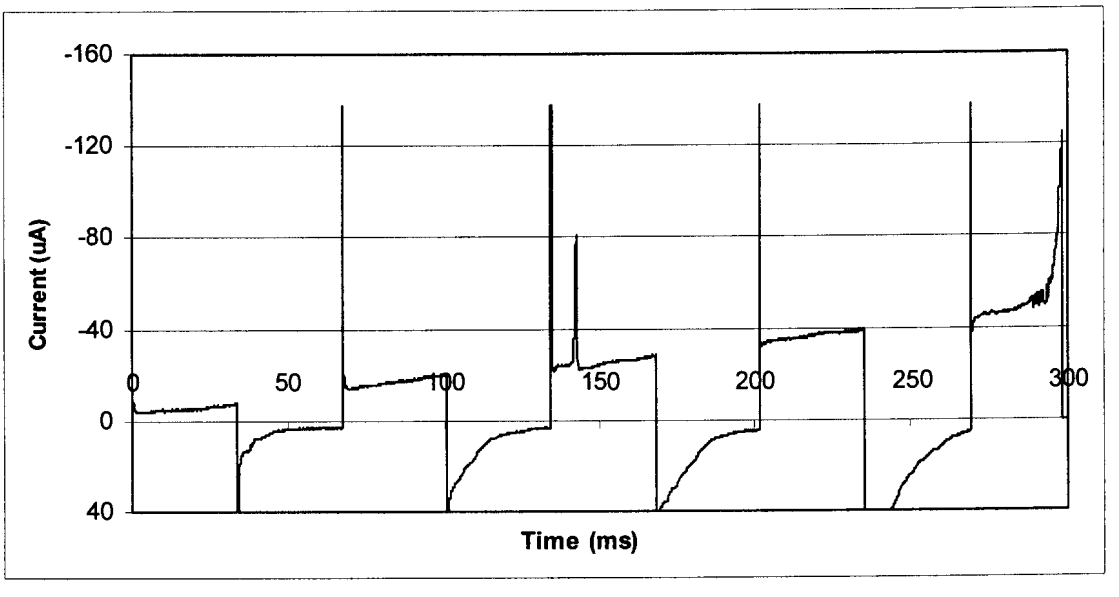

Fig. 7.13 Measured skin current due to bipolar square wave stimulation (Fig 4.8).

The versatility of the model is emphasized by the favorable comparison between measured and simulated results for square wave stimulation. The current increases linearly during negative cycles. During positive cycles the current is rectified, while simultaneously the linear conductance increase continues independent of stimulus polarity. The conductance increase only becomes evident at the start of the next negative cycle.

8 DISCUSSION AND SUMMARY

8.1 ELECTRICAL MODEL OF THE SKIN

Good correspondence between simulated and measured results was obtained. The model can account for all the skin impedance phenomena observed over the investigated voltage and frequency range, except the electrical breakdown. The least successful part of the model is the modeling of the positive phase rectification. Comparison of Fig. 7.10 with Fig. 7.11 shows that the positive current peaks are too low compared with the negative current peaks at extended simulation times. Clearly this aspect of the skin VCC needs further investigation before it can be accurately modeled. The relationship between the percentage hydration of the lipid bilayers and their conductance is not accurately quantified. Furthermore, modeling of the electro-osmotic flow within these layers is beyond the scope of this study. Other effects may need to be taken into account. For example, it is possible that electroporation of the lipid membranes may influence the degree to which electro-osmosis can affect the percentage hydration of these membranes. A reservoir of water is known to exist in the corneocytes on either side of the lipid bilayers. When the lipid membrane is highly porated, water may be able to enter the membrane more easily during electro-osmosis. This could reduce the influence of electro-osmosis on the hydration level of the lipid bilayer, since water which is transported away is replenished from the external reservoir.

8.2 DIAGNOSTIC INFORMATION HYPOTHESIS

It was stated in the introduction that one of the study goals was to lay the foundation for an explanation of the variable rectification at skin zones related to diseased or healthy internal organs seen by Szopinski et al [4]. The authors stimulated the skin on the ear auricle with a dry point electrode (diameter 1 mm) at points that are thought to correspond to particular internal organs, until breakdown occurred. They then measured the skin resistance at the point with the point electrode polarized first negatively (Rneg) and then positively (Rpos) to determine the ratio Rneg / Rpos. It was observed by the authors that at points corresponding to internal organs where tissue damage was present (due to pathology), the

ratio Rneg / Rpos tended towards zero, whereas at points corresponding to healthy organs the ratio tended towards one. Therefore, the degree of rectification measured after inducing breakdown at the skin zone on the ear auricle depended on the health condition of the particular internal organ linked to that zone.

From the conclusions of this study a hypothesis can be advanced to explain how internal organs could cause electrical rectification at remote skin zones. Szopinski hypothesized that diseased or damaged organs may cause antidromic stimulation of sensory nerves that reach the skin [39]. It is well known that antidromic stimulation of sensory nerves result in increased capillary membrane permeability [40]. This allows extravasation of protein molecules (mainly albumin) in the blood plasma [41],[42]. Intercellular fluid has the same composition as blood plasma except that the concentration of protein in blood plasma is much higher than in intercellular fluid [41],[42]. Ordinarily the large protein molecules cannot permeate through the capillary wall.

The protein molecules are negatively charged. Therefore during positive cycles, the protein molecules in the extracellular fluid are attracted to the electrode on the skin surface. The albumin molecule is an ellipsoid 38 by 150 Å [42]. The estimate of w0 = 1.6 kT in experiment 6 translates to an electropore diameter of about 63 Å (from the relation r = 5nm/w0 [16]). The protein molecules are too big to enter the electropores in the lipid bilayer. Instead they block the electropores, reducing conductance during positive cycles. It was shown by Chernomordik [43] that large molecules act as pore blockers in electroporated bilayer membranes, if the size of the molecule is comparable to the electropore diameter. The current during positive cycles is therefore dependent on the concentration of blood plasma proteins in the extracellular fluid, which is in turn dependent on the frequency of nervous impulses reaching the skin.

It was observed during this study that rectification occurs at high voltages before the skin breaks down (Fig. 4.8, 4.5). This was ascribed to electro-osmosis. After breakdown the lipid bilayer membranes are highly porated, which may reduce the rectifying effect of electro-osmosis, as explained previously. This could account for the lack of rectification seen by Szopinski et al [4] at sites related to healthy organs.

8.3 SUMMARY OF RESEARCH CONTRIBUTIONS

8.3.1 Electroporation

The theoretical description of electroporation in bilayer membranes derives from Indenbom [13] and Chizmadzhev [14]. The electrical properties of in-vitro skin in the voltage range 30-50 V had been attributed to electroporation by Pliquett [2], Chizmadzhev [3], and Indenbom [13]. The hypothesis that electroporation is primarily responsible for the non-linear nature of the VCC of the dry skin is new, as well as the explanation why electroporation in the voltage range 10-20 V would not have been observable in the experiments described in [2],[3] and [13], namely that in-vitro skin that had been soaked in electrolyte solution, would not exhibit electroporation because in the lower voltage range the sweat ducts would predominate as current conductors and obscure the relatively small current attributable to electroporation of the stratum corneum. In addition duration of the measurement pulses used in [2], [3] and [13] were too short to induce significant electroporation in the lower voltage range. In order to substantiate this hypothesis measurements were done on various aspects of the skin VCC in the voltage range 10-20 V (experiment 3) from which it was inferred that these measured results are predicted by the theoretical description provided by [13] and [14].

The contribution of this research to the modeling of electroporation is furthermore that the theoretical description of electroporation given by [13] and [14] with the experimentally determined values of parameters such as effective electrode area etc. and the values of parameters derived from experiment 3 led to the conclusion that areas of electroporation in dry skin should be modeled as 15 bilayers in series.

8.3.2 Electro-osmosis

The asymmetry of the skin VCC had been attributed to electro-osmosis by previous authors ([6] and [9]). These authors suggested that water is electro-osmotically transported through the sweat ducts. This idea has been questioned by other authors and was excluded from the more recent model presented by Panescu [7]. The hypothesis confirmed by the experiments reported here is that electro-osmosis may instead occur within the microscopic spaces between the lipid bilayers, since the aqueous regions between these layers is thought to be the primary route of ionic transport through the lipid bilayers. The evidence in support of this hypothesis is presented in experiment 4. A further contribution of this

research is to indicate that the existing mathematical description of electro-osmosis would not be applicable in this situation. Based on this hypothesis equations were introduced to model the effect of electro-osmosis that would describe the rectification observed in experiment 4 and be consistent with the current dependence of electro-osmotic transport from [9].

8.3.3 Trans-epidermal water loss

TEWL is a well known phenomenon. Although other authors have indicated that the collection of moisture due to TEWL under a dry electrode would decrease the impedance, it has not been explicitly included in previous dry electrode models, as done in the models presented in this dissertation.

8.3.4 Skin Breakdown Hypothesis

Experiments 6 and 7 disproved hypotheses regarding the cause of the resistance breakdown of the dry skin found in literature, namely sweat gland activation [7] and electroosmotic filling of sweat ducts [9]. A new hypothesis is reported here, namely that breakdown is due to rupture of the lipid bilayer membranes in the stratum corneum. Evidence in support of this hypothesis is presented in section 5.10.

8.3.5 Diagnostic information hypothesis

Szopinski et al [4] reported a dependence of the electrical parameters of the skin on the health status of internal organs. A hypothesis is presented here (section 8.2) that is a first attempt to explain this phenomenon.

9 REFERENCES

1 MR Prausnitz, The effects of electric current applied to skin, *Advanced Drug Delivery Reviews*, vol. 18, pp. 395-425, 1996.

2 U Pliquett and R Langer, Changes in the passive electrical properties of the human stratum corneum due to electroporation, *Biochim. Et Biophys. Acta*, vol. 1239, pp. 111-121, 1995.

3 YuA Chizmadzhev, Electrical Properties of skin at moderate voltages: Contribution of appengeal macropores, *Biophysical J.*, vol. 74, pp.843-856, 1998.

4 J Szopinski, D Pantanowitz and G Jaros, Diagnostic accuracy of organ electrodermal diagnostics, *SAMJ*, vol. 88, pp. 146-150, 1998.

5 JL Mason and NAM Mackay, Pain sensations associated with electrocutaneous stimulation, *IEEE Trans. Biomed. Eng.*, vol. 23, pp. 405-409, 1976.

6 T Yamamoto, Y Yamamoto and A Yoshida, Formative mechanisms of current concentration and breakdown phenomena dependent on direct current flow through the skin by a dry electrode, *IEEE Trans. Biomed. Eng.*, vol. 33, pp. 396-404, 1986.

7 D Panescu and JG Webster, A Nonlinear Electrical Thermal Model of the Skin, *IEEE Trans. Biomed. Eng.*, vol 41, pp. 672-679, 1994.

8 T Yamamoto and Y Yamamoto, Non Linear Electrical properties of the skin in the low frequency range, *Med.& Biol. Eng & Comput.*, vol. 19, pp. 302-310, 1981.

9 S Grimes, Skin impedance and Electro-Osmosis in the human epidermis, *Med. & Biol. Eng. & Comp.*, vol. 21, pp. 739-749, 1983.

10 WHM Craane-van Hinsberg, JC Verhoef, HE Junginger and HE Bodde, Thermoelectrical analysis of the human skin barrier, *Thermochimica Acta*, vol. 248, pp. 303-318, 1995.

11 R Potts and R Guy, Routes of ionic permeability through the mammalian skin, *Solid State Ionics*, vol. 53-56, pp.165-169, 1992.

12 DR Revis, Skin Anatomy in *http://www.emedicine.com/plastic/topic389.htm*, Shahin Javaheri, Ed., July 25, 2001

13 AV Indenbom and PI Kuzmin, Changes in the Electrical Properties of the Skin Outermost Layer during Pulse Electrotreatment, *Membr. Cell Biol.*, vol. 11, pp. 367-380, 1997.

14 YuA Chizmadzhev, V Zamitsin, JC Weaver and R Potts, Mechanism of electroinduced ionic species transport through a multilamellar lipid system, *Biophysical J.*, vol. 68, pp. 749-765, 1995.

15 T Yamamoto, Y Yamamoto, Electrical properties of the epidermal stratum corneum, *Med. Biol. Eng.*, vol. 14, pp. 151-158, 1976.

16 R Glaser, S Leikin, L Chernomordik, V Pastushenko a A Sorkirko, Reversible electrical breakdown of lipid bilayers: formation and evolution of pores, *Biochim. et Biophys. Acta*, vol. 940, pp. 275-287, 1988.

17 DA Edwards, A linear theory of transdermal transport phenomena, *J. Pharm. Sci, vol. 83*, pp. 1315-1334, 1994.

18 S Grimnes, Pathways of ionic flow through human skin in vivo, *Acta Dermato-Venereologica*, vol. 64, pp 93-98, 1984.

19 RR Burnette and D Marrero, Comparison between the iontophoretic and passive transport of thyrotropin releasing hormone across excised nude mouse skin, *J. Pharm. Sci.*, vol. 75, pp 738-743, 1986.

20 D Panescu and JG Webster, The Mosaic Electrical Characteristics of the Skin, *IEEE Trans. Biomed. Eng.*, vol. 40, pp. 434-439, 1993.

21 C Cullander and RH Guy, Sites of iontophoretic current flow into the skin: identification and characterization with the vibrating probe electrode, *J. Invest. Derma.*, Vol 97, pp 55-64, 1991.

22 JA Bouwstra, MA De Vries, GS Gooris, W Bras, J Brussee and M. Pone, Thermodynamic and structural aspects of the skin barrier, *J. Controlled Release*, vol. 16, pp. 209-220, 1991.

23 JA Bouwstra, GS Gorris, JA van der Spek and W Bras, The structure of human stratum corneum determined with small angle X-ray scattering, *J. Invest. Dermatol.*, vol. 97, pp. 1005-1012, 1991.

24 RO Potts, GM Golden, ML Francoer, VHW Mak and RH Guy, Mechanism and enhancement of solute transport across the stratum corneum, *J. Controlled Release*, vol. 15, pp. 249-260, 1991.

25 UF Pliquett and CA Gusbeth, Perturbation of human skin due to application of high voltage, *Bioelectrochem. and Bioenerg.*, vol. 51, pp. 41-51, 2000.

26 L Chernomordik, SI Sukharev, SV Popov, V Pastushenko and A Sorkirko, The electrical breakdown of cell and lipid membranes: the similarity of phenomenologies, *Biochim. et Biophys. Acta*, vol. 902, pp. 360-373, 1987.

27 A Vader, J Sherman and D Luciano, *Human Physiology: The mechanisms of body function 7th Edition*, Boston MA: WCB McGraw Hill, 1998.

28 FS Knox, TL Wachtel, GR McCahan and SC Knapp, Thermal properties calculated from measured water content as a function of depth in porcine skin, *Burns*, vol. 12, pp. 556-562, 1986.

29 S Grimnes, Dielectric breakdown of human skin in vivo, *Med. & Biol. Eng. & Comput.*, vol. 21, pp. 379-381, 1983.

30 MR Neuman, Biopotential Electrodes, in *Medical Instrumentation: Application and design 3rd Edition*, JG Webster, Ed., NY: John Wiley and Sons, 1998, pp. 190.

31 J Weaver and YuA Chizmadzhev, Theory of electroporation: A review, *Bioelectrochem. and Bioenerg*, vol. 41, pp. 135-160, 1996.

32 SH White, D Mirejovsky and GL King, Structure of lamellar lipid domains and corneocyte envelopes of murine stratum corneum. An X-ray diffraction study, *Biochemistry.*, vol. 27, pp. 3725-3732, 1988.

33 A Alonso, N Meirelles, M Tabak, Effect of hydration upon the fluidity of intercellular membranes of stratum corneum., *Biochim. et Biophys. Acta*, vol. 1237, pp. 6-15, 1995.

34 C Lee, W Lin and J Wang, Mechanical aspects of lipid-bilayer phase transition studied by differential confocal microscopy, Paper CTuR4 delivered at the Conference on Lasers and Electro Optics, Baltimore, Maryland, USA 2001.

35 MJ Pikal, S Shah, Transport mechanisms in iontophoresis. II. Electroosmotic flow and transference number measurements for hairless mouse skin, Pharm. Res., vol. 7, pp 213-221, 1990.

36 DW Fawcett and RP Jensh, *Bloom and Fawcett's Concise Histology 2nd Edition*, London: Hodder Arnold, 2002

37 RT Fenner, *Finite element methods for engineers,* London: Macmillan, 1975.

38 VC Rideout, *Mathematical and computer modeling of physiological systems*, Englewood Cliffs NJ, Prentice Hall, 1991, pp 171-187.

39 J.Z. Szopinski, Habilitation Thesis, Silesian Medical Academy, Poland, 2003

40 SD Brain, P Newbold and R Kajekar, Modulation of the release and activity of neuropeptides in the microcirculation, *Can.J.Physiol.Pharmacol.*, vol. 73, pp. 995-8, 1995.

41 M Kleiner, Biochemistry 6th Edition, St. Louis : Mosby, 1962

42 A White, Principles of Biochemistry 5th Edition, NY: McGraw-Hill, 1973

43 LV Chernomordik, Breakdown of lipid bilayer membranes in an electric field, *Biochim. et Biophys. Acta*, vol. 739, pp. 203-213, 1983.

10 APPENDICES

Programs used for simulations are contained in the appendices. All programs were written for MATLAB for Windows and were run under Windows 98 on an AMD Athlone 2100.

10.1 Appendix 1 Coupled electrical heat transfer model

The program implements the model described in experiment 12. An electrical model is used to calculate the current through the skin, from which the power dissipated in the skin is determined. A 1D axisymmetric finite element heat transfer model estimates the resulting distribution of heat through the stratum corneum. The skin temperature affects the parameters of the electrical model. The skin temperature and current is estimated iteratively at incremental time steps.

10.1.1 Setup finite element matrices

```
%****************** Define Constants **********
pc = 2e-12; %J/um3/C
k = 1e-7;
h1 = 5e-11; %htop+hbot / thickness
T1inf = 25;
h2 = 1e-8; %was 3e-8
T2inf = 30;
dz = 15; % Stratum corneum depth (um)
N = 24;
n = 5;

K = zeros(N+1);
C = zeros(N+1);
F0 = zeros(N+1,1); %forcing function without heat sources
F = zeros(N+1,1);
R = zeros(N+1,1); %Radius
Q = zeros(N,1);
%****************** Impliment Geometry **********
for i=1:N
Edof(i,:) = [i i i+1];
end
for i = 1:n
r2 = i*2.;
R(i+1) = r2;
end
for i = n+1:N
r2 = r2 + 2.*(1+(i-n)/5);
R(i+1) = r2;
end
bc = [N+1 29];
%****************** Setup System Equations *******
for i = 1:N
[Ke,Ce,Fe] = spr1axi(pc,k,h1,h2,dz,0,T1inf,T2inf,R(i),R(i+1));
[K,F0] = assem(Edof(i,:),K,Ke,F0,Fe);
[C] = assem(Edof(i,:),C,Ce);
end
%****************** Add forcing function *********
TC0 = ones(N+1,1);
```

```
TC0 = TC0*29;
nhist = [];
```

10.1.2 Main program

```
%**************Define Constants******************
global dT;
e = 1.602e-19;
k = 1.381e-23;
T = 300;
n = 0.15;
B = e/(k*T);
H = 1.3;
h = 5e-9;
R0 = h/2;
M =(pi*R0^2*H/h);
w0 = 1.5;
m = 14;
Gb = 5.e-4;
U0 = 0;
g = M*(w0-n*B*U0/m)/(w0*exp(w0-n*B*U0/m)-n*B*U0/m);
N0 = 1E6;
G = N0*g/m;
G1 = N0*g/20;
Y0 = [N0,0,G,0,29,N0,G1];

Y=Y0;
T =[0];
st =[0 TC0(1) Q(1) Y0(1:7)];
dt = 1.e-3;
time = 0;
TC = zeros(size(TC0));
dT = 0;
iter = 0;
%*********************Main Loop************************%
while ((time < 10000.e-3) & (TC(1)<45)),
  Tode = -1;
  iter = 0;
%*******Iterate couppled Heat transfer and Electrical equation***%
  while( abs(TC(1)-Tode) > 0.01),
        [T1,Y1] = ode45('difeq',time,time+dt,Y0,1.e-10);     %Solve differential equation
        Qode = Y1(length(Y1),4)*1E-8/dt/3;                   %Calculate heat output by R
        Q(1:5) = ones(5,1)*Qode;                             %Use as input to finite element model
        F=F0;
        for i = 1:N                                          %Assemble finite equations
              [Fe] = spr1axif(Q(i),R(i),R(i+1));
              [F] = assemf(Edof(i,:),F,Fe);
        end
        Tfin = dt;
        ntimes = [Tfin];
        nhist = [];
        ip = [dt Tfin 1 1 0 ntimes nhist];
        TC = step1(K,C,TC0,ip,F,bc);                         %Solve finite element equation
        dT = (TC(1)-TC0(1))/dt;                              $Calulate Temperature rate of change to input
                                                             %to differential equation
        Tode = Y1(length(Y1),5);                             %Temperature change in R
        if iter > 2
              dt = 1e-3;
              end;
        if iter > 10;
              iter
              return;
              end;
```

```
        iter = iter + 1;
 end
 time = time+dt;
 Y0 = Y1(length(Y1),:);
 S = [time TC(1) Q(1) Y0(1:7)];
 Y0(4) = 0;                                  %reset power dissipation to 0
 TC0 = TC;
 st = [st' S']';
 if  dt < 10.e-3
%        dt = dt + 1e-3;
 end
end
```

10.1.3 System of Differential Equations

```
function yp = circuit(t,y) %Simple RC LPF with electroporation of RC resistor

global dT;
N0 = 1E6;
Alpha = 4.2;
K = 10E3;
m = 14;
U = 21;
dUdt = 0;
e = 1.602e-19;
k = 1.381e-23;
T = 300;
n = 0.15;
B = e/(k*T);
w0 = 1.5;
H = 1.3;
h = 5e-9;
R0 = h/2;
M =(pi*R0^2*H/h);
C = 10.e-9;
Gb = 5.e-4;
Tcrit = 40;

g = M*(w0-n*B*y(2)/m)/(w0*exp(w0-n*B*y(2)/m)-n*B*y(2)/m);
v = n*B*y(2)/m;
w = w0 - v;
dgdu = -M*(n*B*(w0*exp(w)-v)+w*(-n*B*w0*exp(w)-n*B))/((w0*exp(w)-v)^2);

if y(5) < Tcrit
        yp(1) = K*(exp(Alpha*(y(2)/m)^2)-y(1)/N0);
else
        yp(1) = (1+y(5)-Tcrit)*K*(exp(Alpha*(y(2)/m)^2)-y(1)/N0);
end

yp(2) = (-y(2)*(y(3)*300E-6  +Gb)+U*Gb)/C;      %dUm/dt
yp(3) = g*yp(1)/m + y(1)/m*dgdu*yp(2)/m;        %dG/dt G is Conductace.cm^-2
yp(4) = y(2)^2*y(3);                            %dP/dt
yp(5) = dT;                                     %dT/dt

yp = yp';
```

10.2 APPENDIX 2 Electroporation / Electro-Osmosis model

The program implements the electrical model of the skin shown in Fig 7.1 by solving the system of differential equations (7.1) - (7.8) described in section 7.2. The current through the skin is calculated as a function of time due to a voltage stimulus.

10.2.1 Constants

```
Re = 40e3; %bulk resistance
f = 12.5;
Vpp = 20;
C = 1e-9;
Gi = 200e-9;
A0 = 1;
dAdt = 1/8;
Adef = 100e-6;
k1 = -1e10;%osmotic decay constant
k2 = 0;
k3 = 1E9;%current integral
k4 = 1e2;
N0 = 1E6;
Alpha = 4.8;
K = 1E3;
m = 15;
e = 1.602e-19;
k = 1.381e-23;
T = 300;
n = 0.15;
B = e/(k*T);
w0 = 1.8;
H = 1.3;
h = 5e-9;
R0 = h/2;
Mg =(pi*R0^2*H/h);
```

10.2.2 Main Program

```
clear;
format short e;
constants;                                  %define constanst (9.2.1)
Y0 = [0 N0 0];                              %initial conditions
Y = Y0;
t = [0];
time = 0;
div = 40;
dt = 1/(f*div);
dt = 1e-3
for i =1:80
        [T1,Y1] = ode23('tempeq',time,time+dt,Y0,1.e-7);   %solve differential equation
        Y0 = Y1(length(Y1),:);                             %get initial condition for next timestep
        Y = [Y' Y1']';                                     %store calculated values
        t = [t' T1']';
        end
        time = time+dt;
end

t = t(2:length(t));                         %ignore extra 0
Y = Y(2:length(Y(:,1)),:);
```

```
ut= [Y(:,1)];
nt= [Y(:,2)];
ht= [Y(:,3)];
```

10.2.3 System of Differential Equations

```
function yp = tempeq(t,y)

V = Vpp*sin(2*pi*f*t);
A = A0+t*dAdt;

um = abs(y(1));
g = Mg*(w0-n*B*um/m)/(w0*exp(w0-n*B*um/m)-n*B*um/m);
Rm = m/(g*y(2)*Adef);
Gm = 1/(Rm*(1+y(3)/50));

yp(1) = ((V-y(1))/Re - y(1)*(Gm+A*Gi))/(C*A);      %dUm/dt
yp(2) = K*(exp(Alpha*(y(1)/m)^2)-y(2)/N0);         %dN/dt

if y(1)>0                                          %dH/dt
yp(3) = y(1)*Gm*k3-y(3)*k2;
else
yp(3) = -y(3)*y(1)*Gm*k1;
end;
yp = yp';
```